B-MYB and FOXM1 drive cell division through cooperative regulation of cell cycle genes.

HARVARD
Kenneth C. Griffin

GRADUATE SCHOOL
OF ARTS AND SCIENCES

DISSERTATION ACCEPTANCE CERTIFICATE

The undersigned, appointed by the

Division of Medical Sciences

Committee on Virology

have examined a dissertation entitled

B-MYB and FOXM1 drive cell division through cooperative regulation of cell cycle genes

presented by Hembly G. Rivas

candidate for the degree of Doctor of Philosophy and hereby certify that it is worthy of acceptance.

Signature: Nick Dyson
Nick Dyson (Dec 4, 2023 15:29 EST)

Typed Name: Dr. Nicholas Dyson

Signature: Karen Cichowski
Karen Cichowski (Dec 6, 2023 10:24 EST)

Typed Name: Dr. Karen Cichowski

Signature: Zuzana Tothova
Zuzana Tothova (Dec 4, 2023 11:47 EST)

Typed Name: Dr. Zuzana Tothova

Signature: Karl Munger
Karl Munger (Dec 4, 2023 12:51 EST)

Typed Name: Dr. Karl Münger

Date: December 04, 2023

B-MYB and FOXM1 drive cell division through cooperative regulation of cell cycle genes.

A DISSERTATION PRESENTED

BY

HEMBLY G. RIVAS

TO

THE DIVISION OF MEDICAL SCIENCES

IN PARTIAL FULFILLMENT OF THE REQUIREMENTS

FOR THE DEGREE OF

DOCTOR OF PHILOSOPHY

IN THE SUBJECT OF

VIROLOGY

HARVARD UNIVERSITY

CAMBRIDGE, MASSACHUSETTS

DECEMBER 2023

Dissertation advisor: Professor James A. DeCaprio Hembly G. Rivas

B-MYB and FOXM1 drive cell division through cooperative regulation of cell cycle genes.

ABSTRACT

Transcription facilitates cell cycle division and progression as it orchestrates the timely expression of genes crucial for each cell cycle phase. Two waves of gene expression prime the cell for replication: the first wave (DNA replication genes) produces the needed cell machinery for DNA replication, and the second wave of gene expression (mitotic genes) encodes the mitotic regulators required for cell division. The B-MYB/MuvB(MMB)-FOXM1 complex coordinates the expression of mitotic genes. This dissertation investigates the inter-dependence between B-MYB and FOXM1 and their requirement for mitosis.

We show that knockout of MMB-FOXM1 complex components B-MYB, LIN54, or FOXM1 confers resistance to CHK1 and ATR inhibition. In addition, we demonstrate that the loss of B-MYB impedes arrest following contact inhibition. Cell cycle kinetic studies reveal that the knockout of B-MYB or FOXM1 has profound effects on the progression of every cell cycle phase. These findings indicate the MMB-FOXM1 complexes function as global coordinators of cell cycle progression and establish the MMB-FOXM1 as a crucial signaling node in response to cellular stress.

During early S phase, B-MYB binds to MuvB to form the MMB complex. The MMB complex recruits FOXM1, and both B-MYB and FOXM1 contribute to activating mitotic genes. In this dissertation, we extend these findings by showing that MMB

enhanced FOXM1 binding to DNA, and B-MYB-mediated recruitment of FOXM1 was critical for the onset of mitotic gene expression. We found that FOXM1 was required to properly dissociate B-MYB from DNA in G2 and degradation of B-MYB and other DNA machinery in mitosis. These findings prove that B-MYB and FOXM1 functionally cooperate and rely on mutually interdependent interactions to activate mitotic genes.

The CHR motif, recognized by the MuvB complex, is primarily enriched at mitotic gene promoters, while canonical MYB and forkhead DNA motifs are less abundant. Current models propose that B-MYB and FOXM1 stabilize MuvB complexes at CHR elements by binding largely non-sequence-specific DNA. Using high-resolution chromatin profiling, we show that B-MYB and FOXM1 binding is correlated but also distinct. We observed that B-MYB binding was enriched at mitotic gene promoters and contained canonical MYB and CHR DNA recognition motifs. In addition, we found that MuvB component LIN9 binding follows the pattern of BMYB rather than FOXM1. We demonstrate that FOXM1 binds to mitotic and DNA damage gene promoters. FOXM1 gene targets were enriched for canonical forkhead DNA recognition motifs. Combining nascent transcript analysis (PRO-seq), RNA-seq, and Cut&Run sequencing, we define FOXM1 as a critical transcriptional driver of cell cycle gene expression. Collectively, these findings indicate that B-MYB and FOXM1 cooperatively regulate the expression of cell cycle genes, where the MMB complex defines mitotic genes through association with MYB and CHR recognition motifs and enhances recruitment of FOXM1 to mitotic gene promoters, where FOXM1 drives transcription of mitotic genes and DNA repair genes.

Contents

Listing of figures

Acknowledgments

First and foremost, I am incredibly grateful to my Ph.D. advisor, Professor James A. DeCaprio, MD, for his invaluable advice, continuous support, and patience. Jim's dedication to student development, diversity, and inclusion unknowingly shaped my training through the CURE summer research program even before graduate school. Jim's commitment to fostering a collaborative and intellectually stimulating environment has inspired me to push the boundaries of my research. I feel truly fortunate to have had such a dedicated and inspiring advisor who not only shared his wealth of knowledge but also instilled in me the confidence to navigate the challenges of graduate school.

I want to also thank the members of my dissertation advisory committee, Peter Sicsinski, Ph.D., and Kenneth Kaye, M.D., for their helpful suggestions and guidance over the years. A special thank you to my committee chair, Professor Nickolas Dyson, Ph.D., for facilitating collaborations, providing thoughtful feedback, and kind encouragement. I would also like to thank Karen Cichowski, Ph.D., Zuzana Tothova, M.D. Ph.D., and Karl Munger, Ph.D., for agreeing to serve on my dissertation defense committee and for taking the time to read this dissertation.

I will forever be thankful to my former undergraduate research advisors. I remember fondly my time as a PREP scholar in Professor Marta Gaglia's lab at Tufts Medical School. Thank you, Marta, for your mentorship, honesty, and thoughtful advice. I want to thank Professor Adan Colon-Carmona, Ph.D., from the University of Massachusetts Boston, for recognizing my potential and providing guidance on navigating the higher education system, enabling me to pursue and achieve my aspirations.

Completing my studies would have been an impossible task without the unwavering support of my family, which extends to my aunts, uncles, and cousins. Thank you to my parents, Merari and Samuel Rivas, for their boundless patience and steadfast belief in me. Their encouragement has been a constant source of strength, guiding me through the challenges and triumphs. Their sacrifices and resilience allowed me to follow my dreams. I am profoundly thankful to my siblings, Brian, Caleb, and Rachel Rivas, for their love and support.

Le quiero dar gracias a mis amados abuelos, Genoveva Pinto y Toribio Rivas, por sus oraciones que nunca fallaron y por siempre recordarme de que Dios tiene un proposito para mi vida. Gracias a la comunidad de mi iglesia y Pastor Rev. Dr. David Martinez por sus oraciones y apoyo. Mi vida es más rica gracias a las relaciones, los valores y el apoyo que todos ustedes me han brindado.

I want to extend a special thanks to all my friends for their friendship throughout my journey in graduate school. Their encouragement, camaraderie, and understanding have been instrumental in making this academic endeavor manageable and enjoyable. I will not forget the late-night shifts together in lab with Julia Schnabel, uplifting conversations with Joanna Rodrigues and Varsha Ananthapadmanabhan, and shared moments of celebration with Mona Ahmed and Camille Cushman; their support has been a constant source of inspiration. The challenges of graduate school were also made

more bearable by Alexis Dickinson and Vania Aguilar; I am truly grateful for your friendship, the good laughs and fun nights out, and for enriching my world.

I would also like to thank Gabriel Cruz. Whether providing a listening ear during stressful times or celebrating small victories, his presence has provided comfort and motivation. Thank you, Gabe, for your unwavering belief in my abilities, even during moments of self-doubt. I am profoundly thankful for your love and understanding and for making this academic journey more fulfilling and memorable.

This section would not be complete if I did not acknowledge Camille Cushman's invaluable role in shaping my experience throughout graduate school. Thank you for being an unwavering source of support and camaraderie throughout the highs and lows of graduate school. Your encouragement, help, and understanding have been invaluable companions on this challenging path. When we met, I knew I had found a lifelong friend, and I can't wait to see what life has in store.

AUTHOR CONTRIBUTIONS FOR CHAPTER 1

In this introductory chapter, the sections “1.1.1: The protein RB represses G1/S genes and reinforces the Restriction Point.” and “1.1.2: The DREAM complex functions in parallel with RB to suppress cell cycle genes.” were adapted from a published book chapter co-authored with James A. DeCaprio[112].

This research was supported by the U.S. Public Health Service grants R35 CA232128-03S1 to H.G.R. and R35CA232128 to J.A.D.

1

Introduction

1.1 Two broad waves of transcription coordinate cell division.

The cell cycle progression is the gradual and highly coordinated series of events a cell undergoes as it prepares to subsequentially divide. The mammalian cell cycle is divided into four phases: Gap 1 (G1), DNA synthesis (S), Gap 2 (G2), and mitosis (M). Transcription is pivotal for cell cycle progression as it orchestrates the timely expression of cyclins and many other genes required for each cell cycle phase. More than 1000 cell cycle-dependent genes have been identified in several genome-wide

studies[140,4,116,50,106,86,29,40,80]. Two waves of gene expression prime the cell for replication: the first wave (G1/S genes) produces transcripts for the cell machinery needed for DNA replication, and the second wave of gene expression (G2/M genes) encodes the transcripts for mitotic regulators required to complete cell division[116,40,8].

Several transcription factors coordinate the repression and activation of cell cycle genes. Repressive transcription complexes, composed of proteins like protein retinoblastoma (Rb) and pocket proteins 130 and p107, inhibit the expression of G1/S genes and prevent entry into S phase. Conversely, activating transcription complexes like E2F transcription factors, B-MYB, and FOXM1 are positive regulatory proteins that facilitate the expression of cell cycle genes essential for cell cycle progression. The dynamic regulation of cell cycle genes (summarized in 1.1) ensures the coordinated progression of the cell cycle and contributes to the precise onset of cellular events necessary for faithful cell division.

1.1.1 The protein RB represses G1/S genes and reinforces the Restriction Point.

The Restriction Point is a critical control step in the cell cycle. It acts as a decision point in late G1 phase, where environmental conditions, such as growth factors, determine whether a cell proceeds to enter S phase and undergo DNA replication or exits the cell cycle into a non-dividing state (G0 phase)(Reviewed in[112]).

The RB protein is central to the Restriction Point, which plays a decisive role in the timing and reinforcement of the G1 checkpoint. RB, the product of the retinoblastoma tumor suppressor gene (RB1), is expressed in all normal cells, including quiescent and proliferating cells. RB functions, in part, as a transcriptional repressor of the activating E2F family of transcription factors (Reviewed in[32]). During G0 phase, an unphosphorylated form of RB binds to E2F and represses the expression of cell cycle-

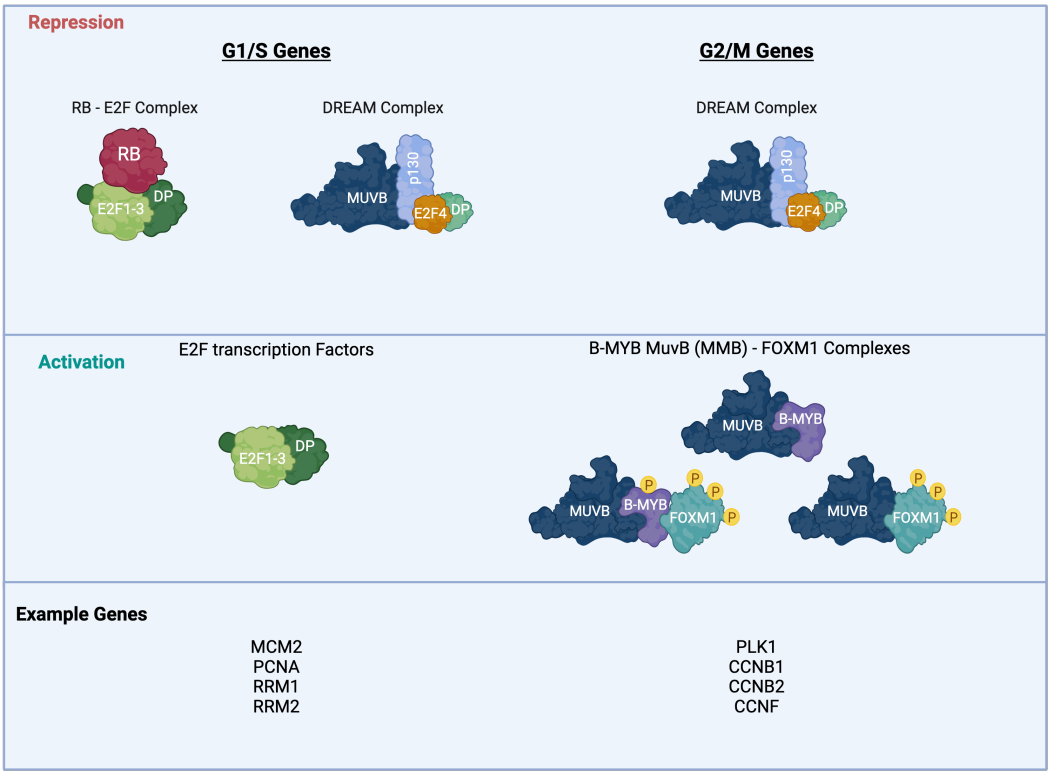

Figure 1.1: Transcriptional Regulation of Cell Cycle Genes. Transcription Factor complexes regulate cell cycle gene expression. Un-phosphorylated RB represses E2F-dependent early cell cycle genes during quiescence. The DREAM complex component LIN54 binds through its CxC DNA-binding domain to recognize both E2F and CHR DNA elements to repress early and late genes and weakly bind the CHR-like elements (CLE). Additionally, E2F4/DP proximity to the cell Cycle-dependent element (CDE) can support DREAM binding to late cell cycle genes. Cooperatively, cyclin D-CDK4/6 initiates the phosphorylation of RB and promotes DREAM complex disassembly. Cyclin E-CDK2 hyperphosphorylates RB, thereby depressing the activation of E2F-activating transcription factors. Release of MuvB from DREAM leads to association with B-MYB, which functionally switches MuvB to an activating transcriptional complex. B-MYB-MuvB and FOXM1-MuvB complexes sequentially bind late cell cycle genes. The binding of B-MYB to MuvB is required to recruit FOXM1.

dependent genes that contain E2F binding sites in their promoter[21,48,138]. Progressive phosphorylation of RB relieves its inhibitory effect on E2F transcription factors, permitting their activation and subsequent stimulation of cell cycle progression beyond the restriction point through the expression of G1/S genes required for DNA replication (Reviewed in[112]).

RB undergoes mono-phosphorylation and subsequent multi-phosphorylation at multiple sites by cyclin-dependent kinases (CDKs) as the cell progresses through the G1 phase, regulating its function in a cell-cycle dependent manner[121]. Growth factors stimulate cyclin D-cyclin-dependent kinase (CDK) 4 complex activity in early G1, which promotes mono-phosphorylation of RB. Cyclin D-CDK4 can phosphorylate RB on 15 serine or threonine residues within a CDK phosphorylation consensus motif (S/T)P[98]. Phosphorylation of RB by cyclin D-CDK4 precludes additional phosphorylation by cyclin D-CDK4[121]. Fourteen forms of mono-phosphorylated RB interact with E2F/DP proteins, with each isoform yielding distinct levels of E2F regulation. Mono-phosphorylation of RB controls both protein interactions and its transcriptional repressor activity. Additionally, mono-phosphorylated RB plays a role in suppressing the activation of E2Fs upon DNA damage signaling[121].

Continued activity of Cyclin D-CDK4 can lead to the activation of Cyclin E, which in complex with CDK2 phosphorylates RB on multiple CDK(S/T)P sites. While mono-phosphorylated RB (cyclin D-CDK4 dependent) retains binding and repression of the activating E2Fs, multi-phosphorylated RB (cyclin E-CDK2 dependent) is unable to bind E2F or repress its activity[98]. The cyclin E-CDK2-dependent multi-phosphorylation of RB releases it from E2F transcription factors. The activating E2Fs, E2F1, E2F2, and E2F3 promote the expression of the several hundred G1/S genes required for DNA synthesis, such as ribonucleotide reductase components RRM1 and RRM2,

replication factor MCM2, and DNA replication complex component PCNA[40] (Figure 1.1). Thus, cyclin E activity toward RB enables cells to pass the Restriction Point and become committed to cell cycle entry. This period of G1, when RB is hyperphosphorylated and cells have committed to S phase entry but before DNA synthesis begins, is referred to as the G1/S transition phase of the cell cycle.

1.1.2 THE DREAM COMPLEX FUNCTIONS IN PARALLEL WITH RB TO SUPPRESS CELL CYCLE GENES.

In addition to RB, p107 (RBL1) and p130 (RBL2) are two RB-like proteins with critical roles in the transcriptional regulation of cell cycle genes. Collectively known as the "pocket proteins," RB, p107, and p130 share extensive homology in a large portion of their central or "pocket" domain, which mediates interaction with various protein partners, including E2F and viral oncoproteins[20]. While pRB is the most extensively studied among these proteins regarding its role in regulating the restriction point, p107 and p130 overlap with pRB in cell cycle control. p107 and p130, similar to pRB, interact with E2F transcription factors and contribute to repressing cell cycle genes.

The DREAM complex is comprised of DP, either RB-like protein p130 or p107, a repressor E2F4 or E2F5, and the five-protein core complex termed MuvB (multivulva class B) consisting of LIN9, LIN37, LIN52, LIN54, and RBBP4 (Figure 1.1)[115]. DREAM imposes its repressive function on cell cycle-regulated genes by recognizing two distinct promotor elements. The MuvB core component LIN54 binds directly to cell cycle gene homology region (CHR) sites in promoters of cell cycle-regulated genes (Figure 1.1). In addition, DREAM components p130/p107 and repressor E2F4/5 bind to E2F sites[107,143]. RB and DREAM bind and repress an overlapping set of E2F-

dependent gene promoters and cooperate to restrict cell cycle entry.

The DREAM complex has a dominant role during G0 and early G1[124]. During these phases, phosphorylation of the MuvB component LIN52 by the kinase DYRK1A enables p130 binding to the MuvB core to form the DREAM complex[76]. Activation of the cyclin D-CDK4 complex phosphorylates p130, releasing p130 and E2F4/DP from the MuvB core, and reduces the binding of p130 to E2F sites in cell cycle-regulated promoters (Figure 1.1).

1.1.3 The MMB-FOXM1 complexes coordinate G2/M gene expression.

The disassociation of the DREAM complex releases the MuvB core complex to serve as a platform for the recruitment and assembly of additional regulatory factors, such as B-MYB and FOXM1 (Reviewed in[94]). Transcription factors B-MYB and FOXM1 sequentially interact with MuvB and orchestrate the G2/M transcriptional program required for cell division and the faithful execution of mitosis (Figure 1.2)[116,77,30,16,120].

B-MYB, encoded by the *MYBL2* gene, is ubiquitously expressed across different cell types; however, protein levels fluctuate in a cell cycle-dependent manner reaching peak levels during S phase[137,72,79,153]. In early S phase, B-MYB binds to MuvB, forming the MMB complex (Figure 1.2)[116]. Multi-site phosphorylation of B-MYB by cyclins-CDK complexes is necessary for activation and maximum transcriptional activity[113,151,117,123,64]. Conversely, phosphorylation of B-MYB also marks it for degradation[15].

Like B-MYB, FOXM1 is ubiquitously expressed and protein phosphorylation fluctuates in a cell cycle-dependent manner[73,101,71,116,16,11]. In its unphosphorylated form, FOXM1 exists in S phase cells in an autoinhibited state[141,73,103]. With 15 canonical

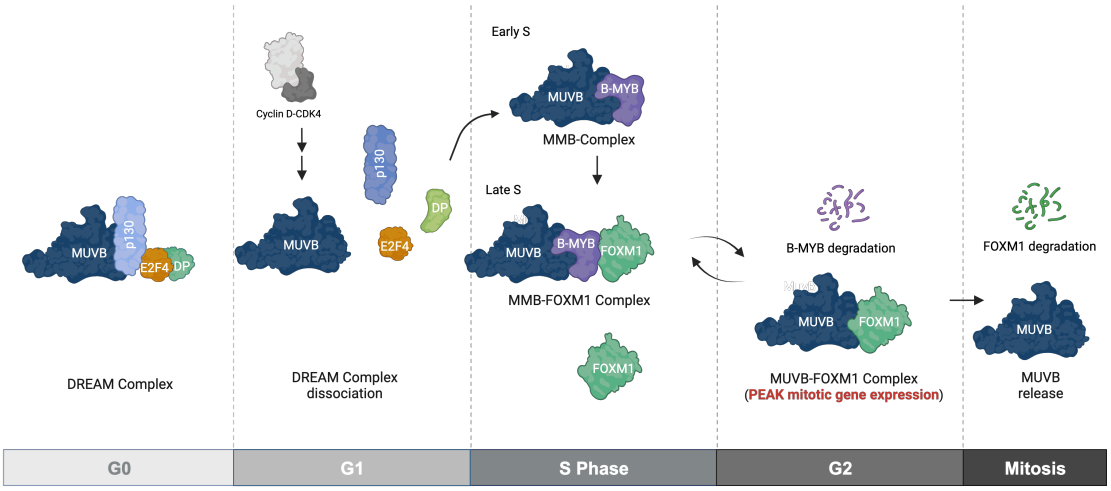

Figure 1.2:

Sequential formation of MMB, MMB-FOXM1, and FOXM1-MuvB complexes activates G2/M gene expression. B-MYB associates with MuvB in the early S phase, forming the MMB complex as a crucial platform for FOXM1 recruitment (forming MMB-FOXM1). During the G2/M phase transition, B-MYB undergoes degradation, and peak expression of G2/M genes correlates with the FOXM1-MuvB complex bound to CHR elements of G2/M promoters.

CDK-dependent phosphorylation sites spanning the c-terminal domain of FOXM1, cyclin-CDK complexes progressively phosphorylate FOXM1[2,73,103,84]. In addition to cyclin-CDKs, the PLK1 kinase and the DNA damage regulator CHK2 kinase also phosphorylate FOXM1[43,130,89]. Hyperphosphorylation of FOXM1 correlates with peak G2/M gene expression (Figure 1.2)[116]. Despite our understanding of B-MYB and FOXM1 activation, it is unclear how these factors functionally cooperate to activate G2/M gene expression. Knockdown of either B-MYB or FOXM1 reduces late cell cycle gene expression[116], suggesting that both transcription factors act as activators of G2/M gene expression.

B-MYB and FOXM1 regulate G2/M gene expression[73,116]. Several Chromatin Immunoprecipitation (ChIP) studies have shown that B-MYB and FOXM1 bind to several overlapping G2/M gene promoters[116,16,30,120]. Whether B-MYB cooperates with FOXM1 to activate G2/M genes is unclear. Knockdown experiments targeting B-MYB have demonstrated decreased FOXM1 levels and decreased expression of downstream G2/M target genes, suggesting FOXM1 requires B-MYB for expression and activity[116,30]. These findings, coupled with protein-protein interaction studies, suggest B-MYB and FOXM1 directly bind and are interdependent in orchestrating the transcriptional activation of G2/M genes[17,30]. However, whether B-MYB serves an essential role in enabling FOXM1 recruitment to gene promoters during cell cycle progression remains unclear.

B-MYB and FOXM1 both contain DNA-binding domains. B-MYB includes a DNA-binding domain known as the MYB DNA-binding domain[7]. This domain is a feature of the MYB family of transcription factors, including MYBL1(MYB) and MYBL2 (B-MYB). The MYB domain consists of one to four imperfect repeats of approximately 50 amino acids, forming a helix-turn-helix structure[99]. FOXM1 contains

a conserved Forkhead Box (FOX) DNA-binding domain[78]. The FOX domain is a winged-helix DNA-binding domain that allows FOXM1 to recognize forkhead DNA sequences (FKH) in the promoter regions of target genes.

Whether FOXM1 binds directly to G2/M gene promoters is contentious. Our lab reported that the forkhead (FKH) motif was enriched in cell cycle promoters in HeLa cells bound by LIN9 and B-MYB, suggesting that FOXM1 is recruited to G2/M promoters in a DNA sequence-dependent manner[116]. Since the original report, several genome-wide studies have presented conflicting models of FOXM1 recruitment to DNA. Therefore, whether FOXM1 binds directly to DNA or depends on co-factors like B-MYB or LIN54 is unclear.

1.1.4 The transcription factor FOXM1 is involved in the replication stress response.

The ATR-CHK1 pathway plays a central role in ensuring the faithful duplication of DNA during S phase[118,19,69,26]. The ATR (ataxia telangiectasia and Rad3-related protein) kinase coordinates DNA replication origin firing, replication fork stability, cell cycle checkpoints, and DNA repair (reviewed in[118]). ATR and co-factors are recruited to replication protein A (RPA)-bound, single-stranded DNA structures generated at sites of active DNA replication or DNA damage caused by replication stress (Reviewed in[118]). During replication stress, ATR phosphorylates and activates the checkpoint kinase 1 (CHK1)[132,149]. Activated CHK1 phosphorylates the CDC25 phosphatases and WEE1 kinase, two critical regulators of CDK1 activity. Consequently, CDC25 phosphatases become inhibited, and WEE1 activity increases, resulting in decreased CDK1 activity through increased phosphorylation of the inhibitory Y15 site on CDK1 (Reviewed in[25]). ATR activity in S phase controls the subsequent

duration of G2[119]. Interestingly, ATR inhibition prematurely activates FOXM1, deregulating the S/G2 transition and leading to early mitosis and under-replicated DNA. Whether FOXM1 alone or the MMB-FOXM1 complex is involved in the ATR-CHK1 response is unclear.

1.1.5 Understanding the MMB-FOXM1 complex presents potential avenues for therapeutic intervention.

Elevated levels of B-MYB and FOXM1 are associated with worse prognostic outcomes in several types of cancers. Increased expression of FOXM1 and B-MYB has been linked to more aggressive tumor behavior, higher tumor grade, increased proliferation, and poorer patient outcomes in various cancers, including breast cancer, ovarian cancer, colorectal cancer, and others[5,12,47]. As pivotal transcription factors that govern the expression of genes required for DNA replication and mitosis, B-MYB and FOXM1 likely exert their oncogenic potential through uncontrolled cell cycle progression and cell proliferation. An imbalance in cell cycle control, leading to unrestrained cellular proliferation, is a hallmark of cancer. Indeed, the knockdown of MYBL2 or FOXM1 in various cancer cell lines hinders cell cycle progression and cellular viability[12,93]. FOXM1 has been associated with increased genomic instability and aneuploidy[73]. High FOXM1 levels have been linked to resistance to chemotherapies like cisplatin[13,27]. Similarly, increased expression levels of B-MYB lead to resistance to DNA damaging agent Doxorubicin[12]. Understanding how B-MYB and FOXM1 influence key cellular processes related to proliferation, genomic stability, and tumor progression will expand our understanding of basic cell cycle processes and inform our interpretation of clinical data for cancers that overexpress these transcription factors.

AUTHOR CONTRIBUTIONS FOR CHAPTER 2

Dr. David Kozono, Peter Deraska, and Hunter D. Reavis generated the sgEV and sgLIN54-1 cell lines in 2.1. The sgFOXM1 K.O. cell lines used in 2.1 were generated by Dr. Timothy Branigan and Larissa Sambel. I would like to thank Dr. Camille H. Cushman for assistance with the Prexasertib sensitivity curves in 2.4. Julia Schnabel performed the RNA purification and RT-qPCR in 2.5.

All other cell lines, assays, and experiments were conceived and performed by Hembly G. Rivas with input from James A. DeCaprio. This research was supported by the U.S. Public Health Service grants R35 CA232128-03S1 to H.G.R. and R35CA232128 to J.A.D.

The published version of Figure2.1 can be found under the following citation: Branigan, T. B., Kozono, D., Schade, A. E., Deraska, P., Rivas, H. G., Sambel, L., Reavis, H. D., Shapiro, G. I., D'Andrea, A. D., and DeCaprio, J. A. (2021). MMB-FOXM1-driven premature mitosis is required for CHK1 inhibitor sensitivity. Cell Rep 34, 108808.

The study of the cell cycle responsible for the reproduction of cells [is] important and might even illuminate the nature of life.

Sir Paul Nurse, Ph.D.

2

The role of the MMB-FOXM1 complex in replication stress and cell cycle progression.

2.1 Abstract

The cell cycle progression is the gradual and highly coordinated series of events a cell undergoes as it prepares and subsequently divides. Transcription is pivotal for cell cycle progression as it orchestrates the timely expression of genes crucial for each cycle phase. The MMB-FOXM1 complexes promote cell cycle progression by ac-

tivating the transcription of G2/M genes involved in mitosis. The regulatory role of the MMB-FOXM1 complexes in other parts of the cell cycle is less well-understood. In this chapter, we examined the individual contributions of MMB-FOXM1 components in regulating replication stress and cell cycle progression. We generated LIN54, B-MYB, and FOXM1 knockouts in the human A549 cell line. Knockout of LIN54, B-MYB, or FOXM1 conferred resistance to checkpoint kinase ATR and CHK1 inhibition. Knockout of B-MYB or FOXM1 did not affect the overall cell doubling time but led to an increase in the proportion of cells in G2/M. Synchronization assays with B-MYB and FOXM1 KOs revealed that knockout of B-MYB uniquely impaired contact inhibition. In contrast, B-MYB and DOXM1 KO cells were arrested in G1 upon CDK4 inhibition. Cell cycle kinetic assays demonstrated that the knockout of FOXM1 quickened S phase progression, while the knockout of B-MYB significantly delayed entry into mitosis. Knockout of B-MYB or FOXM1 impaired G2 phase progression, indicating critical but distinct roles for B-MYB and FOXM1 in regulating cell cycle progression. These discoveries offer insights into the mechanisms behind small molecule inhibitors being actively investigated in clinical trials and suggest perturbations of B-MYB and FOXM1 may have distinct impacts on cell cycle progression and cancer.

2.2 INTRODUCTION

The cell cycle is comprised of four distinct phases: G1 (Gap 1), S (DNA Synthesis), G2 (Gap 2), and M (mitosis), during which the cell grows, duplicates its DNA, and ultimately divides into two identical daughter cells. Key checkpoints precisely regulate and ensure that growth conditions, DNA integrity, and proper chromosome seg-

regation are met before advancing to the next phase ([112] and reviewed in [102]). These checkpoints are known as the G1 phase checkpoint (the restriction point), intra-S checkpoint, and mitotic checkpoint, respectively. Transcription plays a pivotal role in regulating these checkpoints by orchestrating the timely expression of genes crucial for each cycle phase (Reviewed in [8]). Two waves of transcription coordinate cell cycle progression: the first wave (G1/S genes) produces the transcripts for DNA replication machinery, and the second wave of gene expression (G2/M genes) produces the transcripts for mitotic regulators required for chromatin segregation. Successful cell cycle progression is essential for cell proliferation and ensuring the accurate transmission of genetic information from mother to daughter cells. One of the hallmarks of cancer is uncontrolled proliferation, a consequence of defective cell cycle checkpoints, which underlies cancer development and tumor growth ([57]).

Several transcription factors coordinate the repression and activation of cell cycle genes (Reviewed in [41]).The B-MYB-MuvB (MMB) and MuvB-FOXM1 complexes drive G2/M gene expression ([116,77,30,108,126,53,95,16]). The composition of the MuvB core complex (LIN9, LIN37, LIN52, LIN54, and RBBP4) is fixed throughout the cell cycle. It serves as a platform for the assembly of co-repressors and co-activators at transcription start sites of cell cycle genes (Reviewed in [115,60,94]). During quiescence, phosphorylation of the MuvB component LIN52 by the kinase DYRK1A enables p130 binding to the MuvB core to form the transcriptional repressor DREAM complex ([76]). Midway through G1, the cyclin D- cyclin-dependent kinase 4 (CDK4) complex phosphorylates p130 to initiate dissociation of the DREAM complex([125]). Sequential recruitment of transcriptional activators B-MYB and FOXM1 throughout S and G2 phase switches MuvB from a repressor to an activator complex ([116,30,16]). The MMB-FOXM1 complex promotes cell cycle progression by activating the transcrip-

tion of G2/M genes involved in DNA replication, mitosis, and checkpoint control. However, several studies suggest roles for B-MYB and FOXM1 in early cell cycle progression, which precede the discovery of the MMB-FOXM1 complex.

Pioneering studies focused on the role of B-MYB in cell cycle progression suggest that B-MYB serves a critical role in promoting G1/S progression ([139,62,82,44]). Knockdown of B-MYB in megakaryocytic or HepG2 cells results in a decline in S-phase progression, suggesting B-MYB is required for efficient entry into S-phase in certain cell lines ([139,82,44]. Whether the role of B-MYB in G1/S progression occurs in the context of the MMB-FOXM1 complex is unknown.

In addition to G2/M genes, FOXM1 has been implicated in transactivating various genes involved in DNA damage response like NBS1, Csk1, Skp2 (crucial for DNA damage recognition) and EXO1, XRCC1, Polβ/ε (involved in DNA damage repair) (Reviewed in [152]). Early mouse studies proposed that FOXM1 regulates checkpoint proteins like p21 and p27 ([66,136]), which inhibit the activity of cyclin-CDK complexes, thus overriding cell cycle arrest signals and promoting progression into S phase. Recent studies have expanded on the role of FOXM1 in checkpoint control, demonstrating that ATR-CHK1 activity during S phase controlled a CDK1-directed FOXM1 phosphorylation switch, linking G2/M gene expression with the progression of DNA replication([118]).

Moreover, knockout of FOXM1 or MuvB DNA-binding component LIN54 reduced DNA replication in S phase, and conferred resistance to CHK1 inhibition([11]), suggesting that the MMB-FOXM1 complexes may be critical downstream components of an ATR-CHK1 replication stress response.

The regulatory role of the MMB-FOXM1 complexes in other parts of the cell cycle is less well-understood. In addition, mounting work suggests MMB-FOXM1 may be

at a nexus of several stress responses that suppress cell proliferation and progression. Inhibition of MMB-FOXM1 formation is an attractive therapeutic approach for cancers driven by B-MYB or FOXM1 overexpression. Additional insights into B-MYB and FOXM1 function and regulation could significantly impact the development of inhibitors and clinical treatment approaches.

Here, we investigated the roles of B-MYB and FOXM1 in regulating cell cycle kinetics and response to replication stress.

2.3 Methods

2.3.1 Cell Culture

Human non-small cell lung carcinoma (NSCL) A549 and human, human embryonic kidney 293 cells (HEK293T), telomerase reverse transcriptase (hTERT)- immortalized RPE-1 cells were obtained from the ATCC (American Type Culture Collection). Cell lines were confirmed free from mycoplasma contamination using the e-Myco Mycoplasma PCR Detection Kit (Bulldog Bio 25233). hTERT-RPE-1 cells were transduced with pLV hUbC-dCas9-T2A-GFP listed in 2.1 for constitutive expression of the Cas9 endonuclease and sorted for GFP positivity. Cells were cultured in RPMI (Life Technologies, 11875119) or DMEM/F-12 (Life Technologies, 11320033), supplemented with 10% FBS and 1% penicillin-streptomycin (Life Technologies 15140163). B-MYB and FOXM1 knockouts were generated from polyclonal populations by 10-fold serial dilutions to a final concentration of 0.5-1 cells/100 l of media. sgRNAs against target genes are listed in Table 2.3.

!b

Table 2.1: Expression Vectors

Plasmid	Origin	Catalog Number
lentiCRISPR v2	Sanjana et al. 2014[122]	Addgene Plasmid 52961
pLV GG hUbC-dsRED	Kabadi et al. 2014[65]	Addgene Plasmid 84034
pLV hUbC-dCas9-T2A-GFP	Kabadi et al. 2014[65]	Addgene Plasmid 53191

Table 2.2: Reagents

Reagent	Supplier	Catalog Number
Thymidine	Sigma Aldrich	T1895
Abemaciclib (iCDK4-1)	Selleck Chem	S5716
Palbociclib (iCDK4-2)	Selleck Chem	S1116
Prexasertib (iCHK1)	Selleck Chem	S7178
Berzosertib (ATRi-1)	Selleck Chem	S7102
AZ20 (ATRi-2)	Selleck Chem	S7050

2.3.2 Cell Cycle Synchronizations

For single thymidine blocks, 1 x 10^6 (60 mm plate) cells were plated into 2 mM thymidine-containing RPMI media for 20 h. Cells were seeded at high density (confluent) for contact-inhibition conditions and left for six days. For CDK4 inhibition experiments, cells were treated with inhibitors listed in Table 2.2. To release from synchronization, cells were washed twice with pre-warmed 37°C PBS, trypsinized, re-seeded using pre-warmed 37°C RPMI media, and collected at the times denoted.

2.3.3 Lentivirus Infection

Lentivirus was produced by transfecting 293T cells with either the plentiCRISPRv2 vector with a single guide or the pLV GG hUbC-dsRED multiplex guide vector encoding four guides against the target of interest (sgRNA target sequences listed in Table 2.3 and plasmids listed in Table 2.1) and lentiviral second-generation packaging

Table 2.3: Oligonucleotides: sgRNA sequences

sgRNA ID	Target sequence	Origin
sgNTC-1	CTGAAGGTGTCTGGCAGAGC	Doench and Fusi et al. 2016[28]
sgNTC-2	TGGTTCCGTAGGTCGGTATA	Doench and Fusi et al. 2016[28]
sgNTC-3	GAACTCAACCAGAGGGCCAA	Doench and Fusi et al. 2016[28]
sgNTC-4	GCCCCGCCGCCCTCCCCTCC	Doench and Fusi et al. 2016[28]
sgMYBL2-1	CAAGGTGCTGGGCAACCGCT	Benchling CRISPR Guide RNA Design Tool
sgMYBL2-2	GGTGGTTGTGCCAGCGTTCA	Benchling CRISPR Guide RNA Design Tool
sgMYBL2-3	GGGCCGGGGGGATGTCTCGG	Benchling CRISPR Guide RNA Design Tool
sgMYBL2-4	GGGCCCCGGGCCGCGCTCGA	Benchling CRISPR Guide RNA Design Tool
sgFOXM1-1	CATGCCCAACACGCAAGTAG	Benchling CRISPR Guide RNA Design Tool
sgFOXM1-2	TGAGAATCAGTGGCCGACGG	Benchling CRISPR Guide RNA Design Tool
sgFOXM1-3	GTGAATCTTCCTAGACCACC	Benchling CRISPR Guide RNA Design Tool
sgFOXM1-4	ATGGCCACTACTTGCGTGTT	Benchling CRISPR Guide RNA Design Tool

vectors (psPAX2 and VSV-G) using polyethyleneimine (PEI) in serum-free media. Lentivirus-containing media was collected 48 h after transfection and filtered through a 0.45 μm filter before use. Lentivirus was directly applied dropwise to cells and spin-fected as described in the Broad Optimization of lentiviral transduction using spinfection protocol (https://portals.broadinstitute.org/gpp/public/dir/download?dirpath=protocols/production&filename=Optimization_of_Lentiviral_Spinfection_Oct2018.pdf).

2.3.4 Doubling Assay

Cells were seeded at 5 x 10^4 cells in 60 mm dishes and counted every three days for nine days. On days 3,6, and 9, cells were washed with warm PBS, trypsinized, and resuspended in 10 mL warm media. 10uL of cell suspension was used for counting, and the remaining fraction was used to re-plate cells at 5 x 10^4 per new 60mm dish. Cell counts were determined using the LUNA-FX7 high throughput automated cell counter (Logos Biosystems). The population doubling rate (n) was calculated using

the following formula: n = (log N − log N_0) / log 2), where N is the total number of viable cells counted across the nine days, and N_0 is the total viable cells at day 0. The doubling rate (d) was calculated using the formula: d = (t/n), where t is time (9 days = 216 h) and n is the doubling rate.

2.3.5 Viability Assays

1 x 10^3 cells in 100 μl media were seeded per 96-well one day before drug treatment. The next day, 100 μl of media with 2X drug concentration was added to achieve the final concentrations shown. 72 h post-treatment, cells were incubated at room temperature for 30 mins before quantification of viability using CellTiter-Glo (Promega) on an M200 Infinite plate reader (Tecan).

2.3.6 Cell Cycle Distribution Assay

Cell cycle distribution was determined as previously described[11]. Briefly, cells were treated with 10 μM EdU (Click Chemistry Tools, 1149-100) for 1 h before collection. Cells were fixed in 4% formaldehyde in PBS for 15 mins at room temperature before being permeabilized in 70% ethanol at -20°C overnight. Incorporated EdU was labeled using a CLICK reaction (2 mM $CuSO_4$, 100 μM THPTA, 100 mM sodium ascorbate, and 2 μM Alexa 647 Azide in PBS) by rotating for 30 mins at room temperature protected from light. Samples were then washed thrice with 1% BSA in PBS and incubated with the primary antibody against pS10 histone H3-PE conjugate (listed in 2.4) in 1% BSA in PBS overnight at 4°C. After three washes with 1% BSA in PBS, DNA was stained with a 1 μg/mL DAPI, 100 ng/mL RNase A staining solution for 1 h at room temperature protected from light before analysis by flow cytometry (BD LSRFortessa) at the Dana-Farber Flow Cytometry Hematologic Neoplasia and Jimmy

Fund Core.

2.3.7 IMMUNOBLOTTING

Cell pellets were lysed in EBC buffer (120 mM NaCl, 5 mM EDTA, 50 mM Tris-Cl (pH 8.0), 0.5% (v/v) Nonidet P-40, and right before using: 1 cOmplete^{TM} mini protease inhibitor tablet [Sigma Aldrich, 11836153001] and 1 PhosSTOP^{TM} tablet), and protein content was quantified by Bradford assay. For immunoblot, lysates were separated in a 4-20% SDS-PAGE gel, transferred to a nitrocellulose membrane, blocked in 5% milk, and incubated with primary antibody at 4°C overnight. A list of the primary antibodies used can be found in Table 2.4. Blots were imaged with either SuperSignal West Pico (ThermoFisher PI34080) or Immobilon Western Chemiluminescent HRP Substrate (Millipore WBKLS0500).

Table 2.4: Antibodies Used for Immunoblot or Flow Cytometry

Target	Catalog Number
MYBL2	Millipore MABE866
FOXM1	CST 20459S
LIN37	Bethyl A300-BL2983
TBP	ProteinTech 66166-1-Ig
Phospho-Rb (Ser807/811)	CST 9308S
Rb	CST 9309S
MCM2	CST 3619S
PCNA	CST 2586S
RRM1	CST 8637S
RRM2	CST 65939S
PLK1	CST 4513S
CDC20	CST 14866S
Cyclin B1	CST 4138S
Phospho-YAP (Ser127)	CST 13008S
YAP/TAZ	CST 8418S
MOB1	CST 13730S
LATS1	CST 9153S

Table 2.5: RT-qPCR primers for Cell Cycle Genes

Name	Sequence	Primer Bank ID
RRM1 Forward	GCCGCCAAGAACGAGTCAT	157266329c1
RRM1 Reverse	AGCAGCCAAAGTATCTAGTTCCA	
RRM2 Forward	CACGGAGCCGAAAACTAAAGC	260064011c1
RRM2 Reverse	TCTGCCTTCTTATACATCTGCCA	
PCNA Forward	ACACTAAGGGCCGAAGATAACG	33239449c3
PCNA Reverse	ACAGCATCTCCAATATGGCTGA	
PLK1 Forward	CCTGCACCGAAACCGAGTTAT	34147632c3
PLK1 Reverse	CCGTCATATTCGACTTTGGTTGC	
CCNB1 Forward	AACTTTCGCCTGAGCCTATTTT	356582356c3
CCNB1 Reverse	TTGGTCTGACTGCTTGCTCTT	
CDC20 Forward	GCTTTGAACCTGAACGGTTTTG	118402581c3
CDC20 Reverse	TCTGGCGCATTTTGTGGTTTT	
TBP Forward	CCACTCACAGACTCTCACAAC	285026518c1
TBP Reverse	TCTGGCGCATTTTGTGGTTTT	

2.3.8 RT-qPCR of Cell Cycle Genes

Total RNA was purified from A549 cells using the RNeasy Plus Mini kit (Qiagen 74034). Reverse transcription was performed using the High-Capacity cDNA Reverse Transcription kit (ThermoFisher 4368814) with random primers according to the manufacturer's instructions. qPCR was performed on the cDNA using the primers listed in 2.5 and Brilliant III Ultra-Fast qPCR Master Mix (Agilent) using a MxAria (Agilent). Relative RNA expression was calculated using the Cq method and TBP as a reference gene. All PCR primers were obtained from the MGH PrimerBank, a public resource for optimized PCR primers (https://pga.mgh.harvard.edu/primerbank/).

2.4 Results

2.4.1 Impairment of the MMB-FOXM1 complex confers resistance to CHK1 and ATR inhibition.

CRISPR screens to identify genes required for CHK1 inhibitor (CHK1i) sensitivity were performed in A549 and NCI-H460 cells using the Brunello human genome-wide lentiviral gRNA pooled library[28]. A549 and NCI-H460 cells were grown for approximately three weeks in the continuous presence of 100 nM or 50 nM prexasertib, respectively. The genes *MYBL2*, *FOXM1*, and *LIN54* were all among the top hits in both screens, implying the MMB-FOXM1 complex may contribute to CHK1i sensitivity.

To determine if the knockout of B-MYB and FOXM1 resulted in CHK1i resistance, a panel of clonal A549 cell lines with two independent sgRNAs chosen from the Brunello library targeting FOXM1 and LIN54 was generated (Figure 2.1A). Compared to the sgNTC, there were no significant differences in the growth rate of any of the individual sgLIN54 or sgFOXM1 clones over 10 days (Figure 2.1B). Knockout of LIN54 or FOXM1 increased resistance to CHK1 inhibitor prexasertib (CHK1i) and ATR inhibitors berzasertib (ATRi-1) and AZ20 (ATRi-2)(Figure 2.1C-E).

2.4.2 Knockout of B-MYB or FOXM1 leads to accumulation of cells in G2 phase.

To determine the specific contributions of B-MYB and FOXM1 in conferring resistance to CHKi. We generated a panel of clonal B-MYB and FOXM1 knockouts in A549s using CRISPR-Cas9-mediated gene editing. A549s were transduced with pLenti-CRISPR V2-puromycin with a single guide against a non-targeting control (sgNTC), MYBL2 (sgMYBL2), or FOXM1 (sgFOXM1) designed using the Benchling CRISPR Guide RNA Design Tool (https://www.benchling.com/crispr).

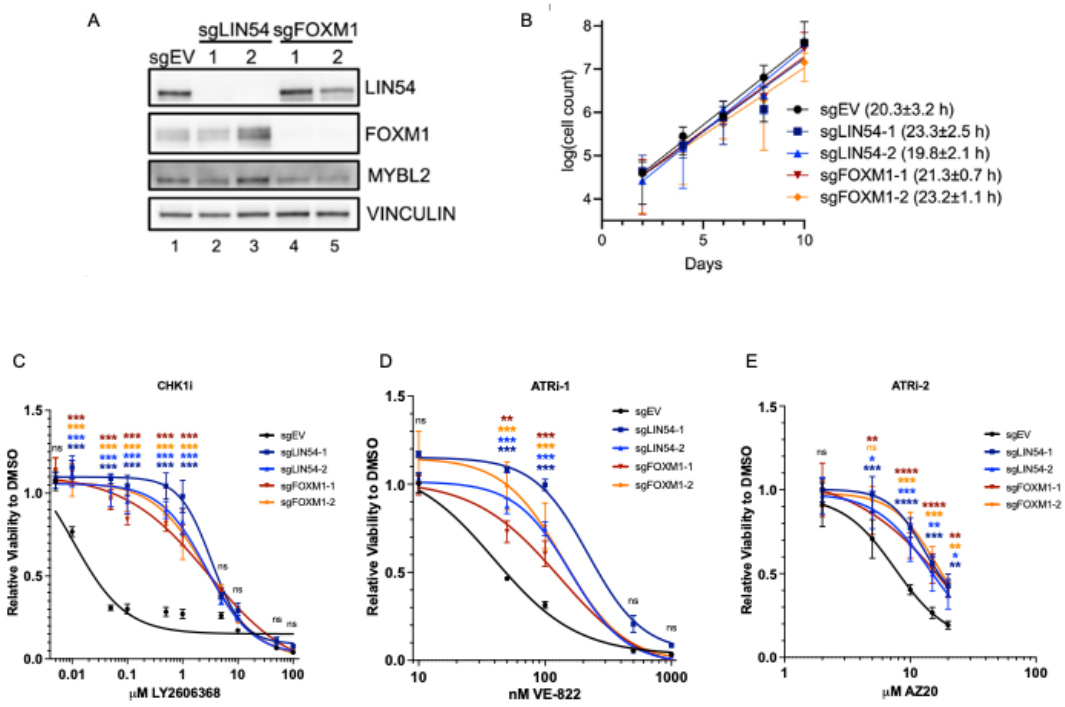

Figure 2.1: LIN54 and FOXM1 components are required for CHK1i sensitivity in A549 cells. A. Immunoblot of MMB-FOXM1 components in A549 LIN54 KO and FOXM1 KO cell lines. **B.** 10-day growth curve and doubling time of A549 EV, LIN54 KO, and FOXM1 KO cells. n=3. Mean ś SEM. **C-E** Viability curves of A549 EV, LIN54 KO, and FOXM1 KO cells in the presence of increasing concentrations of CHK1i or ATR inhibitors (ATRi) for 72 h. CHK1i (C), ATRi-1 (berzosertib) (D), and ATR-2 (AZ20) (E). Viability was assessed using Cell-Titer Glo and normalized to DMSO for each cell line. N=3.

Knockout of B-MYB and FOXM1 was confirmed by immunoblot of lysates of cells growing in sub-confluent asynchronous conditions (Figure 2.2A).

Neither B-MYB nor FOXM1 was essential for A549 cell viability as there was no significant difference in the growth rate of either sgMYBL2 or sgFOXM1 compared to sgNTC (Figure 2.2BC). Flow cytometry analysis of the distribution of cells per each cell cycle phase revealed, however, that knockout of MYBL2 and FOXM1 resulted in the increased fraction of cells in G2 phase compared to sgNTC (Figure 2.2D). The effect was specific to G2, as no significant changes in the mitotic marker histone H3 pS10 were observed in mitosis sgMYBL2 or sgFOXM1 cells compared to sgNTC. However, distinct differences in S phase were observed for sgMYBL2 and sgFOXM1. The knockout of FOXM1 significantly increased the number of cells in S phase. In contrast, the knockout of B-MYB significantly reduced the percentage of cells in S phase compared to sgNTC.

We asked whether these findings were reproducible by generating knockout cell lines in normal human retinal epithelial cells hTERT RPE-1 stably expressing Cas9 and a GFP reporter (Figure 2.3A). Cells were infected with a multiguide vector with an RFP reporter gene and four sgRNAs that were expressed independently from RNA polymerase III promoters targeting either *MYBL2* or *FOXM1*. Dual positive GFP&RFP cells were sorted one week after infection to generate a polyclonal knockout population. Lysates were immunoblotted to access the degree of knockout (Figure 2.3B). Despite several efforts, we were unable to knockout FOXM1 in RPE-1 cells. Multiguide MYBL2 (mxgMYBL2) knockout cells were viable, and knockout did not affect growth compared to the non-targeting control (mxgNTC) (Figure 2.3C). Like A549 cells, mxgMYBL2 cells had fewer cells in the G1 phase and accumulated cells in G2/M (Figure 2.3D). These data demonstrate that B-MYB was dispensable for A549

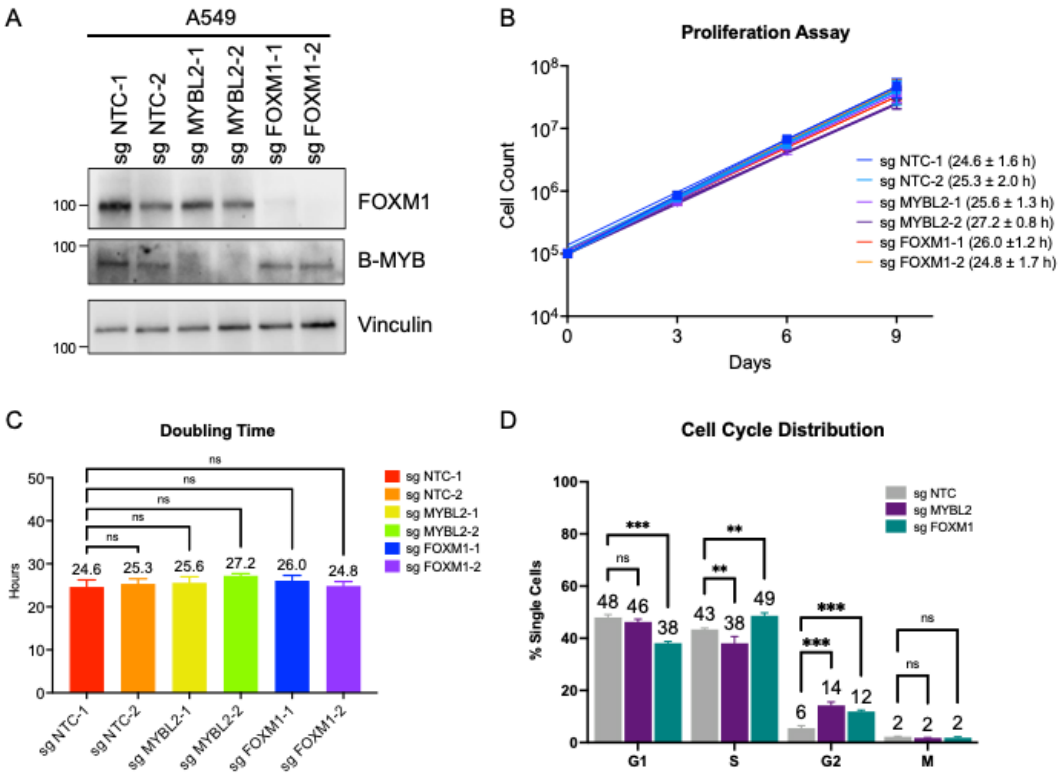

Figure 2.2: A549 cells with knockout of B-MYB or FOXM1 accumulate in G2/M phase but maintain wild-type doubling time. A. Representative western blots of whole-cell lysates from A549 transduced with short guides against non-targeting Control (NTC), MYBL2, and FOXM1 KO cells treated with thymidine for 24 h. **B.** Proliferation assay of a panel of clonal knockout cell lines over nine days. **C.** Calculated doubling time for a panel of clonal knockout cell lines. Statistics were calculated by two-way ANOVA comparing to sgNTC. 0.1(ns), 0.03(*), 0.002(**), <0.0001(***). The error bar represents SEM. N=3. **C.** Cell cycle profile of A549 control and KO cells. Two-way ANOVA calculated statistics. 0.1(ns), 0.03(*), 0.002(**), <0.0001(***). Error bars represent SEM. N=3

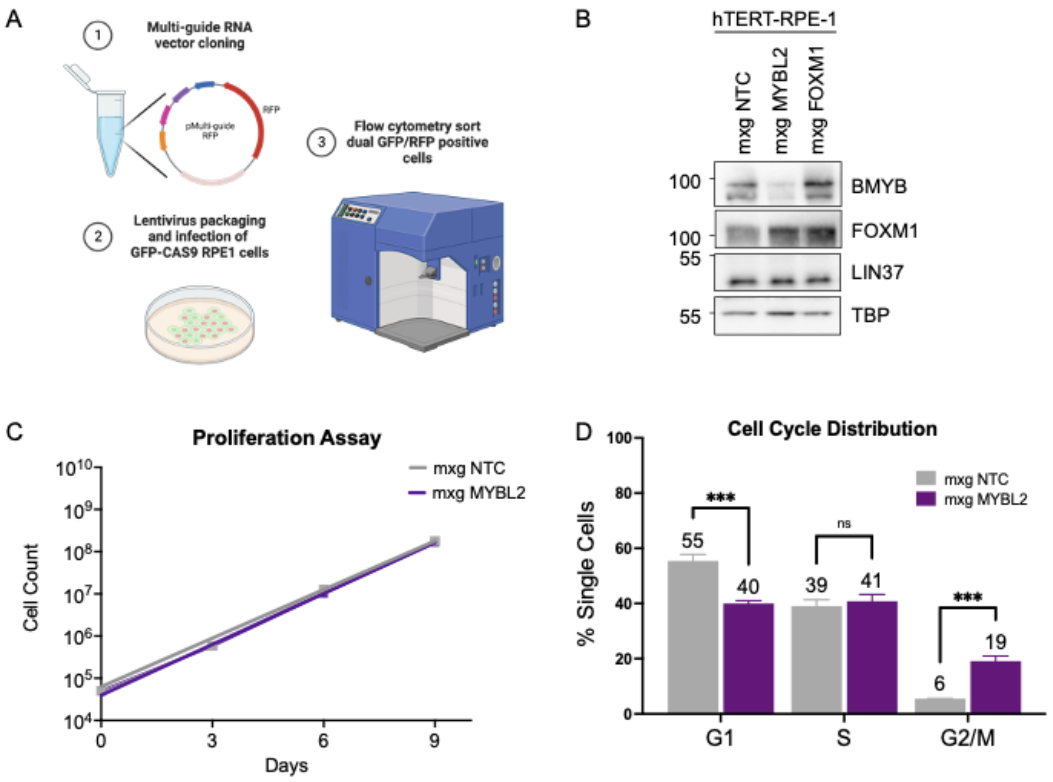

Figure 2.3: Knockout of B-MYB in non-cancerous hTERT-RPE1 accumulates cells in G2/M phase. A. Schematic of generation of multiguide polyclonal cell lines. 1) an RFP reporter gene and four sgRNAs expressed independently from RNA polymerase III promoters were incorporated into a lentiviral vector using the Golden Gate cloning method. 2) Lentivirus was generated to infect GFP-positive CAS9 expression hTERT-RPE1 cells. 3) Dual GFP&RFP positive cells were sorted to generate a polyclonal population. **B.**Representative western blots of whole-cell lysates from hTERT-RPE1 transduced with four short guides (multiguide = mxg) against non-targeting control (mxgNTC) or MYBL2 KO (mxgMYBL2), growing in sub-confluent asynchronous conditions **C.** Proliferation assay of polyclonal knockout cell lines over nine days. **D.** Cell cycle profile of hTERT-RPE-1 mxgNTC and mxgMYBL2 KO cells. Statistics were calculated using two-way ANOVA compared to mxgNTC. 0.1(ns), 0.03(*), 0.002(**), <0.0001(***). Error bars represent SEM. N=3.

and RPE-1 cell viability.

We sought to validate if B-MYB confers resistance to CHK1 and ATR inhibitors in our newly generated A549 knockout cell lines. The clonal A549 knockout cell line panel was treated with CHK1 inhibitors prexasertib. Cells with sgMYBL2 or sg-FOXM1 KO showed increased resistance to CHK1 inhibition (Figure 2.4A-B).

2.4.3 KNOCKOUT OF B-MYB ARRESTS CELLS IN G2/M FOLLOWING CONTACT-INHIBITION.

A hallmark of cancer is dysregulated cell cycle and progression, which can lead to uncontrolled cell division, allowing cancerous cells to proliferate and form tumors. Knockout of B-MYB or FOXM1 in two separate cell types resulted in dysregulation of the cell cycle. To expand our understanding of B-MYB and FOXM1 involvement in cancer development, we investigated how the knockout of B-MYB or FOXM1 affected cell cycle progression. We chose to synchronize cells in G0/G1 by contact inhibition to facilitate the observation and comparison of the different cell cycle phases across our knockout cell populations. Cells were seeded at high density (confluent) in a compact monolayer and left for six days to trigger contact-mediated inhibition and synchronization to G1 phase. To determine if contact inhibition led to a reduction of cells in S phase and an increase in G1 cells, cells were pulsed on day 6 for 1 h with EdU, harvested, and analyzed by flow cytometry. 94% of the sgNTC cells were enriched in G1, while 6% remained in S and G2/M phases (Figure 2.4B), demonstrating that growth of the A549 cells was arrested as indicated by enrichment of cells in G0/G1. Similarly, sgFOXM1 growth was attenuated by contact inhibition, with 88% of cells in G1 and 12% in S and G2/M phases.

In contrast, only 69% of sgMYBL2 were in G1, while almost a third (31%) remained in S/G2/M, significantly more than both sgNTC and sgFOXM1. Similarly, an

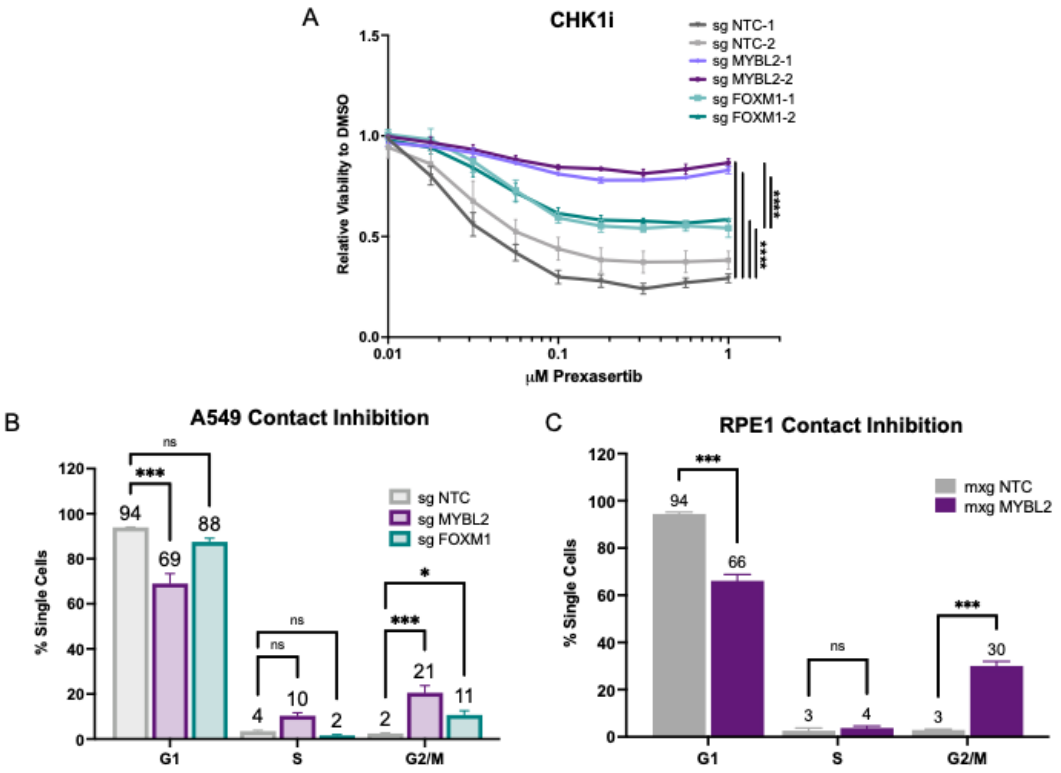

Figure 2.4: Knockout of B-MYB or FOXM1 conferred resistance to CHK1 inhibition, while oss of B-MYB impairs contact inhibition. A Viability curves of A59 sgNTC, sgMYBL2, and sgFOXM1 KO cells in the presence of increasing concentrations of prexasertib (iCHK1). Viability was assessed using Cell-Titer Glo and normalized to DMSO-treated control for each cell line. Prexasertib treatments n=3. Statistics were calculated by two-way ANOVA comparing to sgNTC. 0.1(ns), 0.03(*), 0.002(**), <0.0001(***). **B.** Cell cycle distribution of A549 sgNTC, sgMYBL2, and sgFOXM1 following 6-day contact inhibition. Statistics were calculated by two-way ANOVA comparing to sgNTC. 0.1(ns), 0.03(*), 0.002(**), <0.0001(***). Error bars represent SEM. N=3. **C.** Cell cycle distribution of hTERT-RPE1 mxgNTC and mxgMYBL2 cell line following 6-day contact inhibition. Statistics were calculated by two-way ANOVA comparing to sgNTC. 0.1(ns), 0.03(*), 0.002(**), <0.0001(***). Error bars represent SEM. N=3.

increased fraction of cells in G2/M was observed in the mxgMYBL2 RPE-1 KO (Figure 2.4C), suggesting that knockout of B-MYB mitigates contact inhibition in cells and leads to the retention of S and G2/M cells. These results demonstrated that contact inhibition is ineffective at synchronizing sgMYBL2 knockouts despite effectively synchronizing FOXM1 knockout cells.

To determine if the sgMYBL2 knockouts were actively cycling under contact inhibition, protein and RNA lysates were harvested from subconfluent and confluent cultures of the panel of clonal A549 KO cells (Figure 2.5). Contact inhibition conditions promote de-phosphorylation of RB at serine 807/811 [121]. sgNTC and sgFOXM1 had decreased phosphorylated S807/S811 RB levels, suggesting RB may be in a relatively low phosphorylated state under contact inhibition (Figure 2.5A). Notably, sgMYBL2 demonstrated decreased but slightly higher levels of phosphorylated S807/S811 RB compared to sgNTC and sgFOXM1, suggesting a small portion of RB may remain phosphorylated under contact inhibition.

To determine if cell cycle genes were expressed under contact inhibition, we assessed the expression of a panel of genes by immunoblot and RT-qPCR (Figure 2.5). In all cell lines, decreased protein and mRNA levels of G1/S genes RRM1 and RRM2 correlated with hypo-phosphorylation of RB, although protein levels of DNA replication machinery like MCM2 and PCNA persisted. The decreased G1/S mRNA and protein levels and decreased phosphorylation at residues S807/S811 of RB indicate that RB was dominantly repressing cell cycle gene expression under contact inhibition (Figure 2.5A&B). Protein levels of PLK1, CDC20, and Cyclin B1, encoded by G2/M genes, were similarly decreased in sgNTC and sgFOXM1 cells after contact inhibition, but low levels persisted in the sgMYBL2 cells (Figure 2.5A). This effect was specific at the protein level as PLK1, CDC20, and Cyclin B1 mRNA levels were all

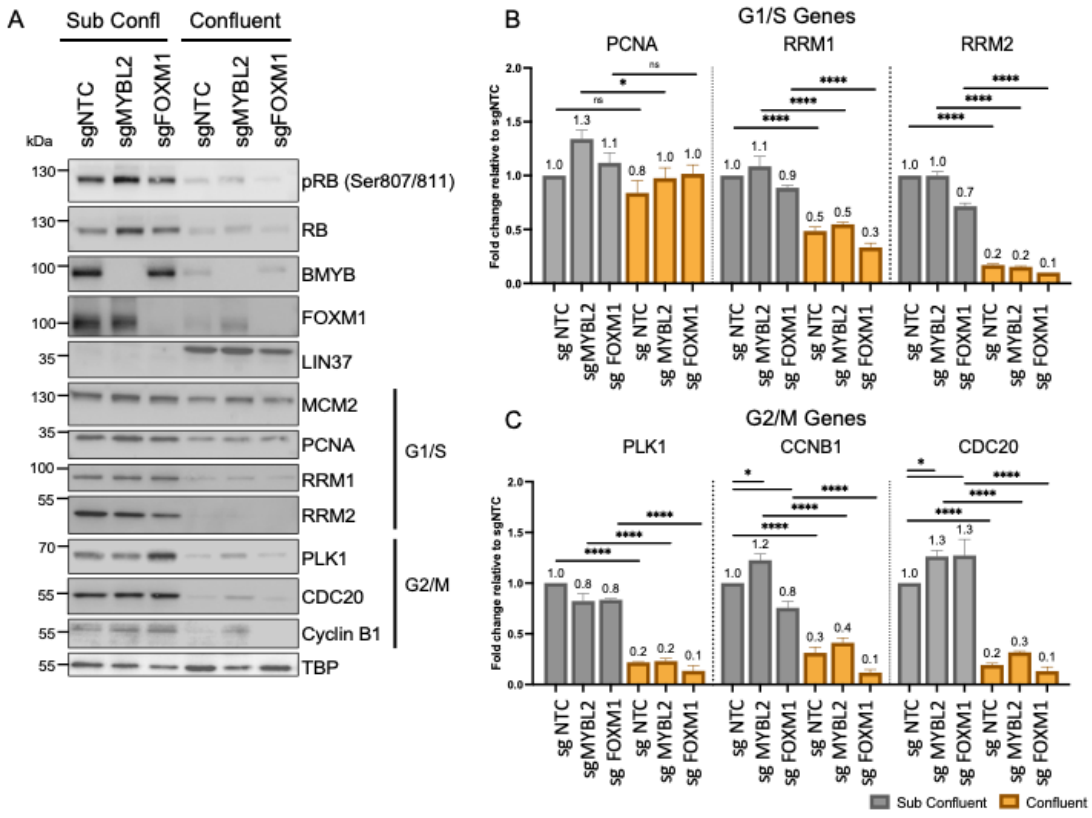

Figure 2.5: B-MYB knockouts express low levels of G2/M proteins under contact inhibition. A. immunoblot of cell cycle protein expression of contact-inhibited cells. **B-C.** RT-qPCR analysis of mRNA of cell cycle genes under contact inhibition conditions. Statistics were calculated by two-way ANOVA comparing to sgNTC. 0.1(ns), 0.03(*), 0.002(**), <0.0001(***) Error bars represent SEM. N=3.

reduced across all cell lines following contact inhibition (Figure 2.5A&C), suggesting continued levels of G2/M proteins or the failure to degrade G2/M proteins might be facilitating cells to cycle under contact inhibition.

The transcription factor YAP physically interacts and cooperates with the MMB complex to activate a subset of G2/M genes[105,51,39]. Under contact inhibition, the Hippo pathway promotes phosphorylation of YAP at serine 127, leading to YAP translocation to the cytoplasm and prevention of YAP transactivation of genes[51]. Given the critical role of YAP in the response to contact inhibition and the physical association of YAP with MMB, we examined whether the phosphorylation of YAP was impaired in B-MYB knockouts. Immunoblot of phospho-YAP and Hippo pathway kinases revealed no difference in the level of expression between knockouts and Control cells (Figure1.6A), suggesting the Hippo signaling pathway was activated, and YAP was potentially translocating to the cytoplasm under high cell density in the sgMYBL2 knockout.

2.4.4 Knockout of B-MYB or FOXM1 differentially alters G2/M phase kinetics.

As an alternative synchronization strategy, we considered CDK inhibitors as tools to help synchronize cells to G1. During quiescence, an unphosphorylated form of RB binds to activating E2F transcription factors, thus repressing the expression of cell cycle-dependent genes that contain E2F binding sites in their promoter[21,48,138]. Passage through the restriction point depends on RB phosphorylation. Once cells have been rendered competent for cell cycle entry, cyclin D-CDK4 activity promotes mono-phosphorylation of RB[121]. Mono-phosphorylation of RB primes RB for cyclin E-CDK2 dependent hyperphosphorylation, which induces RB release from E2Fs and

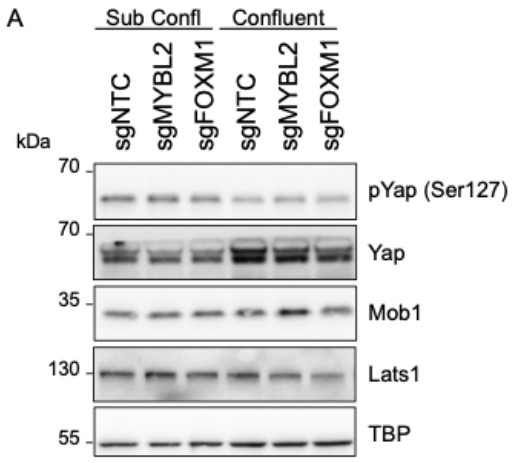

Figure 2.6: The HIPPO signaling pathway is activated under contact inhibition. A. Immunoblot of Hippo-pathway protein expression for contact-inhibited cells.

enables expression of the E2F-dependent genes and entry into S[98].

Abemaciclib and palbociclib are CDK4 inhibitors that reduce the phosphorylation of RB by Cyclin D-CDK complex (reviewed in[36]), thus constraining cells in G1. A549 cells have wildtype RB; therefore, we reasoned that a G1 arrest could be chemically induced by inhibiting CDK4 activity. sgNTC cells were treated with increasing doses of either abemaciclib or palbociclib for 24 h. Treatment with palbociclib resulted in a dose-dependent G1 arrest (Figure 2.7A). In contrast, abemaciclib treatment induced a dose-dependent G1&G2 arrest with 2 μM abemaciclib enriching 20% of cells in G2/M, indicating potential off-target effects (Figure 2.7A). Indeed, recent studies demonstrate that abemaciclib inhibits CDK1-cyclin B and CDK2-cyclin A/E complexes[54], thus resulting in effects in G2/M progression.

Next, we wanted to determine if palbociclib-induced cell cycle arrest was reversible. sgNTC cells were treated with either 1 μM or 2 μM palbociclib for 24 h and then released for 6 h, and the fraction of cells in S phase was measured. While palbociclib at 1 μM and 2 μM effectively synchronized cells in G1 at 24h, release of the 2 μM palbociclib treatment restricted cell cycle re-entry, with S phase levels reaching only 4% after 6 h (Figure 2.7B). In contrast, 24% of cells re-entered S phase following 1 μM palbociclib treatment.

Indeed, treatment of sgMYBL2 and sgFOXM1 cells with 1 μM palbociclib for 24 h (palbo-treat) resulted in more than 88% sgMYBL2 cells in G1 phase and 80% sgFOXM1 cells enriched in G1 phase (Figure 2.7C). Low levels of S/G2/M phase cells remained in the KO cells but were not statistically significant compared to the sgNTC. These results demonstrated that 1 μM palbociclib could effectively synchronize sgMYBL2 and FOXM1 knockout cells.

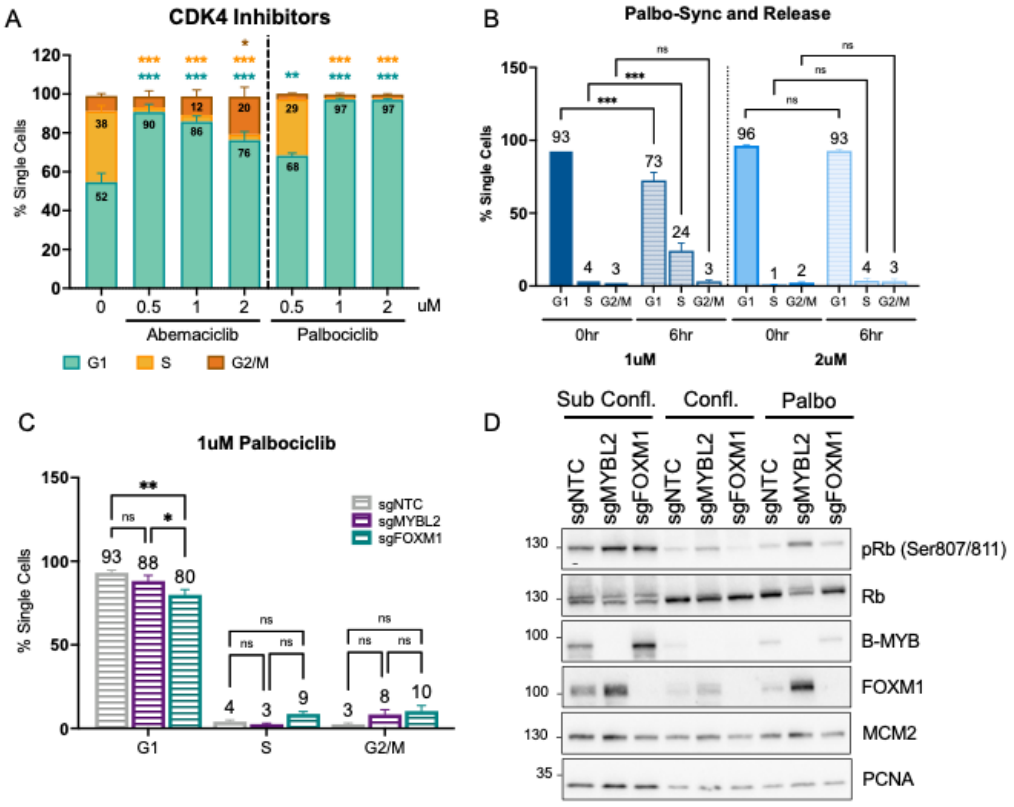

Figure 2.7: Inhibition of CDK4 synchronizes B-MYB and FOXM1 knockouts to G1 phase. A. Cell cycle distribution of sgNTC cells treated for 24 h with increasing doses of CDK4 inhibitors. Statistics were calculated by two-way ANOVA comparing to sgNTC. 0.1(ns), 0.03(*), 0.002(**), <0.0001(***) Error bars represent SEM. N=3. **B.** Cell cycle distribution of sgNTC cells treated and released for 6h following 24 h treatment with palbociclib. Statistics were calculated by two-way ANOVA comparing to 0hr post-release. 0.1(ns), 0.03(*), 0.002(**), <0.0001(***) Error bars represent SEM. N=3. **C.** The cycle profile of A549 sgNTC and KO cells were treated with 1 μM palbociclib for 24 h. Statistics were calculated using two-way ANOVA compared to DMSO-treated sgNTC. 0.1(ns), 0.03(*), 0.002(**), <0.0001(***). Error bars represent SEM. N=3.(**E.**) Cell cycle distribution of sgNTC and KO cells line following 6-day contact inhibition. **D.** Immunoblot of DNA replication machinery expression under contact-inhibition and palbociclib treatment.

It has been reported that prolonged G1 arrest (> 3 days) following CDK4 inhibition decreased replisome components and caused replication stress by impairing origin licensing[23,133]. To access effects at 24 h, protein lysates from subconfluent, confluent, and palbo-treated cells were collected and probed for cell cycle markers by immunoblot. Immunoblotting confirmed that replisome components MCM2 and PCNA levels remained comparable to asynchronous cells following palbociclib arrest, demonstrating no signs of replication stress following 24 h treatment with 1 μM palbociclib (Figure 2.7D).

B-MYB and FOXM1 have been implicated as critical regulators of G1/S and G2/M transitions. One possible explanation for a similar doubling rate between knockouts and sgNTC cells is that knockout of B-MYB and FOXM1 activity alters the rate of progression through certain phases of the cell cycle to offset delays in G2. We investigated how the knockout of B-MYB and FOXM1 affects cell cycle progression kinetics. Cell lines were treated for 24-hrs with 1 μM palbociclib, followed by palbociclib washout and splitting into new plates. Cells were harvested at indicated times (Figure 2.8). At 6 h post-release (hpr), cells began to re-enter the cell cycle with low levels in S phase (Figure 2.8A). At 12 hpr, cells were actively in S phase; at 15 hpr, cells were entering G2/M; by 18 hpr, cells were re-entering the next cell cycle.

To calculate the fold change for each cell cycle phase, we normalized the percentage of cells for each phase to the percentage of cells in asynchronous conditions. In addition, each phase's rate of change per hour was calculated for the first 15 h of the time course to avoid biases from cell cycle re-entry at 18 hpr (Figure 2.9). Knockout of either B-MYB or FOXM1 reduced G2 phase progression compared to sgNTC as KO cells did not peak at 15 hpr (Figure 2.9A), and the percent rate of cells entering G2 per hour was significantly lower for both knockouts compared to sgNTC (Figure

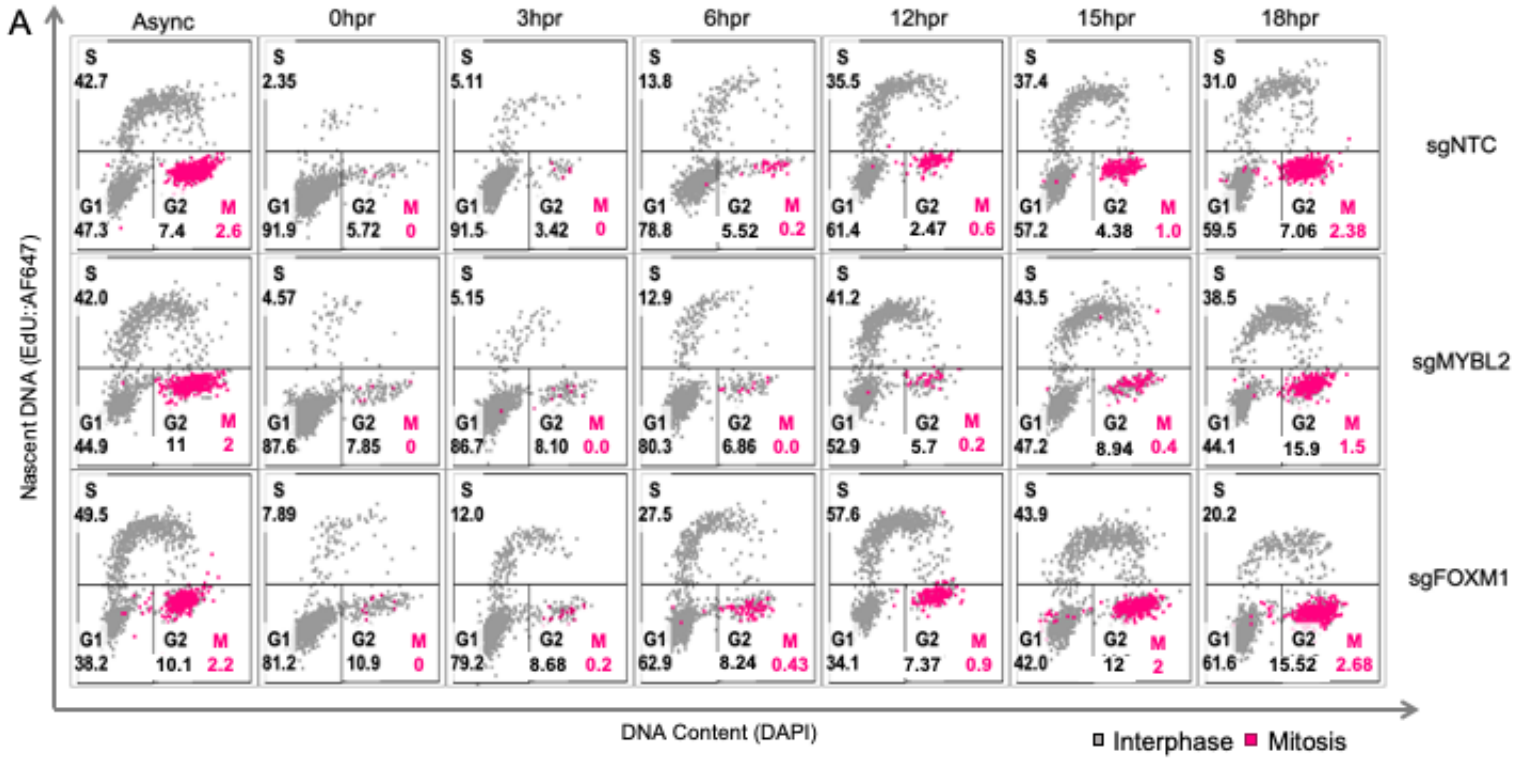

Figure 2.8: Knockout of B-MYB or FOXM1 differentially alters cell cycle kinetics. A. Representative 18-h time course of palbociclib synchronized and released cells. Cells were treated with DMSO or 1 μM palbociclib for 24 h. Cells were harvested or released in warm 37°C media the next day and collected at specified times. Asynchronous cells were used to gate G1, S, and G2 cells. Annotated is the % single cells measured for each phase. Phosphorylated-S10 Histone 3 was used as the mitotic marker and subtracted from the G2/M gate to calculate % Mitotic (M) cells.

2.9B).

Notably, the knockout of FOXM1 quickened early cell cycle kinetics. At 15 hpr, sgFOXM1 had twice the number of cells in mitosis compared to sgNTC cells(Figure 2.9A). In contrast, knockout of B-MYB delayed entry into the G2 phase and M phase, in particular, the percent rate of cells entering mitosis (Figure 2.9B) was significantly lower than FOXM1 knockouts and the sgNTC.

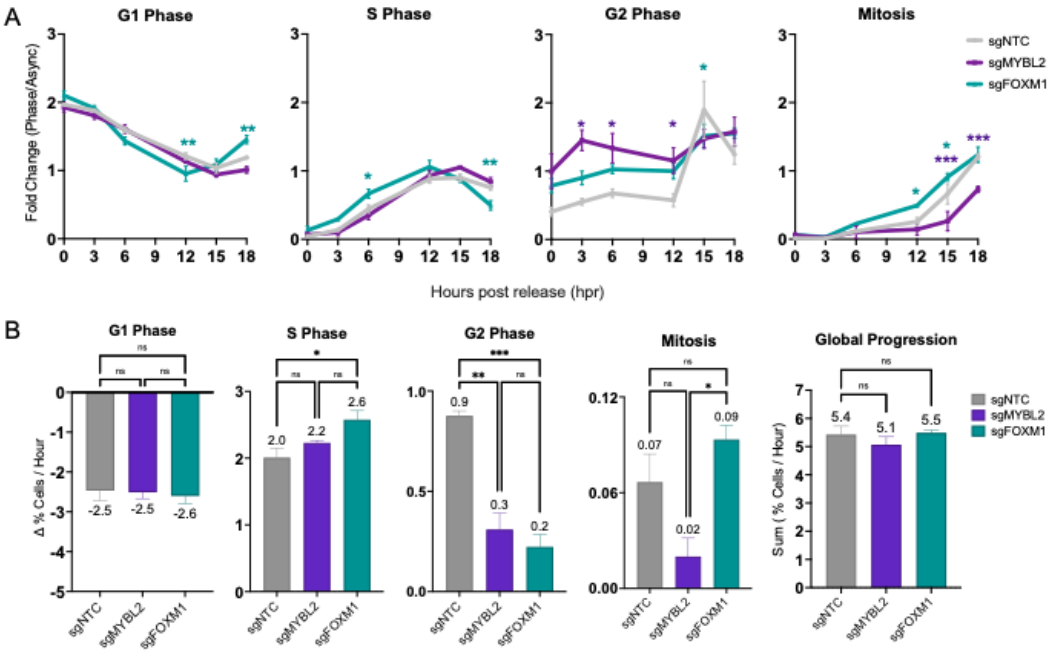

Figure 2.9: Knockout of B-MYB or FOXM1 differentially alters cell cycle kinetics. A. Summary of Cell cycle progression rates through G1 phase, S phase, G2 phase, and M phase were calculated by normalizing the percent of cells in each gate by the Asynchronous sgNTC cell line (n= 3). Statistics were calculated by two-way ANOVA comparing to sgNTC. 0.1(ns), 0.03(*), 0.002(**), <0.0001(***) Error bars represent SEM. N=3. **B.** Summary of the rate of change per hour for each cell cycle phase and the Global progression rate per cell line. Statistics were calculated by two-way ANOVA comparing to sgNTC. 0.1(ns), 0.03(*), 0.002(**), <0.0001(***). Error bars represent SEM. N=3.

2.4.5 Summary of Findings

In this chapter, we investigated the separate functions of MMB-FOXM1 components in the cellular response to replication stress and cell cycle progression. Our study generated LIN54 and FOXM1 knockouts in human A549 cells, B-MYB knockout cells in A549, and hTERT-RPE-1 cells. Knockout of LIN54, B-MYB, or FOXM1 in A549s led to increased resistance against inhibition of either ATR or CHK1. The knockout of B-MYB or FOXM1 resulted in cell enrichment in G2 phase. B-MYB depletion reduced while FOXM1 knockout augmented S phase distributions. Through synchronization assays involving B-MYB and FOXM1 knockout cells, it was evident that B-MYB knockout uniquely affected contact inhibition.

Conversely, both B-MYB and FOXM1 knockout cells displayed sensitivity to CDK4 inhibition. Cell cycle kinetic analyses revealed that FOXM1 depletion hastened S phase progression. In contrast, B-MYB knockout notably delayed entry into mitosis, highlighting that B-MYB and FOXM1 have distinct but crucial roles in regulating proper cell cycle advancement. These findings provide valuable insights into the mechanisms underlying the role of B-MYB in cell-cycle dysregulation, which is a hallmark of tumor cells. Furthermore, these data suggest that B-MYB and FOXM1 have overlapping but different effects on cell cycle progression.

AUTHOR CONTRIBUTIONS FOR CHAPTER 3

The experiments in this chapter were performed by Hembly G. Rivas with input from James A. DeCaprio. This research was supported by the U.S. Public Health Service grants R35 CA232128-03S1 to H.G.R. and R35CA232128 to J.A.D.

An unfertilized egg is a quiescent cell, but then the sperm hits, the doorbell rings, and this whole dinner party rapidly unfolds.

Joan Ruderman, Ph.D.

3

B-MYB and FOXM1 functional activity is interdependent.

3.1 ABSTRACT

During late S phase, B-MYB binds to MuvB to form the MMB complex. The MMB complex recruits FOXM1, and B-MYB and FOXM1 contribute to activating G2/M genes. In this chapter, we investigated the functional interdependence between B-MYB and FOXM1. We show that B-MYB enhanced FOXM1 binding to DNA and

that both B-MYB and FOXM1 binding to DNA are critical for the onset of G2/M gene expression. We found that FOXM1 was required for timely dissociation of B-MYB from DNA and regulation of B-MYB protein levels in mitosis. In addition, FOXM1 knockout resulted in aberrant expression of RRM2 protein, another well-established G1/S gene, suggesting that FOXM1 activity may be crucial for the timely clearance of DNA machinery in mitosis. Both B-MYB and FOXM1 knockout reduced the expression of a wide range of G2/M genes, suggesting that the combined activity of the two transcription factors is required for maximal G2/M gene expression. However, there are differences, as the knockout of FOXM1 impaired G2/M gene expression significantly more than that of B-MYB knockout. These findings demonstrate that B-MYB and FOXM1 synergize and rely on mutually interdependent interactions to activate G2/M genes.

3.2 Introduction

Coordinated transcription of G2/M gene expression facilitates cell cycle progression basally and in response to stress, as discussed in the previous chapter. B-MYB and FOXM1 are significant drivers of G2/M gene expression, and the complex molecular pathways regulating their activity have been the subject of numerous research efforts.

B-MYB and FOXM1 share similar functional, structural, and regulatory features. In quiescence, repressor complex DREAM (DP, RB-like, E2F, and MuvB) and protein RB repress B-MYB and FOXM1 expression[40,96]. In dividing cells, E2F1-3 mediated transcription drives MYBL2 gene expression[56,97], while MMB-FOXM1 complexes promote FOXM1 expression[40]. Multisite, progressive phosphorylation by

cyclin-cyclin-dependent kinase (CDK) complexes stimulate the trans-activating domains of B-MYB and FOXM1[43,89,15,100]. B-MYB activity starts in early S following phosphorylation-mediated release from autoinhibition and disassociation from corepressors N-CoR and SMRT[74]. Phosphorylation of B-MYB correlates with the start of G2/M gene expression[116]. In G2/M phase, FOXM1 auto-inhibition is relieved by cyclin-cdk complexes and PLK1-mediated hyperphosphorylation[2,88,73,17,92]. Hyperphosphorylated FOXM1 correlates with maximal G2/M gene expression. Despite our understanding of B-MYB and FOXM1 expression and activation, it is unclear if B-MYB and FOXM1 cooperate to regulate G2/M progression.

One way in which B-MYB and FOXM1 may cooperate is through recruitment to DNA. Our lab reported that forkhead (FKH) motifs are found at cell cycle promoters in HeLa cells bound by LIN9 and B-MYB, suggesting that recognition of FKH motifs facilitated G2/M gene expression. Immunoprecipitation assays revealed that FOXM1 is sequentially associated with the MMB complex, suggesting MuvB, B-MYB, and FOXM1 bound G2/M gene promoters together.[116]. Since then, several studies have presented conflicting models for how B-MYB and FOXM1 are recruitment to G2/M gene promoters. Chen et al.[17], using U2OS cells, found no enrichment of the FKH motif at cell cycle gene promoters, suggesting a mechanism where FOXM1 recruitment to cell cycle gene promoters depended on interactions with B-MYB and MuvB rather than DNA binding at FKH motif sites. An alternative mechanism presented by Sanders et al.[120], using HEK 293 cells, suggests that the FOXM1 DNA binding domain is required but recognizes DNA in a non-specific manner.

This chapter expands on our understanding of the functional co-dependencies between B-MYB and FOXM1. Specifically, we examined how each transcription factor influences the other's DNA binding, expression, and effect on cell cycle gene expres-

sion. We show that the knockout of B-MYB reduces FOXM1 binding to DNA and delays G2/M gene expression. We found that the knockout of FOXM1 increases the proportion of B-MYB bound to DNA. In addition, we found that FOXM1 knockout severely impaired G2/M expression and the timely regulation of B-MYB and RRM2 proteins in mitosis. These findings indicate that B-MYB and FOXM1 rely on mutually interdependent interactions to regulate DNA binding and expression of G2/M genes and suggest an auto-regulatory feedback loop between B-MYB and FOXM1 cooperatively activates and coordinates G2/M gene expression.

3.3 METHODS

3.3.1 CELL CULTURE

Human non-small cell lung carcinoma (NSCL) A549 cells were obtained from the ATCC (American Type Culture Collection). Cell lines were confirmed free from mycoplasma contamination using the e-Myco Mycoplasma PCR Detection Kit (Bulldog Bio 25233). Cells were cultured in RPMI (Life Technologies, 11875119), supplemented with 10% FBS and 1% penicillin-streptomycin (Life Technologies 15140163).

3.3.2 CELL CYCLE SYNCHRONIZATIONS

For single thymidine blocks, 1 x 10^6 (60 mm plate) cells were plated into 2 mM thymidine-containing RPMI media for 20 h. Cells were seeded at high density (confluent) for contact-inhibition conditions and left for six days. For CDK4 inhibition experiments, cells were treated with inhibitors listed in Table 3.1. To release from synchronization, cells were washed twice with pre-warmed 37°C PBS, re-seeded using pre-warmed 37°C RPMI media, and collected at the times denoted.

Table 3.1: Reagents

Reagent	Supplier	Catalog Number
Palbociclib (PD-0332991)	Selleck Chem	S1116
Nocodazole	Selleck Chem	S2775

3.3.3 Cell Cycle Synchronization

For Palbociclib synchronization and release experiments, cells were treated with 2 μM Palbociclib listed in 3.1 for 24 h. To release from synchronization, cells were washed twice with pre-warmed 37°C PBS, re-seeded using pre-warmed 37°C RPMI media, and collected at the times denoted. For Nocodazole treatments, 2 x 10^6 (60 mm plate) cells were plated into 100 ng/mL Nocodazole-containing RPMI media for 20 h.

3.3.4 Cell Cycle Distribution Assay

Cell cycle distribution was determined as previously described[11]. Briefly, cells were treated with 10 μM EdU (Click Chemistry Tools, 1149-100) for 1 h before collection. Cells were fixed in 4% formaldehyde in PBS for 15 mins at room temperature before being permeabilized in 70% ethanol at -20°C overnight. Incorporated EdU was labeled using a CLICK reaction (2 mM $CuSO_4$, 100 μM THPTA, 100 mM sodium ascorbate, and 2 μM Alexa 647 Azide in PBS) by rotating for 30 mins at room temperature protected from light. Samples were then washed thrice with 1% BSA in PBS and incubated with the primary antibody against pS10 histone H3-PE conjugate (listed in 2.4) in 1% BSA in PBS overnight at 4°C. After three washes with 1% BSA in PBS, DNA was stained with a 1 μg/mL DAPI, 100 ng/mL RNase A staining solution for 1 h at room temperature protected from light before analysis by flow cytometry (BD

LSRFortessa) at the Dana-Farber Flow Cytometry Hematologic Neoplasia and Jimmy Fund Core.

3.3.5 IMMUNOBLOTTING

Cell pellets were lysed in EBC buffer, and protein content was quantified by Bradford assay. For immunoblot, lysates were separated in a 4-20% SDS-PAGE gel, transferred to a nitrocellulose membrane, blocked in 5% milk, and incubated with primary antibody at 4°C overnight. A list of the primary antibodies used can be found in Table 3.2. Blots were imaged with either SuperSignal West Pico (ThermoFisher PI34080) or Immobilon Western Chemiluminescent HRP Substrate (Millipore WBKLS0500).

Table 3.2: Antibodies Used for Immunoblot or Flow Cytometry

Target	Catalog Number
MYBL2	Millipore MABE866
FOXM1	CST 20459S
LIN37	Bethyl A300-BL2983
TBP	ProteinTech 66166-1-Ig
MCM2	CST 3619S
PCNA	CST 2586S
RRM2	CST 65939S
PLK1	CST 4513S
CCNF	CST 81045S
AURKA	CST 14475S
Cyclin B1	CST 4138S
H3	CST 4499S
alpha-Tubulin	CST 3873S
FOXM1 (PE Conjugate)	CST 92319S

3.3.6 RT-QPCR OF CELL CYCLE GENES

Total RNA was purified from A549 cells using the RNeasy Plus Mini kit (Qiagen 74034). Reverse transcription was performed using the High-Capacity cDNA Reverse

Transcription kit (ThermoFisher 4368814) with random primers according to the manufacturer's instructions. qPCR was performed on the cDNA using the primers listed in 3.3 and Brilliant III Ultra-Fast qPCR Master Mix (Agilent) using a MxAria (Agilent). Relative RNA expression was calculated using the Cq method and TBP as a reference gene. All PCR primers were obtained from the MGH PrimerBank, a public resource for optimized PCR primers (https://pga.mgh.harvard.edu/primerbank/). CDDDD

Table 3.3: RT-qPCR primers for Cell Cycle Genes

Name	Sequence	Primer Bank ID
E2F1 Forward	CATCCCAGGAGGTCACTTCTG	168480109c3
E2F1 Reverse	GACAACAGCGGTTCTTGCTC	
RRM2 Forward	CACGGAGCCGAAAACTAAAGC	260064011c1
RRM2 Reverse	TCTGCCTTCTTATACATCTGCCA	
PCNA Forward	ACACTAAGGGCCGAAGATAACG	33239449c3
PCNA Reverse	ACAGCATCTCCAATATGGCTGA	
CCNB1 Forward	AACTTTCGCCTGAGCCTATTTT	356582356c3
CCNB1 Reverse	TTGGTCTGACTGCTTGCTCTT	
CCNB2 Forward	TTGGCTGGTACAAGTCCACTC	332205979c3
CCNB2 Reverse	TGGGAACTGGTATAAGCATTGTC	
CCNF Forward	GGAAAGCGACAGGAGGACAG	118572587c3
CCNF Reverse	TGGCAGACGATCTCACTGGAA	
TBP Forward	CCACTCACAGACTCTCACAAC	285026518c1
TBP Reverse	TCTGGCGCATTTTGTGGTTTT	

3.3.7 Chromatin Fractionation and Flow Cytometry of Transcription Factors

1x10 cells[6] were treated with 10 μM EdU (Click Chemistry Tools, 1149-100) for 1 h before collection. Cells were harvested and permeabilized with CSK buffer (1.5 M Sucrose, 1 M $NaCl_2$, 30 mM $MgCl_2$, 1 M HEPES pH 7.3, 0.1% Triton X-100, Phosstop tablet [Sigma Aldrich 04906837001], and cOmplete Mini Protease Inhibitor

Tablets [Sigma Aldrich, 11836153001]) on ice for 5 mins. Cells were then fixed in 4% formaldehyde on ice for 15 mins. Permeabilized cells were then washed twice with 1% BSA. Incorporated EdU was labeled using a CLICK reaction (2 mM CuSO4, 100 μM TH-PTA, 100 mM sodium ascorbate, and 2 μM Alexa 647 Azide in PBS) by rotating for 30 mins at room temperature protected from light. Samples were then washed thrice with 1% BSA in PBS and incubated with the primary antibody against FOXM1-PE conjugate (listed in 3.2) or FlexAble CoraLite®Plus 550 Antibody labeled B-MYB in 1% BSA in PBS overnight at 4°C. After three washes with 1% BSA in PBS, DNA was stained with a 1 μg/mL DAPI, 100 ng/mL RNase A staining solution for 1 h at room temperature protected from light before analysis by flow cytometry BD LS-Fortessa) at the Dana-Farber Flow Cytometry Hematologic Neoplasia and Jimmy Fund Core.

3.4 Results

3.4.1 B-MYB stabilizes FOXM1 binding to DNA.

Early structural work focused on the DNA binding recognition domain of FOXM1 revealed that FOXM1 had a relatively low affinity to DNA[78], suggesting FOXM1 may require co-factors to bind to DNA. Chromatin immunoprecipitation (ChIP)-qPCR of FOXM1 for a set of G2/M genes in conditional B-MYB knockouts suggested that B-MYB may facilitate FOXM1 binding to G2/M gene promoters[30]. However, ChIP-seq analysis of cell lines expressing either wild-type or DNA-binding domain deficient FOXM1 demonstrated that the FOXM1 DNA binding domain was required for recruitment to gene promoters. Therefore, whether FOXM1 binds DNA in a DNA-mediated or co-factor-dependent mechanism remains unclear. We hypothesized that

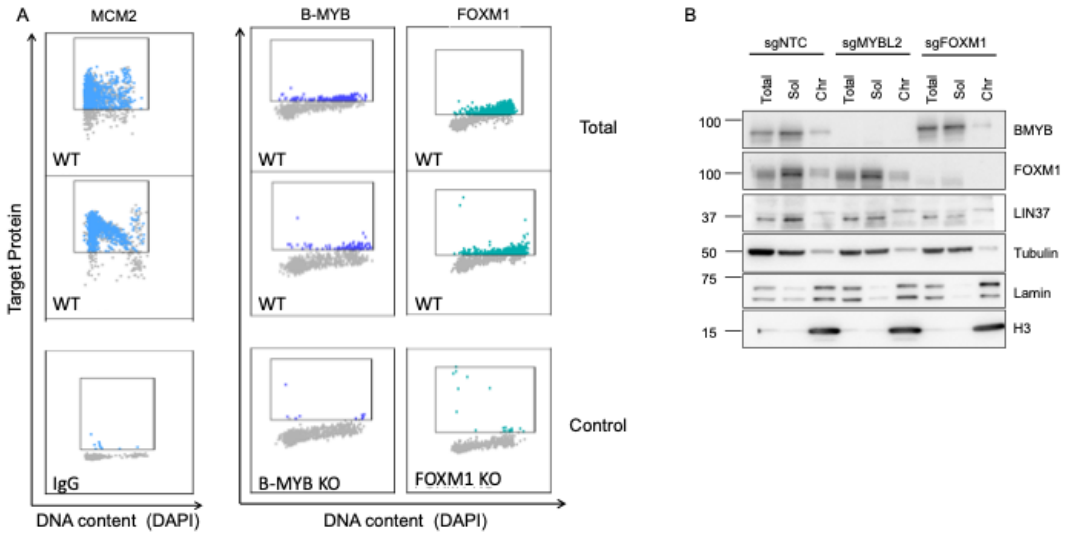

Figure 3.1: Flow cytometric analysis of total and chromatin-B-MYB and FOXM1. A. Gating strategy for defining B-MYB and FOXM1 positive cells. B-MYB and FOXM1 positive cells were defined using sgMYBL2 and sgFOXM1 KO cells. Left: sgNTC cells were fixed and stained with anti-B-MYB or anti-FOXM1 and DAPI (total DNA) to detect total transcription factor levels. Right: Cells were extracted with nonionic detergent to remove soluble proteins, fixed, and stained with anti-B-MYB or anti-FOXM1 and DAPI (total DNA). Purple cells are B-MYB positive, teal cells are FOXM1 positive, and grey cells are negative for either signal. **B.** Transcription factor expression in chromatin-enriched fractions (Chr), cytoplasmic (Sol), or whole cell lysates (Total) was detected by immunoblotting.

FOXM1 can bind to DNA, but B-MYB-FOXM1 interactions enhance FOXM1's association with DNA.

To test this hypothesis, we optimized a chromatin flow cytometry assay to measure chromatin-associated B-MYB or FOXM1 in actively proliferating cells[90]. Nonionic detergent extracted Chromatin fractions were fixed and probed with antibodies against B-MYB, FOXM1, and MCM2 (a chromatin-associated and replication-firing protein) along with DNA content stained (DAPI) and nascent DNA-labeled (EdU) to measure DNA-bound proteins in the various cell cycle phases. The signal detected above KO cell thresholds was considered positive and colored light blue for MCM2, purple for B-MYB, or green for FOXM1 (relevant flow cytometry gating schemes are shown in (Figure 3.1A). B-MYB and FOXM1 protein signal was validated in both total and chromatin-associated fractions by immunoblot (Figure 3.1B).

B-MYB and FOXM1 chromatin-associated signals were superimposed on cell cycle phases to determine the percent positive cells for each phase population. In sgNTC control cells, total FOXM1 and chromatin-associated FOXM1 levels were highest in the G2/M phase (Figure 3.2A). There were no significant differences in total FOXM1 levels between sgMYBL2 and sgNTC. However, knockout of B-MYB significantly reduced chromatin-associated FOXM1 (Figure 3.2B- C), particularly in G2/M. There was no significant difference in the fraction of cells in S phase between sgMYBL2 and sgNTC cells, suggesting the absence of FOXM1 chromatin binding is due directly to the knockout of B-MYB and not changes in the numbers of cells in S phase (Figure 3.2C). These results indicate that B-MYB-FOXM1 interactions enhance and stabilize FOXM1 binding to DNA, as knockout of B-MYB reduces but does not fully impair FOXM1 binding to DNA during G2.

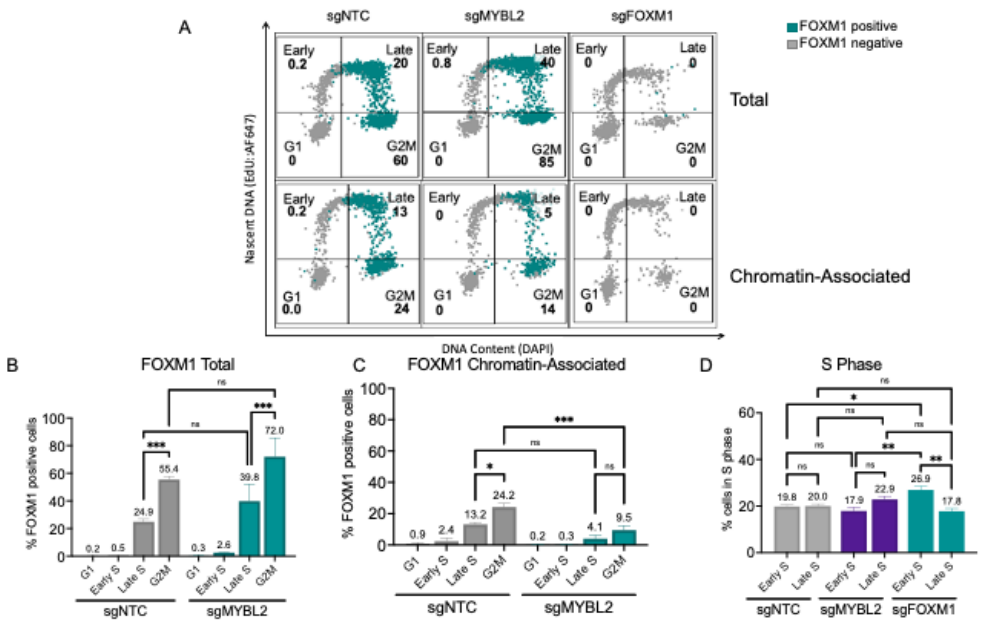

Figure 3.2: B-MYB stabilizes FOXM1 binding to DNA. A. Flow cytometry analysis of FOXM1 total and chromatin-associated in asynchronously proliferating A549 cells. FOXM1-positive cells were gated using sgFOXM1 knockout cells, and the signal was superimposed over cell cycle distributions. **B.** Summary of percent cells with Total FOXM1 (n=3).Statistics were calculated by two-way ANOVA comparing to sgNTC. 0.1(ns), 0.03(*), 0.002(**), <0.0001(***). Error bars represent SEM.**C.** Summary of percent cells with chromatin-associated FOXM1 (n=3). Statistics were calculated by two-way ANOVA comparing to sgNTC. 0.1 (ns), 0.03 (*), 0.002 (**), <0.0001 (***). Error bars represent SEM. **D.** Summary of the percent of cells per each fraction of S phase (n=3).

3.4.2 KNOCKOUT OF FOXM1 INCREASES B-MYB DNA-BINDING

Next, we tested if FOXM1 affects B-MYB binding to DNA. There is no current evidence suggesting FOXM1 regulates B-MYB binding. However, FOXM1 knockdown reduces the expression of mitotic cyclins and CDK1 proteins[116,40]. Phosphorylation by cyclin-CDK complexes regulates B-MYB DNA binding and activation, which suggests FOXM1 activity may be indirectly regulating B-MYB activation and binding to DNA[123,74,70]. In sgNTC cells, B-MYB bound to DNA in S and G2/M phase (Figure 3.3A). Notably, FOXM1 KO cells had higher levels of total and chromatin-associated B-MYB than sgNTC cells (Figure 3.3B-C), revealing that FOXM1 can affect B-MYB binding to DNA through an unknown mechanism.

We probed immunoblots of chromatin-enriched fractions following Palbociclib-synchronization and release to further test the interdependence between B-MYB and FOXM1 in binding to DNA. Cytoplasmic marker α-tubulin was only observed in the total (Tot) unfractionated conditions and in the soluble fraction, whereas chromatin marker Histone H3 was enriched in the chromatin-associated fraction (Figure 3.4A). In sgNTC cells, at 6 h post-Palbociclib release (hpr), B-MYB and FOXM1 signal is observed in the chromatin-associated fraction and progressively accumulated at later time points while remaining largely unchanging in the soluble fraction. FOXM1 signal was observed in the chromatin-associated fraction of sgMYBL2 cells, demonstrating that B-MYB knockout does not abolish FOXM1 binding to DNA and supports our earlier observation in Figure 3.2 that B-MYB was not required for FOXM1 binding. Similarly, an increase in B-MYB signal was observed in the chromatin-associated fraction at 12 hpr, suggesting FOXM1 may be regulating B-MYB association to DNA.

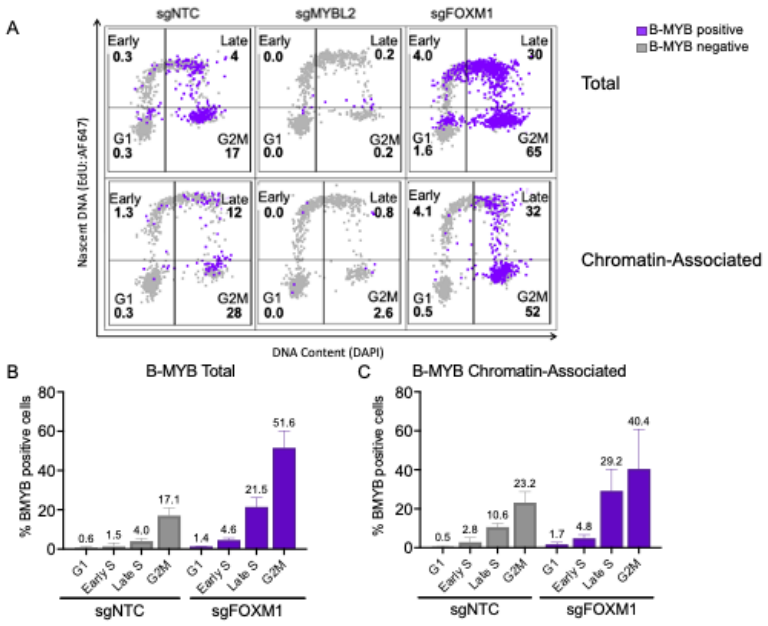

Figure 3.3: Knockout of FOXM1 increases B-MYB DNA-binding. A. Flow cytometry analysis of B-MYB expression in total and chromatin-bound fractions in asynchronously proliferating A549 cells. B-MYB-positive cells were gated using sgMYBL2 knockout cells, and the signal was superimposed over cell cycle distributions. **B.** Summary plots of percent cells expressing B-MYB in the total cell lysate fraction (n=2). Error bars represent SEM.**C.** Summary plots of percent cells expressing B-MYB in the chromatin-bound fraction (n=2). Error bars represent SEM.

3.4.3 B-MYB RECRUITMENT OF FOXM1 INITIATES G2/M GENE EXPRESSION

To measure the direct impact of knockout of B-MYB or FOXM1 on G2/M gene expression, we harvested whole-cell protein lysates from Palbociclib synchronized and released cells and blotted for B-MYB, FOXM1, MuvB component LIN37, and several G2/M proteins. TBP was used as a loading control. B-MYB and FOXM1 proteins were detected in the sgNTC cells at 12 h-post-release from Palbo-sync (Figure 3.4B). In parallel, we observed the expression of cyclin B1, cyclin F, and PLK1 at 12 h-post-release (hpr) in sgNTC cells. In contrast, the appearance of FOXM1 protein was delayed in B-MYB KO cells, with protein levels not reaching levels comparable to that in the sgNTC cells even 24 hpr (Figure 3.4B). Knockout of B-MYB also slowed cyclin F protein expression, suggesting that B-MYB is critical for the proper onset of a subset of G2/M genes. These results indicate that knockout of B-MYB also leads to functional impairment and decreased protein levels of critical mitotic regulators like PLK1 and Cyclin F.

We observed that in FOXM1 KO cells, expression levels of cyclin B1, cyclin F, and PLK1 at 12 h after Palbociclib-synchronization and release were similar to sgNTC cells (Figure 3.4B). However, PLK1 and cyclin F expression were not sustained as levels dropped at 15 h-post-release. Furthermore, cyclin F protein did not reach levels in the FOXM1 KO cells compared with the sgNTC cells even up to 24 h-post-release. These results suggest that FOXM1 may be critical for sustaining or enhancing G2/M gene expression during G2 and into mitosis.

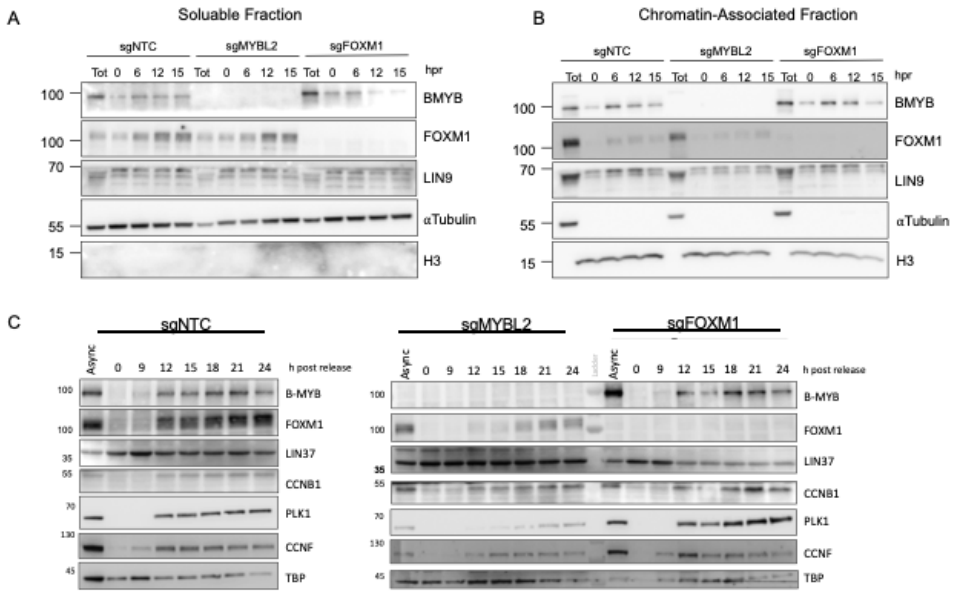

Figure 3.4: B-MYB recruitment of FOXM1 initiates G2/M gene expression. A-B. Immunoblot of soluble (Sol) and chromatin-enriched fractions (Chr) following a 1 μM Palbociclib synchronization and release at the specified time points. Total (Tot) whole-cell protein lysates were harvested from asynchronous conditions from each cell line. **C.** Immunoblot of cell cycle proteins from whole cell lysates extracted following a 1 μM Palbociclib treatment for 24hrs and release at the specified timepoints.

3.4.4 FOXM1 PROMOTES B-MYB DEGRADATION IN MITOSIS

We next wanted to measure how the knockout of B-MYB or FOXM1 affected the expression of G2/M protein levels in mitosis. Cells were treated for 20 h with nocodazole to synchronize cells to Mitosis. In the sgNTC, nocodazole treatment enriched for mitotic regulators PLK1, CCNB1, AURKA, FOXM1 and CCNF((Figure 3.5A), whereas G1/S proteins RRM1, RRM2, PCNA, and B-MYB protein were reduced (Figure 3.5A). In comparison to nocodazole-treated sgNTC control, nocodazole-treated sgMYBL2 cells had reduced PLK1 and CCNB1 protein (Figure 3.5A), suggesting knockout of B-MYB impaired expression of PLK1 and CCNB1. Nocodazole treatment of sgFOXM1 cells, in particular, caused an even greater reduction in PLK1, CCNB1, and CCNF protein levels and led to higher levels of G1/S proteins RRM2 and B-MYB in mitosis (Figure 3.5B). The increase in RRM2 expression was specific to protein levels, as nocodazole treatment reduced RRM2 mRNA in nocodazole-treated sgFOXM1 cells compared to DMSO-treated sgFOXM1 (Figure 3.5B). The aberrant expression of G1/S proteins in nocodazole-treated sgFOXM1 cells suggests that FOXM1 may regulate the controlled degradation of G1/S genes as the cells transition into mitosis.

3.4.5 SUMMARY OF FINDINGS

During early S phase, B-MYB binds to MuvB to form the MMB complex [116]. The MMB complex recruits FOXM1, and all three are required for maximal activation of G2/M genes (Reviewed in [40]). In this chapter, we extend these findings by showing that B-MYB enhanced FOXM1 binding to DNA, and B-MYB-mediated recruitment of FOXM1 was critical for the onset of G2/M gene expression. Unexpectedly,

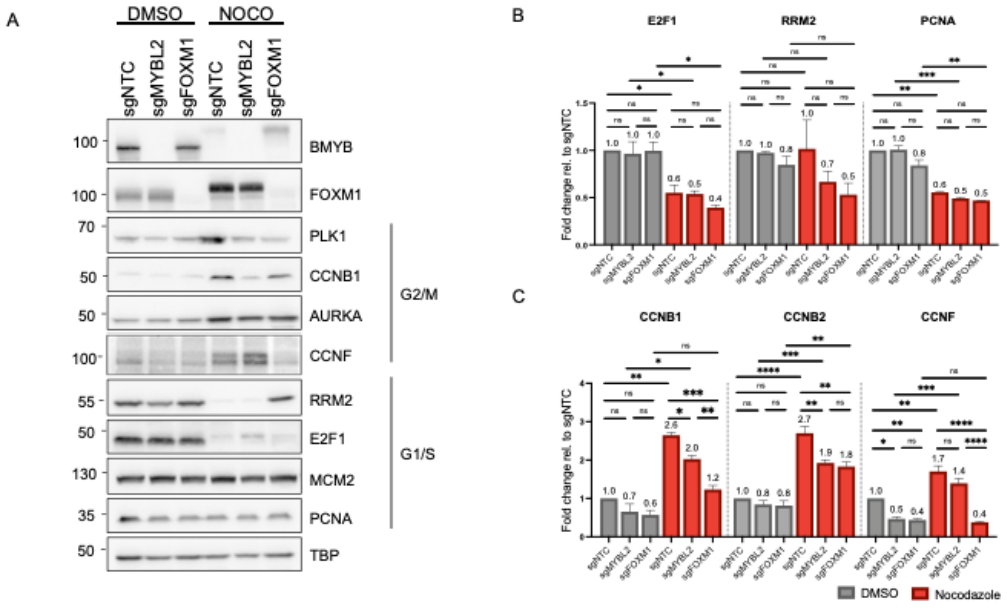

Figure 3.5: FOXM1 severely impairs G2/M gene expression and prevents B-MYB degradation in Mitosis A. Immunoblot of whole-cell lysates from sgNTC and KO cells treated with either DMSO or 100 ng/mL Nocodazole for 20h. TBP was used as a loading control. B. RT-qPCR of a panel of cell cycle genes from sgNTC and KO cells treated with DMSO or Nocodazole for 20h (n=3). Statistics were calculated by two-way ANOVA comparing to sgNTC. 0.1(ns), 0.03(*), 0.002(**), <0.0001(***). Error bars represent SEM.

we found that FOXM1 was involved in regulating total and chromatin-associated B-MYB protein levels through a previously unobserved mechanism. FOXM1 regulation of B-MYB extended into mitosis, as we found that knockout of FOXM1 resulted in persistent levels of G1/S proteins B-MYB and RRM2. In addition, FOXM1 severely impaired G2/M gene expression following nocodazole treatment compared to nocodazole-treated B-MYB knockout cells.

AUTHOR CONTRIBUTIONS FOR CHAPTER 4

The Nascent Transcriptomics Core at Harvard Medical School performed the PRO-seq library construction and data analysis, while sample preparation and clustering analysis were performed by Hembly G. Rivas. The CUT&RUN analysis and integration with PRO-sequencing data sets were carried out by Hanjun Lee[1,2,3] and Dr. Michael Lawrence[1,2], with sample preparation performed by Hembly G. Rivas.

All other sequencing experiments and data analysis were performed by Hembly G. Rivas with input from James A. DeCaprio. This research was supported by the U.S. Public Health Service grants R35 CA232128-03S1 to H.G.R. and R35CA232128 to J.A.D.

*

*[1] Massachusetts General Hospital Cancer Center and Harvard Medical School, Charlestown, MA. [2] Broad Institute of Massachusetts Institute of Technology and Harvard, Cambridge, MA. [3] Department of Biology, Massachusetts Institute of Technology, Cambridge, MA.

" [When] studying how cells divide, any sensible scientist should have expected to find only hopeless complexity. If you think of cell division as a symphony, we knew that the symphony had to be performed by thousands of musicians, each playing a different instrument."

Leland H. Hartwell, Ph.D.

4

B-MYB primes G2/M promoters and FOXM1 transactivates G2/M genes.

4.1 Abstract

The CHR motif, recognized by the MuvB complex, is primarily enriched at G2/M gene promoters, while canonical MYB and forkhead (FKH) DNA motifs are less enriched at G2/M promoters. Current models propose that MuvB specifically binds to CHR sites, while B-MYB and FOXM1 may be recruited to neighboring, non-specific

DNA sequences. We performed Cleavage Under Targets and Release Using Nuclease (CUT&RUN) chromatin profiling and found that B-MYB and FOXM1 binding is correlated but can be distinguished. We observed that B-MYB binding was enriched at G2/M gene promoters and contained canonical MYB and CHR DNA recognition motifs. In addition, we found that MuvB component LIN9 binding follows the pattern of B-MYB rather than FOXM1. We demonstrate that FOXM1 binds to G2/M and DNA damage gene promoters. FOXM1 gene targets were enriched for canonical FKH DNA recognition motifs. Combining nascent transcript analysis (PRO-seq), RNA-seq, and CUT&RUN sequencing, we define FOXM1 as a critical transcriptional driver of cell cycle gene expression. Collectively, these findings indicate that B-MYB and FOXM1 cooperatively regulate the expression of cell cycle genes, where the MMB complex defines G2/M genes through association with MYB and CHR recognition motifs and enhances recruitment of FOXM1 to G2/M gene promoters, where FOXM1 drives transcription of G2/M genes and DNA repair genes.

4.2 Introduction

B-MYB and FOXM1 are cell cycle transcription factors with several functional, structural, and regulatory features. In quiescence, DREAM represses B-MYB and FOXM1 expression[40,96]. In proliferating cells, E2F1-3 mediated transcription drives B-MYB (MYBL2) gene expression[56,97], while MMB complex contributes to FOXM1 expression[40]. Multisite, progressive phosphorylation by cyclin-CDKs and PLK1 stimulates the trans-activating domains of B-MYB and FOXM1[43,89,15,100]. Hyperphosphorylation of B-MYB and FOXM1 correlates with increased transcriptional activity[116]. Notably, the knockdown of either B-MYB or FOXM1 reduces but does not abolish

G2/M gene expression, suggesting that both transcription factors contribute to maximal G2/M gene production([116,101,71,16,11]).

Several lines of evidence suggest that despite these similarities, B-MYB and FOXM1 may serve cooperative but distinct roles in regulating and initiating G2/M genes. For example, B-MYB and FOXM1 are discretely activated. B-MYB transcription is activated in late G1 following cyclin-CDK mediated phosphorylation. In early S phase, FOXM1 is maintained in a relatively low phosphorylated state. During this time, B55, a subunit of protein phosphatase 2A, keeps phospho-FOXM1 levels low through association with FOXM1[2,1]. Starting in late S and into G2 phase, FOXM1 undergoes increased multi-site phosphorylation and reaches a hyperphosphorylated state in M phase[17,73]. In addition to activation, the degradation of B-MYB and FOXM1 is also phase-specific. B-MYB is increasingly ubiquitinated as the cells enter G2 and degraded before mitosis[15], while FOXM1 undergoes proteasomal degradation by APC/C-CDH1 complexes during mitosis[103,73]. Notably, peak gene expression levels of G2/M genes occur in early M when B-MYB is already degraded[80,116], and only FOXM1 remains.

Additionally, both B-MYB and FOXM1 have DNA-binding domains. All G2/M genes harbor a conserved cell cycle genes homology region (CHR) motif (5'-TTYRAA-3') that LIN54 recognizes, the DNA-binding subunit of MuvB[116,96]. In contrast, some G2/M genes contain a canonical MYB (5'-YAAC[GT]G-3'), an FKH DNA recognition motif (5'- RYAAAYA -3'), or a combination of CHR, MYB, and FOXM1 regulatory DNA-elements (Reviewed in[41]). These observations suggest that B-MYB, MuvB, and FOXM1 gene expression regulation may be combinatorial, where both proteins cooperate to transactivate G2/M genes.

In this chapter, we explore the individual contributions of B-MYB and FOXM1 in

Table 4.1: Reagents

Reagent	Supplier	Catalog Number
Palbociclib (PD-0332991)	Selleck Chem	S1116
Nocodazole	Selleck Chem	S2775

the direct transactivation of G2/M genes.

4.3 METHODS

4.3.1 CELL CULTURE

Cells were cultured in RPMI (Life Technologies, 11875119), supplemented with 10% FBS and 1% penicillin-streptomycin (Life Technologies 15140163). Cell lines were confirmed free from mycoplasma contamination using the e-Myco Mycoplasma PCR Detection Kit (Bulldog Bio 25233). Cells were cultured in RPMI (Life Technologies, 11875119), supplemented with 10% FBS and 1% penicillin-streptomycin (Life Technologies 15140163).

4.3.2 CELL CYCLE SYNCHRONIZATION

For Palbociclib synchronization, eight separate 15cm^2 dishes were seeded at 2.5 x 10^6 and treated with 1μM Palbociclib-containing RPMI media for 24 h. Treatment with Palbociclib was staggard such that 0 h and 6 h were collected together while 12 h and 15 h time points were collected 2 h after. For Palbociclib release, two 15 cm^2 were trypsinized, pooled, and re-seeded using pre-warmed 37°C complete RPMI media into three 15cm^2 dishes. For Nocodazole treatments, 2 x 10^6 (60 mm plate) cells were plated into 100 ng/mL Nocodazole-containing RPMI media for 20 h. Reagents are listed in Table 4.1.

4.3.3 CUT&RUN

CUT&RUN SAMPLE PREPARATION

Day One. CUT&RUN samples were processed following the EpiCypher®CUTANA^{TM} CUT&RUN protocol. More than one CUT&RUN reaction was planned for each time point, so cells were batch-processed till the addition of the antibody. Briefly, 55 μL ConA beads were activated by washing twice with 110 μL cold bead activation buffer (20 mM HEPES pH 7.9, 10 mM KCl, 1 mM $CaCl_2$, 1 mM $MnCl^2$). Following washes, ConA beads were resuspended in 55 μL cold bead activation buffer and kept on ice till needed. In parallel, harvested cells were washed once with room temperature (RT) 1x PBS and spun for 3 min at 600 xg at RT. The supernatant was removed, and cells were resuspended in 1 mL RT wash buffer (20 mM HEPES, pH 7.5, 150 mM NaCl, supplemented fresh before each use: 0.5 mM Spermidine, 1x Roche cOmplete^{TM} Mini EDTA-free Protease Inhibitor (Sigma Aldrich 11836153001)). Cells were counted, and 5.5x10^6 cells were used for the CUT&RUN experiment. Cells were spun for 3 min at 600 x g at RT and washed for two washes. After the last wash, cells were re-suspended in 550 μL RT Wash Buffer and then incubated with the activated ConA beads. The bead slurry was gently rocked at RT for 10 min and then placed on a magnet until the slurry cleared. The supernatant was removed and resuspended in 275 μL cold antibody buffer (Wash buffer + added day of 0.01% digitonin + 2 mM EDTA). 50 μL of the cell slurry was aliquoted into individual 8-strip PCR tubes. Antibodies were added at 1:50 dilution for each assigned sample, and the tube strip was incubated on a nutator overnight at 4°C.

Day Two.Tubes were placed on a magnet till the slurry cleared and the supernatant was removed. Quickly, 200 μL cold Digitonin Buffer directly (Wash buffer + fresh

0.01% digitonin) was added to each reaction using a multichannel pipette. Wash the step for a total of two times. After the second wash, the supernatant was removed and discarded. 50 μL cold digitonin Buffer was added to each reaction, and the tube strip was gently vortexed to resuspend beads. 2.5 μL of pAG-MNase (EpiCypher 15-1016) was added to each CUT&RUN reaction and gently vortex to mix. Samples were incubated on a rocker for 10 min at RT. The tube strip was placed on the magnet, and samples were washed twice with cold digitonin wash buffer. After the second wash, the supernatant was removed and discarded. 50 μL cold digitonin buffer was added per reaction, placed on ice, and 1 L 100 mM $CaCl_2$ was added to each reaction. PCR tube trip was placed on a nutator for 2 h at 4°C. Following incubation, 33 μL stop buffer (340 mM NaCl, 20 mM EDTA, 4 mM EGTA, 50 μg/mL RNase A, 50 μg/mL Glycogen, 0.5 ng/reaction Spike-in DNA (EpiCypher 18-1401)) was added to each reaction and gently vortexed to mix. PCR tubes were incubated for 10 min at 37°C in a thermocycler. Samples were briefly spun down and placed on a magnetic stand. The supernatant was transferred to a new PCR tube strip. DNA was purified from the supernatant using the CUTANA^{TM} DNA Purification Kit (EpiCypher, 14-0050). DNA was eluted in 12 μL RNase/DNase-free water (Life Technologies, 10977023) and sent for sequencing.

HIGH THROUGHPUT SEQUENCING AND ANALYSIS

After DNA purification, library preparation and high-throughput sequencing were performed by the Molecular Biology Core Facilities at Dana-Farber Cancer Institute. Samples were sequenced single-end, 75bp with an Illumina Next-Seq 500. Data was analyzed using the ENCODE3 histone replicated ChIP-seq processing pipeline to call narrow peaks. Heatmaps were generated using the deepTools suite of Python tools[109].

CUT&RUN DATA ANALYSIS

Sequence quality was assessed with FastQC (Babraham Bioinformatics), and sequencing reads were trimmed using trim-galore. Reads were aligned to the GRCH38p.13 v101 cDNA library was performed using bwa-mem, then duplicate-marked using sambamba, and filtered to remove reads that were duplicates, had mapping quality <30, had >2 mismatches, or had >1/3 of their sequence soft-clipped. Filtered BAMs were sorted, indexed, and deep tools bamCoverage was used to generate CPM-normalized bigwig files for peak visualization. Bedtools-coverage was used to count reads in 200bp genomic windows tiling the genome. Peak calling was performed using MACS2 [146,37].

Table 4.2: Antibodies Used for CUT&RUN

Target	Catalog Number
IgG	Abcam ab46540
FOXM1	ProteinTech 13147-1-AP
B-MYB	Bethyl A301-656A
LIN9	Bethyl A300-BL2981

4.3.4 RNA-SEQUENCING

A549 sgNTC, sgMYBL2, and sgFOXM1 cells were treated with DMSO or 100 ng/mL Nocodazole for 20 hrs before harvesting. Total RNA was extracted using TRIzol™ (Life Technologies 15596026) according to the manufacturer's recommendation. Novogene Corporation Inc. Sequencing performed poly-A selection, library preparation, and sequencing was performed on the NovaSeq 6000 to >12G (40 million reads) per sample of PE150 reads.

Data Analysis:

Sequence quality was assessed with FastQC (Babraham Bioinformatics) and read alignment to the GRCH38p.13 v101 cDNA library was performed using Salmon[104]. Differential expression analysis was performed using DESeq2[83,150]. Gene ontology analyses were restricted to genes with a HUGO gene symbol and performed using DAVID[58].

4.3.5 PRO-sequencing

Sample Preparation

A549 sgNTC cells were seeded in 12 separate 15cm^2 dishes at 2.5 x 10^6 cells per dish and treated with 1 μM Palbociclib for 24 h. The next day, cells were pooled using warmed 37°C complete RPMI media. One-fourth of the pooled cells were saved and processed at the 0-hour time point. The remaining fraction was used to re-seed three separate 15cm^2 plates, and cells were cultured for 6, 12, and 15 h post-Palbociclib-synchronization. After collection, cells were resuspended in 2 mL room temperature 1x PBS. Cells were then spun down at 500 xg and resuspended in 10 mL cold PBS, and 20 μL was saved for counting cells. Cells were then spun down at 500 xg and resuspended in 250 μL buffer W (10 mM Tris-Cl, pH 8.0, 10 mM KCl, 250 mM Sucrose, 5 mM $MgCl_2$, 1 mM EGTA, 0.5 mM DTT, 10 % (v/v) Glycerol, and protease plus phosphatase inhibitors added right before use), and gently resuspended to ensure single cell solution. Next, 10 mL Buffer P (buffer W + 0.1% (v/v) Igepal CA-630 + 0.05% (v/v) Tween-20) was directly added to the cell suspension, and the sample was incubated on ice for 5 min. Following incubation, samples were spun down 500 xg at 4°C, the supernatant removed, and gently resuspended in 1 mL of buffer W. Follow-

ing gentle resuspension, an additional 9 mL Buffer W was added to each tube. Samples were spun down at 500 xg, supernatant removed, and gently resuspended in 250 μL Buffer F (50 mM Tris-Cl pH 8.0, 40% (v/v) glycerol 4.0 mL, 5 mM $MgCl_2$, 1.1 mM EDTA, 0.5 mM DTT, and protease plus phosphatase inhibitors added right before use). The sample was transferred to a clean 1.5 mL low-binding tube and snap-frozen on dry ice. Samples were stored at -80°C till processing.

PRO-SEQ LIBRARY CONSTRUCTION

Aliquots of frozen (-80°C) permeabilized cells were thawed on ice and pipetted gently to resuspend fully. Aliquots of permeabilized cells were counted using a Luna II Logos Biosystems instrument. For each sample, 1 x 10^6 permeabilized cells were used for nuclear run-on, with 5 x 10^4 permeabilized Drosophila S2 cells added to each sample for normalization. Nuclear run-on assays and library preparation were performed essentially as described in Reimer et al.[110] with modifications noted: 2X nuclear run-on buffer consisted of (10 mM Tris (pH 8), 10 mM $MgCl_2$, 1 mM DTT, 300 mM KCl, 20 μM/ea biotin-11-NTPs (Perkin Elmer), 0.8U/ μL SuperaseIN (Thermo), 1% sarkosyl). Run-on reactions were performed at 37°C. Random hexamer extensions (UMIs) were added to the 3$^{'}$ end of the 5$^{'}$ adapter and the 5$^{'}$ end of the 3$^{'}$ adapter. An adenylated 3$^{'}$ adapter was prepared using the 5$^{'}$ DNA adenylation kit (NEB) and ligated using T4 RNA ligase 2, truncated KQ (NEB, per manufacturers instructions with 15% PEG-8000 final), and incubated at 16°C overnight. 180 μL of betaine buffer (1.42 g of betaine brought to 10 mL) was mixed with ligations and incubated 5 min at 65°C and 2 min on ice before addition of streptavidin beads. After T4 polynucleotide kinase (NEB) treatment, beads were washed once each with high salt, low salt, and 0.25X T4 RNA ligase buffer (NEB) and resuspended in 5$^{'}$ adapter mix (10 pmol 5$^{'}$

adapter, 30 pmol blocking oligo, water). 5' adapter ligation was per Reimer but with 15% PEG-8000 final. Eluted cDNA was amplified 5-cycles (NEBNext Ultra II Q5 master mix (NEB) with Illumina TruSeq PCR primers RP-1 and RPI-X) following the manufacturer's suggested cycling protocol for library construction. A portion of preCR was serially diluted for test amplification to determine the optimal amplification of final libraries. Pooled libraries were sequenced using the Illumina NovaSeq platform.

PRO-SEQ DATA ANALYSIS

All custom scripts described herein are available on the AdelmanLab GitHub (https://github.com/AdelmanLab/NIH_scripts). Dual, 6nt Unique Molecular Identifiers (UMIs) were extracted from read pairs using UMI-tools [10.1101/gr.209601.116]. Read pairs were trimmed using cutadapt 1.14 to remove adapter sequences (-O 1 −−match−read−wildcards−m 20,26). The UMI length was trimmed off the end of both reads to prevent read-through into the mates UMI, which will happen for shorter fragments. An additional nucleotide was removed from the end of read 1 (R1), using seqtk trim (https://github.com/lh3/seqtk), to preserve a single mate orientation during alignment. The paired-end reads were then mapped to a combined genome index, including both the spike (dm6) and primary (hg38) genomes, using bowtie2. Properly paired reads were retained. These read pairs were then separated based on the genome (i.e., spike-in vs primary) to which they mapped, and both these spike and primary reads were independently deduplicated, again using UMI-tools. Reads mapping to the reference genome were separated according to whether they were R1 or R2, sorted via samtools 1.3.1 (-n), and converted to bedGraph format using a custom script (bowtie2stdBedGraph.pl). This script counts each read once at the exact 3' end

of the nascent RNA. Because R1 in PRO-seq reveals the position of the RNA 3' end, the "+" and "-" strands were swapped to generate bedGraphs representing 3' end positions at single nucleotide resolution. Samples displayed highly comparable recovery of spike-in reads. Thus, samples were normalized based on the DESeq2 size factors (see below). Combined bedGraphs were generated by summing counts per nucleotide across replicates for each condition.

Annotated transcription start sites were obtained from human (GRCh38.99) GTFs from Ensembl. After removing transcripts with immunoglobulin, Mt, Mt_tRNA, and rRNA biotypes, the PRO-seq signal in each sample was calculated in the window from the annotated TSS to +150 nt downstream, using a custom script, make_heatmap.pl. This script counts each read one time at the exact 3' end location of the nascent RNA. Given good agreement between replicates and similar return of spike-in reads, bedGraphs were merged within conditions and depth−normalized to generate bigWig files binned at 10bp.

Refinement of gene annotation (proTSScall) using PRO-seq alone

PRO-seq reads were used to identify active transcription start sites using a custom script, proTSScall, available on the NascentTranscriptionCore GitHub (https://github.com/NascentTranscriptionCore/proTSScall). Briefly, PRO-seq 3' read bedGraphs for "+" and "-" strands were separately combined across samples, and the composite read counts were assigned to TSS-proximal windows (TSS to +150nt) using the same filtered TSS annotation described above. TSSs with 9 counts in this window are deemed 'inactive' and the remaining TSSs, deemed 'active', are collapsed to yield 1 dominant TSS per gene, defined as the one with the highest TSS-proximal read count – if the highest read count is shared amongst multiple transcripts, the TSS

furthest upstream, in a strand-aware fashion, is called dominant. Dominant TSSs sharing the same start position are deduplicated as follows: (1) if start positions are equal, the TSS with the longest associated annotated transcript is called dominant; (2) if start positions and transcript lengths are both equal, the TSS associated with the lowest Ensembl gene ID (numerical portion) is dominant.

DIFFERENTIAL EXPRESSION ANALYSIS

Reads were summed within the TSS to TES window for each active gene using the make_heatmap script (https://github.com/AdelmanLab/NIH_scripts), which counts each read one time at the exact 3' end location of the nascent RNA. DEseq2, using the Wald test, was used to determine statistically significant differentially expressed genes. Unless otherwise noted, the default size factors determined by DEseq2 were used.

4.3.6 4SU- RT QPCR

Cells were labeled with complete RMPI containing 500 μM 4sU (Sigma Aldrich, T4509) for 30 mins before isolating RNA with an RNeasy RNA extraction kit (Qiagen, 75144). Total RNA (100 μg) was incubated in biotinylation buffer (10 mM Tris [pH 7.4], 1 mM EDTA) and 200 μg HPDP-biotin (EZ-link HPDP-biotin; Life Technologies, A35390) with constant rotation at room temperature for 1.5 hr. RNA was then purified using the RNA Clean & Concentrator^{TM}-25 K (Thomas Scientific, 1159U73). RNA was resuspended in DEPC-treated water and mixed with 50 μl Dynabeads MyOne streptavidin C1 (New England Biolabs, S1420S) that had been prewashed twice with 1X wash buffer (100 mM Tris [pH 7.5], 10 mM EDTA, 1 M NaCl, 0.1% Tween 20). Samples were rotated for 15 min at RT, then washed 6Œ at RT wash

buffer. Samples were eluted with 100 μM DTT, and the RNA was precipitated with ethanol before RT-qPCR. Relative RNA expression was calculated using the Cq method and TBP as a reference gene. Fold-change was calculated in reference to the 0 hr control. All PCR primers were obtained from the MGH PrimerBank, a public resource for optimized PCR primers (https://pga.mgh.harvard.edu/primerbank/).

Table 4.3: RT-qPCR Primers for Cell Cycle Genes

Name	Sequence	Primer Bank ID
CCNB1 Forward	AACTTTCGCCTGAGCCTATTTT	356582356c3
CCNB1 Reverse	TTGGTCTGACTGCTTGCTCTT	
CCNF Forward	GGAAAGCGACAGGAGGACAG	118572587c3
CCNF Reverse	TGGCAGACGATCTCACTGGAA	
TBP Forward	CCACTCACAGACTCTCACAAC	285026518c1
TBP Reverse	TCTGGCGCATTTTGTGGTTTT	

4.4 Results

4.4.1 B-MYB and FOXM1 bind to promoters of cell cycle genes.

To explore the differences between B-MYB and FOXM1 DNA-binding, we performed CUT&RUN[128] using antibodies specific for B-MYB, FOXM1, and LIN9, the central scaffold protein of the MuvB complex (Figure 4.1A). We confirmed antibody specificity by comparing target CUT&RUN signals to an IgG control from asynchronous and synchronized cells. Macs2 software was used to call B-MYB and FOXM1 peaks on the asynchronous and synchronized samples. We first analyzed the composite profile of B-MYB and FOXM1 peaks across all genes (Figure 4.1B). In agreement with their roles in transcriptional activation, we found a general enrichment of B-MYB and FOXM1 peaks near the Transcription Start Site (TSS) of genes. Notably, for cell cycle genes, we found the average peak signal near TSS was at least

2-fold higher than the signal found near the TSS of all genes, particularly near G2/M gene transcription start sites (Figure 4.1C).

A heat map illustrates B-MYB and FOXM1 binding sites at 413 well-established cell cycle genes[40] in G2/M synchronized cells, 15 hours post-release from palbociclib-synchronization (Figure 4.2A). Despite the overlap between B-MYB and FOXM1 peaks, B-MYB binding was enriched and specific at G2/M gene transcription start sites, whereas FOXM1 bound at both G1/S and G2/M gene transcription start sites (Figure 4.2B).

To explore the binding differences between B-MYB and FOXM1 at cell cycle genes, we calculated a B-MYB/FOXM1 binding intensity ratio (binding signals) for the 413 cell cycle genes based on peak height detected at -500 bp to +500 bp relative to the TSS (Figure 4.3A). The stronger the B-MYB peak, the smaller the ratio number grew, while a strong FOXM1 peak resulted in a large ratio number. We found that B-MYB and FOXM1 binding signals for cell cycle genes were strongly correlated (Spearman's p= 0.623). When analyzing cell cycle genes by cell cycle phase, we found that B-MYB and FOXM1 binding was also correlated irrespective of phase. However, the top 10 G1/S genes had a slightly stronger FOXM1 binding signal (Figure 4.3B), suggesting that FOXM1 bound significantly more to G1/S genes than B-MYB. In contrast, the top 10 G2/M genes shared similar binding signals between B-MYB and FOXM1 (Figure 4.3C).

4.5 B-MYB, NOT FOXM1, GOVERNS G2/M SPECIFICITY.

We wondered if the promoters of B-MYB-specific or FOXM1-specific genes contained consensus binding sites for B-MYB-, FOXM1-, or MuvB-binding sites. We

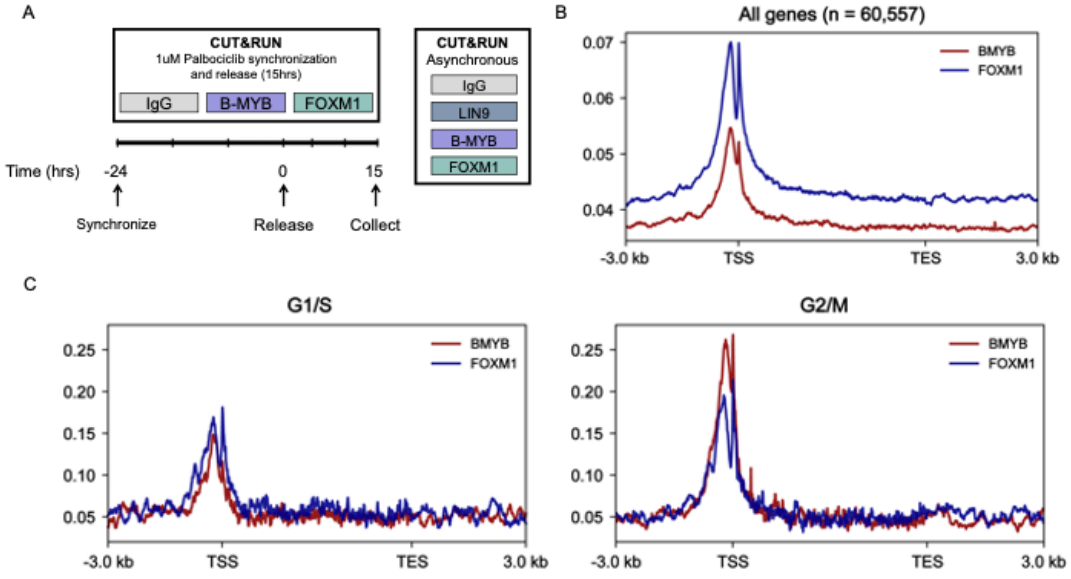

Figure 4.1: B-MYB and FOXM1 binding is enriched at transcription start sites of cell cycle genes A. Schematic of experimental design and conditions collected for CUT&RUN.**B.** Global metagene indicates that B-MYB and FOXM1 are mostly present at the Transcription Start Site (TSS) of genes as opposed to the transcription end site (TES) **C.** Metagene analysis of well-established G1/S and G2/M cell cycle genes ([40]) reveals that B-MYB and FOXM1 signal is highest at G2/M transcription start sites (TSS).

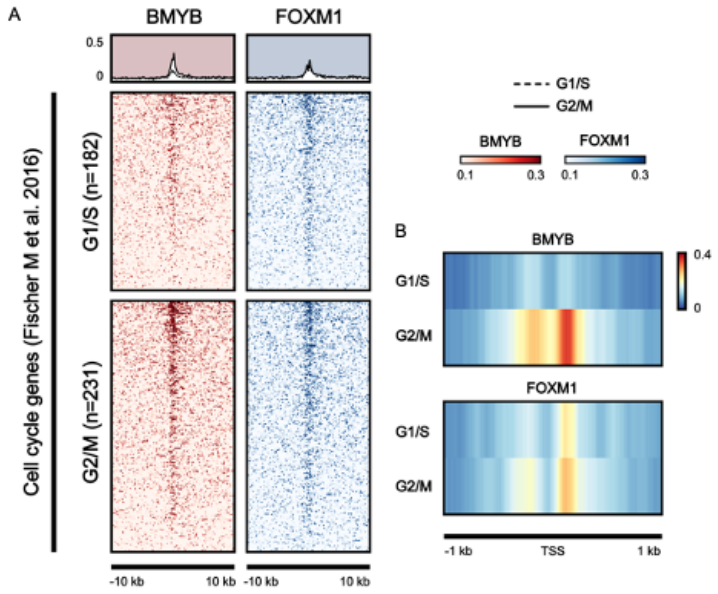

Figure 4.2: B-MYB and FOXM1 bind to overlapping cell cycle gene promoters. A. Heat maps of CUT&RUN datasets from synchronized cells (15 h post-Palbociclib release) for B-MYB and FOXM1 across 10,000 bp and 10,000 bp from the transcription start site (TSS) of cell cycle gene set previously described by (Fischer et al., 2016). **B.** B-MYB and FOXM1 peak signal between -500 bp and 500 bp from the TSS at cell cycle genes.

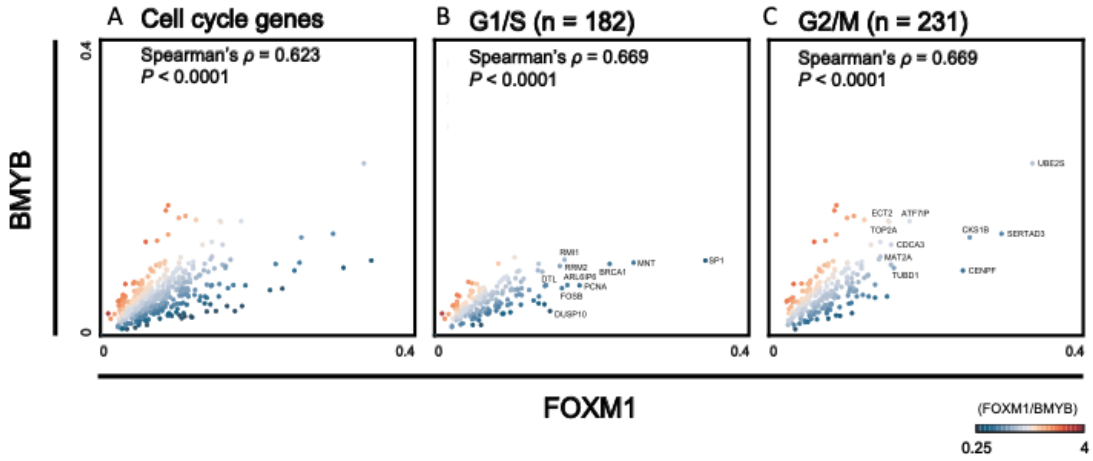

Figure 4.3: B-MYB and FOXM1 binding is strongly correlated, but there are differences. A-C. Scatter plots of the binding signal ratio of B-MYB and FOXM1 on cell cycle gene promoters. The B-MYB peak signal divided by the FOXM1 peak signal binding was used to compare the binding strength between the two transcription factors. The peak signal was based on peaks detected at -500 bp to +500 bp relative to the TSS. Spearman's coefficients are shown across the different cell cycle gene groups. Annotated are the top 10 genes for each cell cycle phase.

performed motif enrichment analysis on FOXM1-specific and B-MYB-specific gene targets. HOMER analysis revealed that for B-MYB-specific genes, consensus sequences for MYB and CHR (cell cycle gene homology) were among the top five significantly enriched motifs (Figure 4.4A), providing additional validation that B-MYB and LIN9 bound specifically and cooperatively to these gene promoters [126,116,16]. The FOXP1 FKH motif was the most significantly enriched DNA motif for FOXM1-specific genes. Gene ontology (GO) analysis of B-MYB- and FOXM1-specific genes revealed that B-MYB-specific genes were enriched in mitotic cytokinesis, regulation of cell cycle process, mitotic sister chromatid segregation, whereas FOXM1-specific genes enriched for DNA metabolic process, DNA recombination, and DNA repair. (Figure 4.4B). Based on our DNA motif and gene ontology analyses, these data suggest that B-MYB governs G2/M specificity, whereas FOXM1 cooperates but has a distinct function regulating the cellular DNA damage response.

4.6 FOXM1 PROMOTES NASCENT RNA TRANSCRIPTION THROUGHOUT THE CELL CYCLE.

DNA binding by a transcription factor is an initial regulatory step required for gene expression. DNA binding, however, does not necessarily indicate the synthesis of RNA. Several steps can be directly measured to understand the dynamic control mechanisms that cells employ to modulate gene activity in response to internal and external cues (reviewed in [142]). Nascent mRNA provides real-time information about ongoing transcription, and mature RNA reflects the culmination of transcriptional and post-transcriptional processing. We aimed to study DNA binding parallel to nascent and mature RNA levels to understand how B-MYB and FOXM1 regulate active gene expression of cell cycle genes.

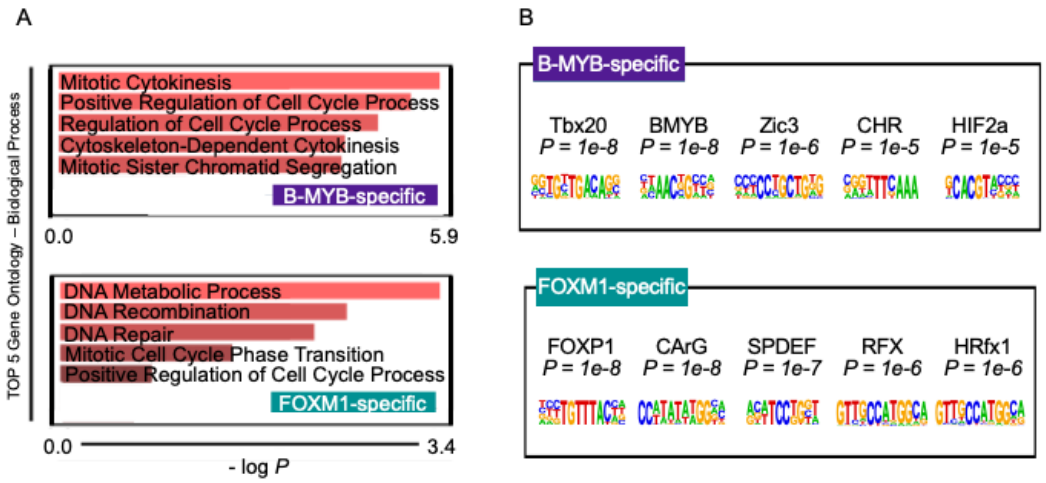

Figure 4.4: B-MYB binds specifically to G2/M gene promoters, and FOXM1 binds to G2/M and DNA repair gene promoters. A. Homer motif analysis of B-MYB- and FOXM1-specific genes identified from PCA clustering in panel A. **B.** Gene ontology analysis of B-MYB- and FOXM1- specific gene sets. The top five pathways are shown for each transcription factor.

First, we wanted to understand if chromatin binding was indicative of active gene expression for B-MYB and FOXM1. Typically, transcription is assayed by measuring mature mRNA molecules globally by RNA-seq or selectively of candidate genes by RT-qPCR. A recent comprehensive study of the transcriptional landscape across the cell cycle revealed a gap between transcription and the accumulation of RNA levels. This suggests that the transcriptional activation of cell cycle genes precedes the accumulation of the transcribed products[80]. Indeed, several studies comparing RNA-seq and nascent RNA sequencing techniques indicate delays and limitations of steady-state RNA levels in reflecting fluctuations of rapidly expressed or degraded transcripts[91]. All current cell cycle nascent RNA studies have been performed using unsynchronized or single-phase synchronized cells[80,135,111,145].

We employed precision nuclear run-on sequencing (PRO-seq)[87] to measure the dynamic transcriptional changes throughout one cell division round following palbociclib release. PRO-seq libraries were prepared for A549 sgNTC cells treated with palbociclib and collected at 0-, 6-, 12-, or 15 hours post-release, with two biological replicates per time point (Figure 4.5A). We identified 1,585 differentially expressed protein-coding genes being actively transcribed in one or more time points with a false-discovery rate (FDR) < 0.05 (Figure 4.5B). Of these genes, roughly 15% (234) were detected across all time points, whereas about 32% (507) were uniquely detected at 6- hours post-release (hpr), and about 17% (265) of actively transcribed genes overlapped between 12- and 15-hpr.

Gene ontology (GO) analysis using the Database for Annotation, Visualization, and Integrated Discovery (DAVID)[58] revealed that genes with peak synthesis at 12-hpr were enriched for GO terms involving "DNA replication" and "DNA Repair" (Figure 4.5B). In contrast, genes highly synthesized at 15-hpr enriched for "Mitotic Spindle

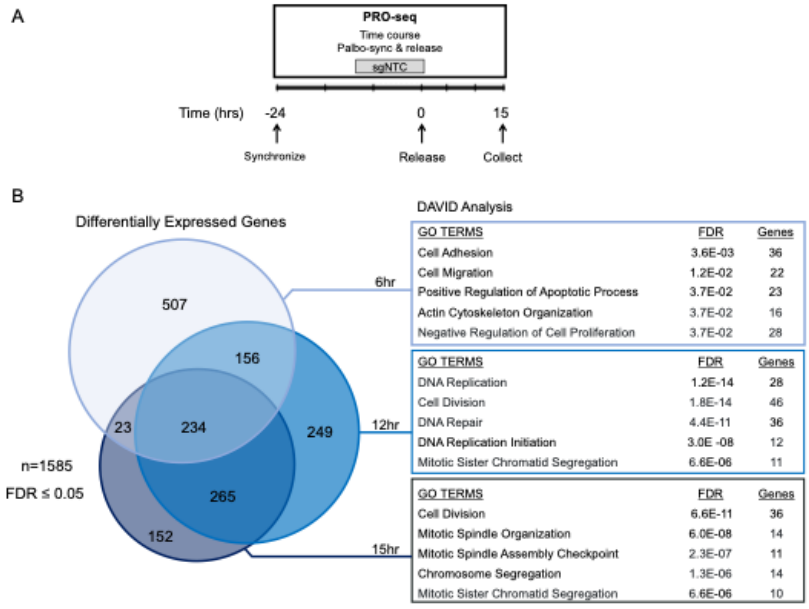

Figure 4.5: Palbociclib-synchronization and release enrich for cell cycle gene synthesis. **A.** Schematic of experimental design and samples collected for PRO-seq **B.** 1585 differentially expressed genes were identified following analysis by DEseq2 and DAVID analysis was conducted.

Organization" and "Chromatin Segregation" pathways (Figure 4.5B), suggesting that most G2/M genes were synthesized at 15-hpr, though the about 17% overlap between these two-time points indicates that synthesis of cell cycle genes may be a progressive process.

Hierarchical clustering was performed to investigate further the synthesis patterns of the top differentially expressed genes (4.6). A silhouette score was used to estimate and give a distribution of the potential number of clusters using the NbClust R package (Figure 4.6A)[14]. The data were z-score normalized and the Euclidean distance between each gene was calculated and plotted (Figure 4.6B). Using the dendrogram to visualize the data's structure and combined with the silhouette analysis from NbClust, these methods suggest that a 6-cluster solution would be an excellent fit for the data. Cluster 4, which peaked at 12-hpr and cluster 5 at 15-hpr, contained the highest number of annotated cell cycle genes[40] (Figure 4.6C). The six gene expression trends were visually represented by clusters for all 1585 differentially expressed genes (Figure 4.7D).

Next, we used a principal component analysis (PCA)-based method to simplify our CUT&RUN data across all conditions and integrate the different datasets. PCA is a dimensionality reduction method that condenses the variation in a data set into its two major principal components (PC1 and PC2). We reasoned that the transcriptional state of the gene (open vs closed chromatin) and binding preference among B-MYB, FOXM1, and LIN9 would be the major variation drivers for the calculated principal components. We observe that B-MYB and LIN9 gene targets clustered together in quadrant IV. In contrast, a subset of FOXM1 gene targets separated out into the first quadrant (Figure 4.7A), suggesting a slight difference in binding between B-MYB and FOXM1. This difference accounted for roughly 15% of the variation in our

CUT&RUN data and was reflected in PC2.

We used the PCA analysis component scores and measured how well each principal component correlated with cell cycle nascent RNA transcripts (Figure 4.8). We observed a right-handed positive shift with nascent gene expression (Figure 4.8A), suggesting that the PC1 component strongly indicates open chromatin accessibility as it correlates positively with high nascent transcription. Comparison of PC2 component to nascent RNA transcription revealed that FOXM1-specific significantly correlated with nascent RNA transcription (Figure 4.8B), implicating FOXM1 as a potent activator of transcription.

4.7 FOXM1 DEPENDS ON B-MYB TO ACTIVATE G2/M GENES.

We employed RT-qPCR of 4sU-labeled nascent RNA to validate our PRO-seq results and explore the role of B-MYB and FOXM1 in initiating the synthesis of G2/M genes. At defined time points, cells were pulse-labeled with 4-thiouridine (4sU), which is incorporated in actively transcribing RNA and can be subsequently isolated from total RNA by coupling to HPDP-biotin and purified over streptavidin beads[45,114]. G2/M gene expression in total and nascent RNA fractions was quantified by RT-qPCR and normalized to housekeeping gene TBP, a non-cell-cycle regulated gene.

We chose to validate two well-established G2/M genes: CCNB1 and CCNF. CUT&RUN in synchronized cells (15-hpr Palbociclib treatment) showed co-occupancy by B-MYB and FOXM1 on the CCNB1 gene promoter (Figure 4.9A), whereas FOXM1, not B-MYB, occupied the CCNF gene promoter (Figure 4.9B). We detected a robust transcriptional activation of CCNB1 and CCNF genes over time for total and nascent RNA in sgNTC cells, indicating the 4sU assay accurately portrays cell cycle transcrip-

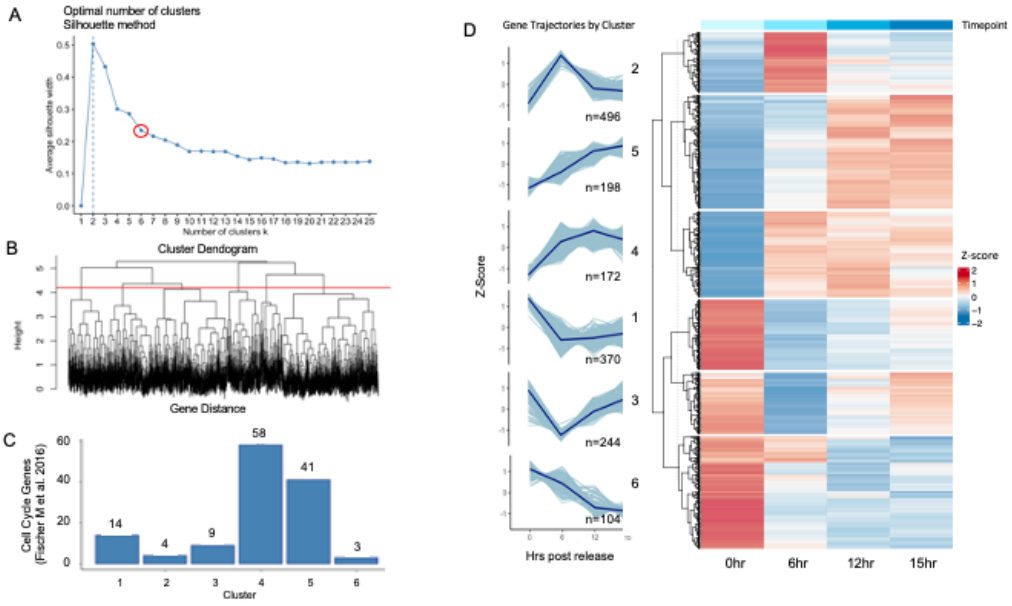

Figure 4.6: Nascent cell cycle gene synthesis peaks at 12 and 15 hours-post Palbociclib-synchronization and release A. Silhouette analysis to determine cluster number for differentially synthesized genes from the PRO-seq dataset. Circled in Red is the optimal cluster number. **B.** Dendrogram of differentially expressed genes. The red line denotes 6 cluster data structures. **C.** Bar graph summarizing the number of cell cycle genes per cluster. The cell cycle gene set was previously described by Fischer et al. 2016. **D.** Heatmap of differentially expressed genes. On the left are gene trajectories for each denoted cluster. The Z-score was calculated by Log2 transforming the normalized counts generated by DESeq.

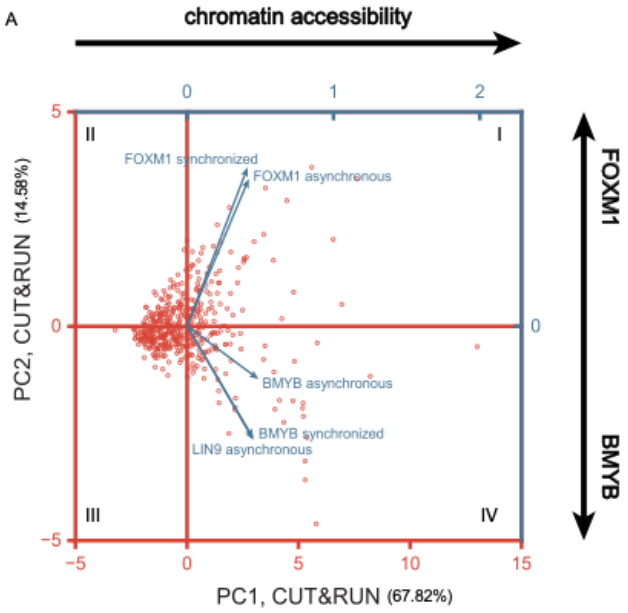

Figure 4.7: Principal component analysis of CUT&RUN data. A. PCA was generated using all CUT&RUN datasets. Each dot represents a cell cycle gene target and its combined chromatin accessibility profile for LIN9, B-MYB, and FOXM1. Binding changes were investigated at in asynchronous and palbociclib 15 hours-post release synchronized samples.

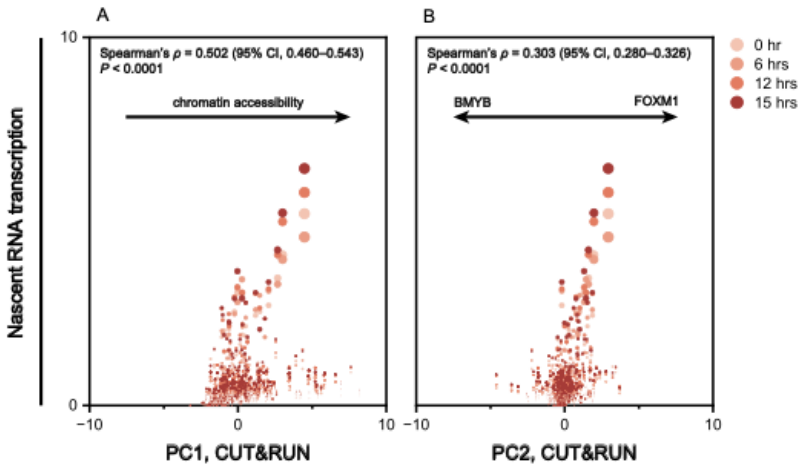

Figure 4.8: FOXM1 binding correlates with active cell cycle gene synthesis. A. Scatter plot of nascent cell cycle transcripts. On the x-axis is the PCA score for PC1 from Figure 3, which captures chromatin accessibility. **B.** Scatter plot of nascent cell cycle transcripts. On the x-axis is the PCA score for PC2 from Figure 3, which captures the differential binding between B-MYB and FOXM1.

tional changes. For CCNB1, expression loss of B-MYB delayed transcriptional activation at early time points, but by 18-hpr, total and nascent RNA reached levels comparable to control (Figure 4.9 C and D). These results suggest that FOXM1 is sufficient and necessary to activate CCNB1 expression. In contrast, loss of either B-MYB or FOXM1 impaired transcriptional activation of CCNF total and nascent RNA levels compared to control (Figure 4.9 E and F), suggesting both B-MYB and FOXM1 are required for the transactivation of CCNF.

4.8 FOXM1 DRIVES G2/M GENE EXPRESSION.

We reasoned that if FOXM1 was the main driver of G2/M genes, then loss of FOXM1 and not loss of B-MYB should impair G2/M gene expression. We performed an RNA-seq analysis of nocodazole synchronized cells to explore further the independent contributions of B-MYB and FOXM1 in regulating G2/M genes (Figure 4.10A). Nocodazole disrupts microtubule polymerization and impairs spindle fiber formation during metaphase, thus arresting cells in early mitosis[38]. G2/M gene expression is at its highest level as cells enter the M phase.

To comprehensively analyze the differences between B-MYB and FOXM1 gene regulation, we performed a hierarchical gene clustering analysis of the top 250 differentially expressed cell cycle genes. A silhouette score was used to estimate the distribution of the potential number of clusters using the NbClust R package (Figure 4.10B)[14]. We concluded five clusters best fit the expression patterns of the data. G2/M genes were primarily upregulated, whereas G1/S genes were mainly downregulated in nocodazole-treated sgNTC, suggesting an enrichment of G2/M gene expression following nocodazole treatment (Figure 4.10C). Cluster 4, comprised of

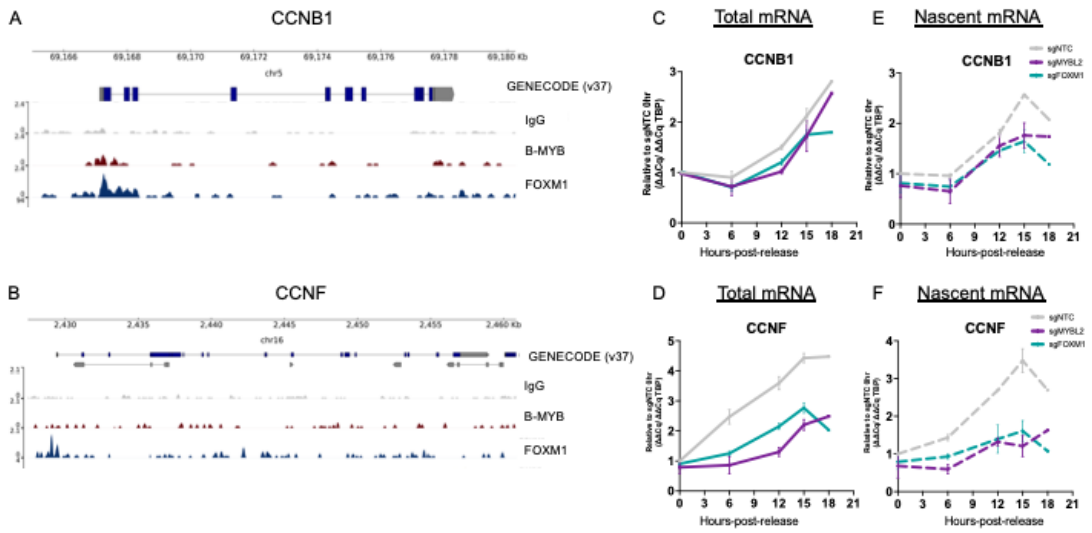

Figure 4.9: FOXM1 binding correlates with active cell cycle gene synthesis. A-B. CUT&RUN gene tracks for B-MYB and FOXM1 synchronized samples. Gene browser shots were generated using the integrative Genomics Viewer (IGV, Broad Institute). **C-D.** Cells were Palbociclib-synchronized and released. Total mRNA levels for G2/M genes for denoted time points. The cell cycle gene was normalized to housekeeping gene TBP total mRNA levels. Data represents fold change relative to 0hr (n=2).**E-F.** Nascent mRNA levels for a panel of G2/M genes at denoted time points. The cell cycle gene was normalized to housekeeping gene TBP nascent mRNA levels. Data represents fold change relative to 0hr (n=2).

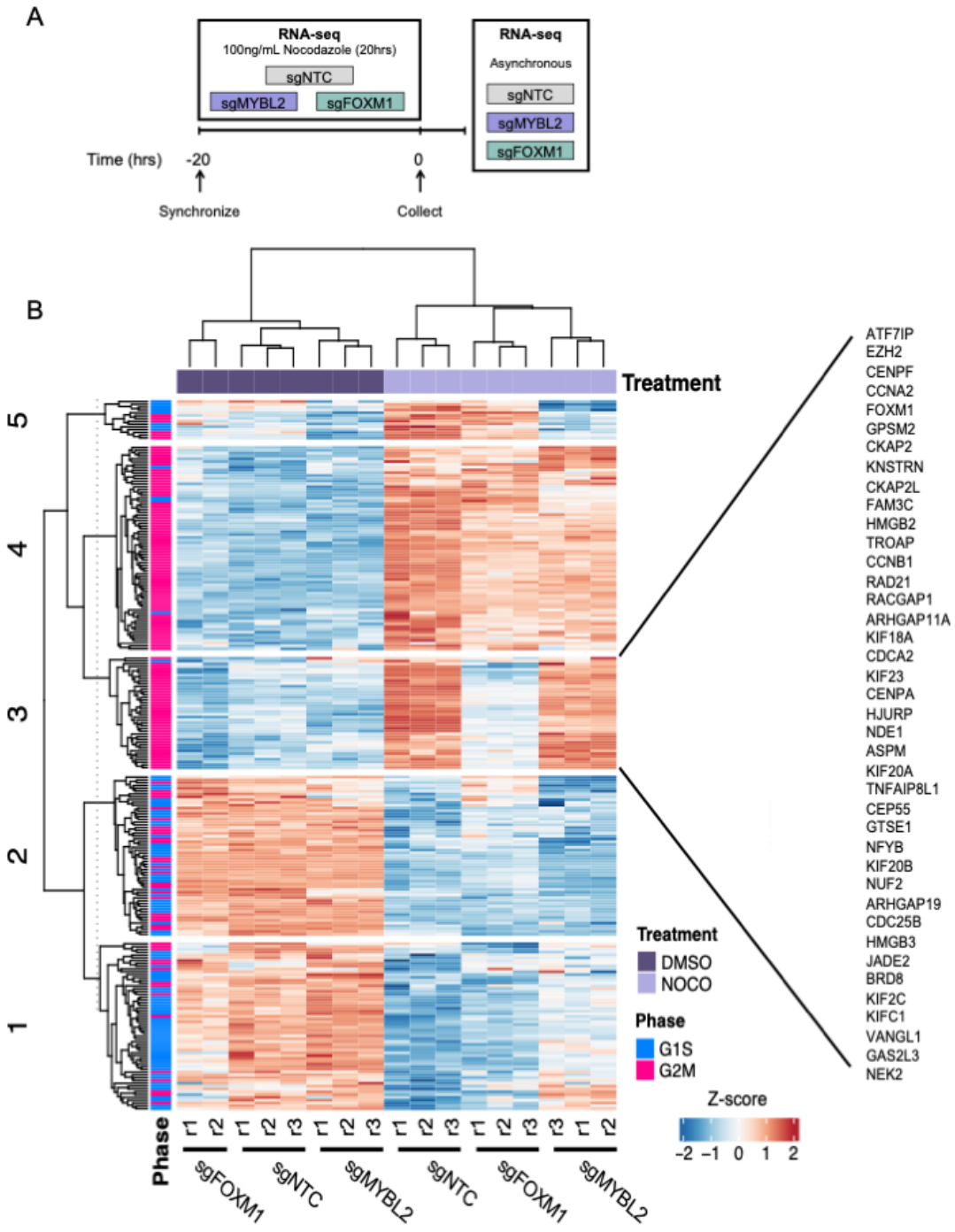

Figure 4.10: Loss of FOXM1 severely impairs G2/M gene expression compared to B-MYB loss. A. Schematic of nocodazole-treated RNA-sequencing experiments. **B.** Heatmap of top 250 differentially expressed cell cycle genes. Gene clusters are denoted on the left. The cell cycle phases for each gene are annotated: G1/S genes are in blue, and G2/M genes are in pink. Cluster 3 genes are highlighted.

G2/M genes, expression was induced in the control; however, loss of either B-MYB or FOXM1 partially impaired this induction, suggesting cooperative transcription between B-MYB and FOXM1 regulates cluster 4 expression. Expression of only a small subset of genes, concentrated in cluster 5, was directly suppressed in the B-MYB KO, suggesting that B-MYB alone facilitates but does not drive G2/M expression.

In contrast, expression of a large portion of G2/M genes, grouped in cluster 3, was suppressed in the FOXM1 KO. CCNB1 was amongst the genes in cluster 3, supporting our observation that FOXM1 is required for the nascent transcription of CCNB1. Overall, FOXM1 KO significantly reduced or completely suppressed the expression of G2/M genes (Figure 4.10C, clusters 3 and 4), implicating FOXM1 as a critical driver of G2/M expression.

4.8.1 Summary of Findings

In this chapter, we focused on understanding the individual contributions of B-MYB and FOXM1 in transactivating G2/M genes. We observed that B-MYB binds preferentially to G2/M gene promoters, while FOXM1 binds to G2/M and DNA damage gene promoters. We found that the MuvB component LIN9 binding correlates with B-MYB but not FOXM1. B-MYB-specific gene targets were enriched for the canonical MYB and CHR motifs. In contrast, FOXM1 gene targets were enriched for FOXP1 FKH DNA recognition motifs. Combining nascent transcript analysis (PRO-seq), RNA-seq, and CUT&RUN sequencing, we define FOXM1 as a critical transcriptional driver of cell cycle gene expression. Collectively, these findings indicate that B-MYB and FOXM1 cooperatively regulate the expression of cell cycle genes, where the MMB complex defines G2/M genes through association with MYB and CHR recognition motifs and enhances recruitment of FOXM1 to G2/M gene promot-

ers, where FOXM1 drives transcription of G2/M genes and DNA repair genes.

5

Discussion

5.1 Summary of Results

This dissertation investigates if B-MYB and FOXM1 cooperate to transactivate G2/M genes. We studied the contributions of the separate MMB-FOXM1 components in the cellular response to replication stress and cell cycle progression. Studies focused on understanding the function of the ssDNA sensor, ATR, during cell division demonstrated that ATR inhibition prematurely activated FOXM1, causing a breakdown of the S/G2 transition and leading to early mitosis, under-replicated DNA, and

DNA damage[118]. Our work generated LIN54, B-MYB, and FOXM1 knockout (KO) in human A549 cells, which were resistant to inhibition of ATR and CHK1, suggesting ATR signaling influences the MMB-FOXM1 complex, not just FOXM1.

Next, we sought to characterize the cell growth and division of B-MYB and FOXM1 knockout cells. Cell proliferation assays revealed that B-MYB KO cells and FOXM1 KO cells had similar cell doubling times compared to sgNTC control. However, cell cycle distribution analysis demonstrated that B-MYB KO cells and FOXM1 KO cells had a higher percentage of cells in the G2 phase than the sgNTC control. Notably, the knockout of B-MYB reduced, while the knockout of FOXM1 increased the percent of cells in the S phase, suggesting differences in cell cycle regulation between B-MYB and FOXM1. Cell cycle kinetic analyses revealed that FOXM1 KO cells had quicker S phase progression. At the same time, B-MYB KO cells had delayed entry into mitosis, suggesting that B-MYB and FOXM1 have shared roles, such as response to ATR and CHK1 inhibition, and distinct roles in regulating cell cycle progression.

Synchronization assays using B-MYB and FOXM1 knockout cells revealed that B-MYB KO uniquely impaired contact inhibition, a hallmark of cancer[57]. Under contact inhibition, the B-MYB KO cells had five times more cells in S phase and significantly fewer cells arrested in G1 than sgNTC control cells and FOXM1 KO cells. The B-MYB KO cells retained low levels of phosphorylated RB protein and several G2/M proteins, unlike the sgNTC control cells and sgFOXM1 KO cells, suggesting active replication under contact inhibition.

In contrast, both B-MYB and FOXM1 knockout cells synchronized well with CDK4 inhibitors, revealing a powerful system to study and directly compare the two knockout cells. These findings provide valuable insights into the mechanisms underlying the role of B-MYB in cell-cycle dysregulation and oncogenesis. Furthermore, these data

suggest that B-MYB and FOXM1 have overlapping but different effects on cell cycle control.

In the third chapter, we showed that B-MYB enhanced FOXM1 binding to DNA, and B-MYB-mediated recruitment of FOXM1 was critical for the onset of G2/M gene expression. In addition, we found that FOXM1 was required to regulate total and chromatin-associated B-MYB, indicating for the first time that the binding of B-MYB and FOXM1 to DNA is mutually dependent. Furthermore, we found that FOXM1 KO led to decreased levels of CCNF/cyclin F in mitosis, FOXM1 resulting in increased levels of cyclin F substrates RRM2. Despite the higher levels of mitotic B-MYB in the FOXM1 KO cells, FOXM1 KO cells had lower mRNA levels of several G2/M genes compared to B-MYB KO cells, suggesting a driving role for FOXM1 in the expression of G2/M genes.

In the fourth chapter, we focused on whether B-MYB and FOXM1 DNA binding was required for G2/M gene expression and whether B-MYB and FOXM1 equally contributed to the activation of G2/M genes. Analysis of CUT&RUN data indicated that B-MYB-specific gene targets were enriched for the canonical MYB and CHR motifs. We observed that FOXM1 gene targets were enriched for FOXP1 FKH DNA recognition motifs. B-MYB was exclusively bound to G2/M gene promoters, while FOXM1 was bound to G2/M and DNA damage gene promoters. This result expands on observations from Chapter Three, suggesting that FOXM1 can bind DNA in a sequence-specific manner and that FKH motif sites facilitate FOXM1 binding to DNA. We show that the MuvB component LIN9 binding correlates with B-MYB but not FOXM1, consistent with the cooperative binding of B-MYB with the MuvB complex to CHR sites[116,40]. Furthermore, we observed that B-MYB and FOXM1-bound gene targets contain MYB and FKH motifs, indicating that B-MYB, FOXM1, and MuvB

binding was due at least in part to specific DNA binding activities of each of these three components. Combining nascent RNA sequencing (PRO-seq), bulk RNA sequencing (RNA-seq), and promoter occupancy (CUT&RUN), we characterized the dynamic expression of G2/M genes at the G2/M phase, which implicated FOXM1 as the critical transcriptional driver of G2/M gene expression.

5.1.1 CRISPR-CAS9 GENE KNOCKOUT OF FOXM1 IS LOW-EFFICIENCY.

We demonstrated that B-MYB was dispensable for cell viability in A549 and hTERT-RPE-1. In contrast, we observed that FOXM1 was dispensable for A549 viability but could not confirm that FOXM1 was dispensible in the hTERT-RPE-1 cell line. Despite significant efforts, we could not generate FOXM1 KO cells in hTERT-RPE-1 cells. This could be due to various reasons. It is possible that FOXM1 KO is not tolerated in hTERT-RPE-1 cells. During this study, the Cimprich group published work using hTERT-RPE-1 FOXM1 knocked down cells, suggesting that acute loss of FOXM1 may be tolerated in hTERT-RPE-1 cells[118]. hTERT RPE-1 are non-cancerous cells and lack the cell cycle deregulation common to most cancer cells. The Dependency Map (DepMAP) database, which holds publicly available data of pan-cancer CRISPR-CAS9 screens, suggests that neither B-MYB nor FOXM1 are common essential genes in cancer cells.

Technical and not biological barriers may be why we could not knockout FOXM1 in hTERT-RPE-1 cells. One possibility is CRISPR-CAS9 guide efficiency, which could prevent the generation of polyclonal knockouts of FOXM1. Many factors affect the efficiency of single guide RNA (sgRNA) [Reviewed in[63]]. The GC content, secondary structure, and sgRNA activity score can all influence efficiency, making it challenging to predict successful guides accurately. We used three separate sgRNA

design algorithm tools with different design algorithms and cut-offs to address this possibility. We tested the top four highest-scoring efficiency and specificity guides but could not knock out FOXM1 in hTERT-RPE-1 cells. To note, hTERT-RPE-1 cells did not grow in single-cell conditions, making it impossible to screen for single-cell knockout clones as was the case for the A549 knockout clones.

An alternative approach and potential future direction for studying the G2/M transcription factors would be to use an inducible degron system[144], which promotes the rapid and targeted degradation of target proteins. A FOXM1-degron module fusion protein would be generated and constitutively expressed in the desired cell line. Subsequently, FOXM1 protein levels could be selectively and rapidly degraded, enabling the precise and reversible loss of FOXM1. One future experiment could test how the degron-mediated knockdown of FOXM1 affects cells directly entering S phase or G2 phase, expanding on the temporal regulation and transactivation of G2/M gene expression.

Generating an inducible degron-mediated knockdown system for FOXM1 could also be a powerful approach for double knockout experiments of B-MYB and FOXM1. This work did not test whether double knockout of B-MYB or FOXM1 was viable in A549 or RPE-1 cells, and lethality may be associated with constitutive knockout of both transcription factors. If this were the case, an inducible FOXM1 degron-tagged cell line could be infected with multi-guide mxgMYBL2 lentivirus to develop an inducible double knockout cell line. If a B-MYB-FOXM1 double knockout is feasible, then an inducible degron-system may be used to try and generate a triple knockout system, where B-MYB, FOXM1, and MuvB component LIN54 are all functionally lost.

5.1.2 THE ATR-CHK1 SIGNALING DEPENDS ON THE MMB-FOXM1 COMPLEX.

The ATR-CHK1 pathway plays a central role in the cellular response to DNA damage during S/G2[118]. As part of a separate project, Dr. Alan D'Andrea's lab from Dana-Farber's Center for DNA Damage and Repair performed a genome-wide CRISPR-Cas9 screen to identify genes that, when lost, confer resistance to CHK1 inhibition ([11]). We validated that B-MYB, KO, LIN54 KO, or FOXM1 KO, in two multiple cell lines, led to a 200-fold resistance to CHK1 inhibition and a 5-fold resistance to ATR inhibition compared to control cells. These observations revealed a critical role for the MMB-FOXM1 complexes in the S phase DNA damage response[11]. Given the robust resistance we observed for LIN54 (MuvB), B-MYB, and FOXM1 knockout cells to CHK1 and ATR inhibitors, it is possible that impairment of MMB-FOXM1 complexes also alters sensitivity to additional DNA replication stress inducers. LIN54, B-MYB, or FOXM1 have been suggested to increase resistance to gemcitabine, fludarabine, cytarabine, and hydroxyurea compared to control empty vector cells, as these inhibitors reportedly activate a strong ATR response[9,85,67].

Future experiments could focus on studying whether B-MYB and FOXM1 knockout affects sensitivity to replication stress inducers, particularly those used clinically for the treatment of solid tumors or hematologic malignancies like Gemcitabine (cytosine analog), Fludarabine (adenosine analog), Cytarabine (cytosine analog), Methotrexate (inhibitor of de novo purine and pyrimidine synthesis), camptothecin (topoisomerase I poison), and doxorubicin (DNA intercalator).

5.1.3 THE ROLE OF B-MYB IN ONCOGENESIS MAY BE MULTI-FACETED.

In this dissertation, we made a novel observation that B-MYB knockout impairs contact inhibition, a phenomenon often associated with cancer cells and tumorigenesis[57]. There are several studies emphasizing how high levels of B-MYB play an important role in different cancer types. For instance, elevated B-MYB expression correlates with poor prognosis in non-small-cell lung cancer patients[34]. B-MYB has been identified as a critical regulator of cell cycle progression in colorectal cancer and is associated with increased cell proliferation[35]. Additionally, studies in ovarian cancer found high B-MYB expression was correlated with poor overall survival[61]. Our work suggests that loss of B-MYB can also dysregulate cell proliferation and promote cancer-like phenotypes.

The mechanism by which loss of B-MYB impairs a cell's ability to contact inhibit is unknown. Recent studies have shown that the transcriptional factor YAP (Yes-associated protein) directly interacts with MMB to activate a subset of G2/M genes ([105,51,39]). YAP is a downstream effector of the Hippo signaling pathway, which senses cell density and cell-to-cell contact([148]). When cells are densely packed, the Hippo pathway is activated, leading to the phosphorylation and cytoplasmic retention of YAP. Hyper-phosphorylated YAP cannot enter the nucleus and is rendered transcriptionally inactive. The YAP and B-MYB interaction may explain the persistent G2/M population we observed in contact-inhibited cells. Immunoblot analysis of phospho-YAP in cells exposed to contact inhibition revealed consistently elevated levels of phospho-YAP across all cell lines, suggesting YAP was inactivated. Contact inhibition of B-MYB KO cells may result in a YAP/B-MYB double knockout mimic. Despite the low levels of a small range of G2/M proteins, it is possible contact-inhibited

B-MYB knockouts do not have the transcriptional capacity to produce high enough levels of CDK1, which coordinates the entry and progression of mitosis[46,129].

In parallel, sustained levels of cell cycle proteins or the failure to degrade G2/M proteins could facilitate cells to continue cycling under contact inhibition. APC/C component CDC20 and Cyclin B1 protein levels, two critical regulatory G2/M genes[40], persisted in the sgMYBL2 knockout cells under contact inhibition. This effect was specific at the protein level as CDC20 and Cyclin B1 mRNA levels were all reduced across all cell lines following contact inhibition. Cyclin B1 accumulates during the G2 phase and forms a complex with CDK1, triggering entry into mitosis[75]. The Cyclin-B-CDK1 complex activates the anaphase-promoting complex/cyclosome (APC/C)-CDH1 complex, which plays a crucial role in the degradation of specific proteins during the G2/M transition, ensuring proper progression through mitosis[131]. Inactivation or reduced APC/C-CDH1 complex activity could lead to a breakdown in the timely degradation of G2/M proteins. Along with the expression of G1/S proteins like PCNA and MCM2 that were detected under contact inhibition, these factors combined could be driving entry into S phase observed in the B-MYB knockout cells.

5.1.4 B-MYB AND FOXM1 BINDING OF DNA IS INTERDEPENDENT.

Before this study, there were three conflicting models proposed for FOXM1 binding to DNA: (1) FOXM1 interacts with MMB and binds directly to gene promoters at sites containing an FKH consensus motif[116], (2) FOXM1 does not directly bind to DNA but is recruited to gene promoters by MMB[16], and (3) FOXM1 binds to non-consensus sequences facilitated by interaction with the MMB complex[120]. We found that B-MYB KO severely impaired but did not abolish FOXM1 binding, suggesting B-MYB enhances FOXM1 DNA binding (Figure 5.1A). CUT&RUN analysis

of FOXM1 binding sites expanded on this observation, demonstrating that FOXM1-specific gene targets contain FKH motifs, suggesting FOXM1 binding is dependent on FKH motif recognition. Therefore, our work supports the first model, or cooperativity between B-MYB and FOXM1, where B-MYB enhances FOXM1 binding of FKH motif recognition sites.

A largely unanswered question is if B-MYB recruits FOXM1 to DNA. Our work suggests that B-MYB facilitates the recruitment of FOXM1 to DNA, as knockout of B-MYB significantly reduced the level of chromatin-association FOXM1 measured by flow cytometry and immunoblot. We could not successfully test the association between endogenous B-MYB and FOXM1 by co-immunoprecipitation (co-IP). We used the FOXM1 knockout-validated antibody for these experiments, which is not validated for co-IPs. This antibody may lack enough specificity for FOXM1 as high background signal and non-specific proteins were observed for both sgNTC control and sgFOXM1 lysates.

An alternative approach to validate B-MYB and FOXM1 association would be to perform Proximity-Labeling mass-spectrometry (APEX-MS)[81]. B-MYB or FOXM1 would be fused to a peroxidase (ascorbic acid peroxidase; APEX). Following treatment of cells with H_2O_2, APEX converts exogenously supplied biotin-phenol to biotin-phenoxyl radicals and promotes the covalent labeling of proteins within a radius of 20nm. Subsequently, the biotinylated proteins can be isolated using Steptavidin. The eluted protein can then be processed and analyzed by MS. This approach would provide a "snap-shot" of the interactome for B-MYB and FOXM1, which paired with the Palbociclib synchronization and release assay to look at the dynamic changes in protein interactors across different points in the cell cycle.

Post-translational modifications of FOXM1 may facilitate recruitment by B-MYB.

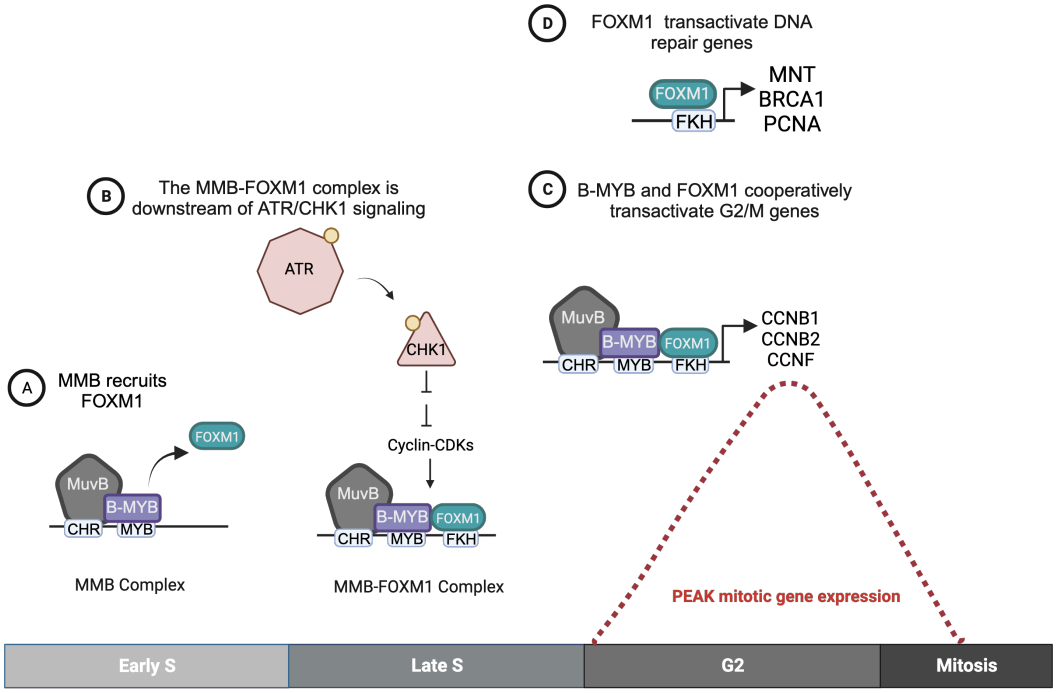

Figure 5.1: B-MYB and FOXM1 cooperatively activate G2/M gene expression A. B-MYB recruits FOXM1 to G2/M gene promoters by enhancing FOXM1 association to DNA. **B.** The MMB-FOXM1 complexes are downstream of the ATR-CHK1 signaling pathway and are required for cellular sensitivity to ATR and CHK1 inhibitors. **C.** MMB recruitment of FOXM1 forms the MMB-FOXM1 complex, which is the complex that transactivates G2/M gene expression. B-MYB and FOXM1 DNA binding are mutually dependent. FOXM1 is a potent transcriptional driver that regulates B-MYB degradation, forming a regulatory feedback loop between the two transcription factors. **D.** FOXM1 binds to promoters of DNA repair genes.

FOXM1 is maintained in a relatively low phosphorylated state in the early S phase. During this time, B55, a subunit of protein phosphatase 2A, keeps phospho-FOXM1 levels low through association with FOXM1 and repression of cyclin A-CDK[2,1]. Starting in the late S and into the G2 phase, FOXM1 undergoes progressive multisite phosphorylation and reaches a hyperphosphorylated state in M phase[17,85,84,73,43]. Phosphorylation at S715 by the cyclin-B1-Cdk1 complex permits association and further phosphorylation by the Polo-Like-Kinase 1 (PLK1)[43]. Recent structural work has demonstrated that phosphorylation of FOXM1 induces a series of conformation changes, from ordered to disordered, which facilitates the PLK1 interaction[89]. It is possible that, like in the case of PLK1, phosphorylation of FOXM1 induces conformational changes that favor the B-MYB-FOXM1 interaction.

CDK-dependent phosphorylation sites span across the entire FOXM1 protein, including the N-terminal autoinhibitory domain that is required for MuvB binding[73,103]. One potential approach to determine whether FOXM1 phosphorylation is necessary for interacting with B-MYB is to alanine mutate the 15 CDK phosphorylation sites spanning the FOXM1 protein. Using our mutant FOXM1 cell lines, we could investigate protein-protein interactions by APEX proximity labeling and conduct further experiments focused on functionally characterizing those interactions.

Cooperative recognition of DNA can occur through many mechanisms. Alternatively, one possibility is MMB binding to DNA increases chromatin accessibility, which exposes DNA to FOXM1 binding. Structural work focused on MuvB assembly and function showed that MuvB bound to trimethylated Histone H3 at lysine 9 (H3K9me3), a chromatin modification known to mark heterochromatin and transcriptionally repressed genes[3]. B-MYB is activated and associated with the MuvB complex in the early S phase, switching MuvB from a transcriptionally repressive to a

transcriptionally activating complex[116]. It is possible that B-MYB binding to MuvB promotes disassociation with repressive H3 marks, recruits epigenetic remodelers for deposition of active transcription marks that increase chromatin accessibility, and exposes naked DNA containing FKH motifs for FOXM1 recruitment.

Structural information is available regarding how MuvB recruits B-MYBv; however, there is no solved structure for the MMB-FOXM1 complex. In the MMB complex, the B-MYB c-terminus directly interacts with MuvB components LIN9 and LIN52[52]. The transcription factor LIN52 is central within the MuvB complex, and a BMYBLIN52 MuvB interface could be a promising target for chemical inhibitors[52]. Whether LIN52 is also essential for binding FOXM1 to B-MYB is unknown.

Future structural work should emphasize elucidating the binding sites and interactions within the MMB-FOXM1 complex, which could also aid in developing targeted therapeutics. Currently, there are also two partial structures solved for FOXM1. Structural details of the FoxM1 DNA-recognition domain identified key contacts between FOXM1 and DNA and suggested the interaction itself could be weak[78]. A more recent study explored the autoinhibition mechanism of FOXM1, solving a solution structure for the negative regulatory and transactivation domains of FOXM1[89]. The group found that a structural switch facilitates activation of FoxM1, where the switch transitions from an ordered to a disordered state that permits phosphorylation and binding to co-factors like PLK1. The development of FOXM1 as a therapeutic inhibitor for cancer is underway[18,147]. A comprehensive understanding of the structural aspects governing the interaction and DNA binding of B-MYB and FOXM1 could play pivotal roles in designing effective inhibitors for cancer treatment.

5.1.5 B-MYB, NOT FOXM1, BINDING IS SPECIFIC TO G2/M GENES.

CUT&RUN analysis of B-MYB and FOXM1 found that B-MYB preferentially bound to G2/M gene promoters, while FOXM1 bound to G2/M and DNA damage genes. B-MYB may function as a pioneer transcription factor for G2/M genes. Our work suggests that B-MYB alone is insufficient for transactivating G2/M genes (Figure 5.1C). Despite elevated levels of B-MYB observed in the FOXM1 KO cells, B-MYB alone could not support G2/M gene expression without FOXM1. In the FOXM1 KO cells where B-MYB chromatin binding is increased, elevated B-MYB could disrupt DREAM complex formation and promote quicker cell cycle progression.

High levels of B-MYB disrupt DREAM complex formation[59,61]. The DREAM complex is a transcriptional repressor complex that works in parallel with RB to repress cell cycle gene expression in G0/G1[124]. De-repression of cell cycle genes accelerates the progression of the cell cycle. Cell cycle kinetic assays revealed that FOXM1 KO cells had quicker S phase entry and progression, while B-MYB KO cells had significantly delayed entry into mitosis. To test whether elevated B-MYB levels disrupt the DREAM complex in FOXM1 KO cells, immunoprecipitation experiments could focus on testing whether the DREAM complex forms in FOXM1 KO cells under contact inhibition.

Interestingly, we observed that FOXM1 KO cells had lower CCNB1 and CCNF mRNA levels than B-MYB KO and sgNTC control, suggesting that FOXM1 could be the primary driver of G2/M gene expression. In line with this result, early studies looking at B-MYB transactivation and function observed that B-MYB is a weak transcriptional activator[42,137].

The biochemical consequences of the association between B-MYB and the MuvB

complex remain unclear and poorly understood. The MMB complex may facilitate the unwinding of compact nucleosomes to increase chromatin accessibility for other transcription factors like FOXM1 to bind DNA and initiate transcription of G2/M target genes.

ATAC-sequencing would directly test whether B-MYB and MuvB cooperate to increase chromatin accessibility at G2/M gene promoters. With our established and validated Palbociclib synchronization and release assay, we could perform ATAC-sequencing at early time points (0, 3, and 6 h post-release) when we know B-MYB is bound to DNA but G2/M genes are not actively expressed. We can compare chromatin accessibility across time points and genetic backgrounds using our sgNTC control, sgMYBL2, and sgLIN54 cell lines. Paired with CUT&RUN of active H3K4me3 and repressive H3K27me3 histones, we could see if enrichment of activating histone mark correlates with increased chromatin accessibility. If B-MYB is critical for unwinding and opening up the TSS of G2/M promoters, G2/M promoter accessibility would be impaired without B-MYB.

5.1.6 FOXM1 TRANSACTIVATES THE EXPRESSION OF G2/M AND DNA DAMAGE GENES.

We found that FOXM1 bound near G2/M and DNA repair gene promoters. Integration of CUT&RUN sequencing and nascent RNA sequencing demonstrated that FOXM1 gene targets significantly correlated with nascent mRNA synthesis, implicating FOXM1 as a potent transcriptional activator. Furthermore, these data support several lines of evidence suggesting FOXM1 plays a crucial role in the DNA damage response.

FOXM1 has been suggested to transactivate several DNA damage sensors, mediators, signal transducers, and effectors (reviewed[152]). Knockdown of FOXM1 has been

shown to regulate the expression of genes involved in DNA repair processes, including homologous recombination and nucleotide excision repair following irradiation or treatment with doxorubicin[55]. A current obstacle in the field is the absence of a unified list of genes regulated by FOXM1. Subsequent efforts could concentrate on mining publicly available RNA-seq data, incorporating data from knockout-generated cell lines, and accounting for potential variations across different cell types to comprehensively examine and delineate FOXM1 gene targets.

Our work and others have shown that FOXM1 plays a crucial role in coordinating cell cycle progression after DNA damage[11,119,134]. Subsequent experiments could focus on characterizing the FOXM1-mediated response to cycle regulators such as CDK (Cyclin-Dependent Kinase) inhibitors, PLK inhibitors, and Aurora Kinase inhibitors that are actively investigated in clinical trials for various cancers. Flavopiridol and Dinaciclib are examples of broad-spectrum CDK inhibitors that have been studied in clinical trials[49,68]. Volasertib is a PLK inhibitor undergoing clinical trials for various cancers[127,31]. Alisertib is an Aurora A kinase inhibitor evaluated in several recent clinical trials[6,10]. It is crucial to determine whether FOXM1 plays a role in the sensitivity to these inhibitors and if a patient's FOXM1 mutation status can be informative for treatment decisions.

5.1.7 A REGULATORY FEEDBACK LOOP BETWEEN B-MYB AND FOXM1 COORDINATES G2/M GENE EXPRESSION.

Our work found that FOXM1 negatively regulated B-MYB binding to DNA. In FOXM1 knockout cells, there was higher total B-MYB protein and chromatin-associated B-MYB protein than sgNTC control cells, suggesting that loss of FOXM1 activity may stabilize B-MYB levels. Currently, the mechanism for B-MYB degradation is

poorly understood. Hyperphosphorylation of B-MYB enhances transcriptional activity[123] and stimulates increased multisite ubiquitination of B-MYB[15]. FOXM1 KO severely impaired cyclin F mRNA and protein levels compared to B-MYB KO and control cells. Cyclin F is a G2/M gene that encodes for an F-box protein belonging to the Skp1-Cullin-F-box (SCF) ubiquitin ligase type family[33]. As a substrate recognition receptor for the SCF family of E3 ligases, cyclin F degrades several G1/S cell cycle proteins like p130[33], activating E2Fs[22], and RRM2[24]. Correlating with the loss of cyclin F protein, we observed aberrant elevated levels of RRM2 in mitosis. Cyclin F has been shown to directly interact with B-MYB via the cyclin box domain to B-MYB[70] and provides an attractive mechanism for B-MYB degradation.

Subsequent experiments could investigate whether the cyclin F knockout leads to the accumulation of B-MYB and RRM2 protein levels during mitosis. The complete set of proteins regulated by cyclin F remains poorly understood. Conducting mass spectrometry experiments with cyclin F knockout cells could unveil the spectrum of cyclin F targets and unbiasedly examine whether B-MYB is directly regulated. If this is the case, conducting experiments involving the overexpression of cyclin F in FOXM1 knockouts could serve as an additional validation step.

Collectively, our work has shown that B-MYB facilitates FOXM1 cooperative binding to DNA and FOXM1, in turn, suppressing B-MYB through a currently unknown mechanism, B-MYB and FOXM1 exist in a regulatory feedback loop that coordinates G2/M expression.

References

[1] Alvarez-Fernández, M., Halim, V. A., Aprelia, M., Laoukili, J., Mohammed, S., & Medema, R. H. (2011). Protein phosphatase 2A (B55) prevents premature activation of forkhead transcription factor FoxM1 by antagonizing cyclin A/cyclin-dependent kinase-mediated phosphorylation. *The Journal of Biological Chemistry*, 286(38), 33029–33036.

[2] Anders, L., Ke, N., Hydbring, P., Choi, Y. J., Widlund, H. R., Chick, J. M., Zhai, H., Vidal, M., Gygi, S. P., Braun, P., & Sicinski, P. (2011). A systematic screen for CDK4/6 substrates links FOXM1 phosphorylation to senescence suppression in cancer cells. *Cancer Cell*, 20(5), 620–634.

[3] Asthana, A., Ramanan, P., Hirschi, A., Guiley, K. Z., Wijeratne, T. U., Shelansky, R., Doody, M. J., Narasimhan, H., Boeger, H., Tripathi, S., Müller, G. A., & Rubin, S. M. (2022). The MuvB complex binds and stabilizes nucleosomes downstream of the transcription start site of cell-cycle dependent genes. *Nature Communications*, 13(1), 526. Number: 1 Publisher: Nature Publishing Group.

[4] Bar-Joseph, Z., Siegfried, Z., Brandeis, M., Brors, B., Lu, Y., Eils, R., Dynlacht, B. D., & Simon, I. (2008). Genome-wide transcriptional analysis of the human cell cycle identifies genes differentially regulated in normal and cancer cells. *Proceedings of the National Academy of Sciences*, 105(3), 955–960. Publisher: National Academy of Sciences Section: Biological Sciences.

[5] Barger, C. J., Branick, C., Chee, L., & Karpf, A. R. (2019). Pan-Cancer Analyses Reveal Genomic Features of FOXM1 Overexpression in Cancer. *Cancers*, 11(2), 251.

[6] Beltran, H., Oromendia, C., Danila, D. C., Montgomery, B., Hoimes, C., Szmulewitz, R. Z., Vaishampayan, U., Armstrong, A. J., Stein, M., Pinski, J., Mosquera, J. M., Sailer, V., Bareja, R., Romanel, A., Gumpeni, N., Sboner, A., Dardenne, E., Puca, L., Prandi, D., Rubin, M. A., Scher, H. I., Rickman, D. S., Demichelis, F., Nanus, D. M., Ballman, K. V., & Tagawa, S. T. (2019). A Phase II Trial of the Aurora Kinase A Inhibitor Alisertib for Patients with Castration-resistant and Neuroendocrine Prostate Cancer: Efficacy and Biomarkers. *Clini-*

cal Cancer Research: An Official Journal of the American Association for Cancer Research, 25(1), 43–51.

[7] Bergholtz, S., Andersen, T. ., Andersson, K. B., Borrebæk, J., Lüscher, B., & Gabrielsen, O. S. (2001). The highly conserved DNA-binding domains of A-, B- and c-Myb differ with respect to DNA-binding, phosphorylation and redox properties. *Nucleic Acids Research*, 29(17), 3546–3556.

[8] Bertoli, C., Skotheim, J. M., & de Bruin, R. A. M. (2013). Control of cell cycle transcription during G1 and S phases. *Nature Reviews. Molecular Cell Biology*, 14(8), 518–528.

[9] Beyaert, M., Starczewska, E., Pérez, A. C. G., Vanlangendonck, N., Saussoy, P., Tilman, G., De Leener, A., Vekemans, M.-C., Van Den Neste, E., & Bontemps, F. (2017). Reevaluation of ATR signaling in primary resting chronic lymphocytic leukemia cells: evidence for pro-survival or pro-apoptotic function. *Oncotarget*, 8(34), 56906–56920.

[10] Blakely, C. M., Gubens, M. A., Allen, G. M., Shah, S., Jereza, M., Bacaltos, B., & Bandyopadhyay, S. (2021). Phase I study of the aurora kinase A inhibitor alisertib in combination with osimertinib in EGFR-mutant lung cancer. *Journal of Clinical Oncology*, 39(15_suppl), 9074–9074. Publisher: Wolters Kluwer.

[11] Branigan, T. B., Kozono, D., Schade, A. E., Deraska, P., Rivas, H. G., Sambel, L., Reavis, H. D., Shapiro, G. I., D'Andrea, A. D., & DeCaprio, J. A. (2021). MMB-FOXM1-driven premature mitosis is required for CHK1 inhibitor sensitivity. *Cell Reports*, 34(9), 108808.

[12] Calvisi, D. F., Simile, M. M., Ladu, S., Frau, M., Evert, M., Tomasi, M. L., Demartis, M. I., Daino, L., Seddaiu, M. A., Brozzetti, S., Feo, F., & Pascale, R. M. (2011). Activation of v-Myb avian myeloblastosis viral oncogene homolog-like2 (MYBL2)-LIN9 complex contributes to human hepatocarcinogenesis and identifies a subset of hepatocellular carcinoma with mutant p53. *Hepatology*, 53(4), 1226–1236. _eprint: https://onlinelibrary.wiley.com/doi/pdf/10.1002/hep.24174.

[13] Carr, J. R., Kiefer, M. M., Park, H. J., Li, J., Wang, Z., Fontanarosa, J., DeWaal, D., Kopanja, D., Benevolenskaya, E. V., Guzman, G., & Raychaudhuri, P. (2012). FoxM1 Regulates Mammary Luminal Cell Fate. *Cell Reports*, 1(6), 715–729.

[14] Charrad, M., Ghazzali, N., Boiteau, V., & Niknafs, A. (2014). NbClust: An R Package for Determining the Relevant Number of Clusters in a Data Set. *Journal of Statistical Software*, 61, 1–36.

[15] Charrasse, S., Carena, I., Brondani, V., Klempnauer, K. H., & Ferrari, S. (2000). Degradation of B-Myb by ubiquitin-mediated proteolysis: involvement of the Cdc34-SCF(p45Skp2) pathway. *Oncogene*, 19(26), 2986–2995.

[16] Chen, X., Müller, G. A., Quaas, M., Fischer, M., Han, N., Stutchbury, B., Sharrocks, A. D., & Engeland, K. (2013). The forkhead transcription factor FOXM1 controls cell cycle-dependent gene expression through an atypical chromatin binding mechanism. *Molecular and Cellular Biology*, 33(2), 227–236.

[17] Chen, Y.-J., Dominguez-Brauer, C., Wang, Z., Asara, J. M., Costa, R. H., Tyner, A. L., Lau, L. F., & Raychaudhuri, P. (2009). A conserved phosphorylation site within the forkhead domain of FoxM1B is required for its activation by cyclin-CDK1. *The Journal of Biological Chemistry*, 284(44), 30695–30707.

[18] Chesnokov, M. S., Halasi, M., Borhani, S., Arbieva, Z., Shah, B. N., Oerlemans, R., Khan, I., Camacho, C. J., & Gartel, A. L. (2021). Novel FOXM1 inhibitor identified via gene network analysis induces autophagic FOXM1 degradation to overcome chemoresistance of human cancer cells. *Cell Death & Disease*, 12(7), 1–13. Number: 7 Publisher: Nature Publishing Group.

[19] Cimprich, K. A., Shin, T. B., Keith, C. T., & Schreiber, S. L. (1996). cDNA cloning and gene mapping of a candidate human cell cycle checkpoint protein. *Proceedings of the National Academy of Sciences*, 93(7), 2850–2855. Publisher: Proceedings of the National Academy of Sciences.

[20] Classon, M. & Dyson, N. (2001). p107 and p130: Versatile Proteins with Interesting Pockets. *Experimental Cell Research*, 264(1), 135–147.

[21] Claudio, P. P., De Luca, A., Howard, C. M., Baldi, A., Firpo, E. J., Koff, A., Paggi, M. G., & Giordano, A. (1996). Functional analysis of pRb2/p130 interaction with cyclins. *Cancer Research*, 56(9), 2003–2008.

[22] Clijsters, L., Hoencamp, C., Calis, J. J. A., Marzio, A., Handgraaf, S. M., Cuitino, M. C., Rosenberg, B. R., Leone, G., & Pagano, M. (2019). Cyclin F Controls Cell-Cycle Transcriptional Outputs by Directing the Degradation of the Three Activator E2Fs. *Molecular Cell*, 74(6), 1264–1277.e7.

[23] Crozier, L., Foy, R., Mouery, B. L., Whitaker, R. H., Corno, A., Spanos, C., Ly, T., Gowen Cook, J., & Saurin, A. T. (2022). CDK4/6 inhibitors induce replication stress to cause long-term cell cycle withdrawal. *The EMBO journal*, 41(6), e108599.

[24] D'Angiolella, V., Donato, V., Forrester, F. M., Jeong, Y.-T., Pellacani, C., Kudo, Y., Saraf, A., Florens, L., Washburn, M. P., & Pagano, M. (2012). Cyclin F-mediated degradation of ribonucleotide reductase M2 controls genome integrity and DNA repair. *Cell*, 149(5), 1023–1034.

[25] de Gooijer, M. C., van den Top, A., Bockaj, I., Beijnen, J. H., Würdinger, T., & van Tellingen, O. (2017). The G2 checkpointa node-based molecular switch. *FEBS Open Bio*, 7(4), 439–455. _eprint: https://onlinelibrary.wiley.com/doi/pdf/10.1002/2211-5463.12206.

[26] de Klein, A., Muijtjens, M., van Os, R., Verhoeven, Y., Smit, B., Carr, A. M., Lehmann, A. R., & Hoeijmakers, J. H. (2000). Targeted disruption of the cell-cycle checkpoint gene ATR leads to early embryonic lethality in mice. *Current biology: CB*, 10(8), 479–482.

[27] de Moraes, G. N., Khongkow, P., Gong, C., Yao, S., Gomes, A. R., Ji, Z., Kandola, N., Delbue, D., Man, E. P. S., Khoo, U. S., Sharrocks, A. D., & Lam, E. W.-F. (2015). Forkhead box K2 modulates epirubicin and paclitaxel sensitivity through FOXO3a in breast cancer. *Oncogenesis*, 4(9), e167–e167. Number: 9 Publisher: Nature Publishing Group.

[28] Doench, J. G., Fusi, N., Sullender, M., Hegde, M., Vaimberg, E. W., Donovan, K. F., Smith, I., Tothova, Z., Wilen, C., Orchard, R., Virgin, H. W., Listgarten, J., & Root, D. E. (2016). Optimized sgRNA design to maximize activity and minimize off-target effects of CRISPR-Cas9. *Nature Biotechnology*, 34(2), 184–191.

[29] Dominguez, D., Tsai, Y.-H., Gomez, N., Jha, D. K., Davis, I., & Wang, Z. (2016). A high-resolution transcriptome map of cell cycle reveals novel connections between periodic genes and cancer. *Cell Research*, 26(8), 946–962.

[30] Down, C. F., Millour, J., Lam, E. W.-F., & Watson, R. J. (2012). Binding of FoxM1 to G2/M gene promoters is dependent upon B-Myb. *Biochimica et Biophysica Acta (BBA) - Gene Regulatory Mechanisms*, 1819(8), 855–862.

[31] Doz, F., Locatelli, F., Baruchel, A., Blin, N., De Moerloose, B., Frappaz, D., Dworzak, M., Fischer, M., Stary, J., Fuertig, R., Riemann, K., Taube, T., & Reinhardt, D. (2019). Phase I dose-escalation study of volasertib in pediatric patients with acute leukemia or advanced solid tumors. *Pediatric Blood & Cancer*, 66(10), e27900.

[32] Dyson, N. J. (2016). RB1: a prototype tumor suppressor and an enigma. *Genes & Development*, 30(13), 1492–1502. Company: Cold Spring Harbor Laboratory Press Distributor: Cold Spring Harbor Laboratory Press Institution: Cold Spring Harbor Laboratory Press Label: Cold Spring Harbor Laboratory Press Publisher: Cold Spring Harbor Lab.

[33] Enrico, T. P., Stallaert, W., Wick, E. T., Ngoi, P., Wang, X., Rubin, S. M., Brown, N. G., Purvis, J. E., & Emanuele, M. J. (2021). Cyclin F drives proliferation through SCF-dependent degradation of the retinoblastoma-like tumor

suppressor p130/RBL2. *eLife*, 10, e70691. Publisher: eLife Sciences Publications, Ltd.

[34] Fan, X., Wang, Y., Jiang, T., Cai, W., Jin, Y., Niu, Y., Zhu, H., & Bu, Y. (2018). B-Myb Mediates Proliferation and Migration of Non-Small-Cell Lung Cancer via Suppressing IGFBP3. *International Journal of Molecular Sciences*, 19(5), 1479.

[35] Fan, X., Wang, Y., Jiang, T., Liu, T., Jin, Y., Du, K., Niu, Y., Zhang, C., Liu, Z., Lei, Y., & Bu, Y. (2021). B-Myb accelerates colorectal cancer progression through reciprocal feed-forward transactivation of E2F2. *Oncogene*, 40(37), 5613–5625.

[36] Fassl, A., Geng, Y., & Sicinski, P. (2022). CDK4 and CDK6 kinases: From basic science to cancer therapy. *Science (New York, N.Y.)*, 375(6577), eabc1495.

[37] Feng, J., Liu, T., Qin, B., Zhang, Y., & Liu, X. S. (2012). Identifying ChIP-seq enrichment using MACS. *Nature Protocols*, 7(9), 1728–1740. Number: 9 Publisher: Nature Publishing Group.

[38] Feng, R., Li, S., Lu, C., Andreas, C., Stolz, D. B., Mapara, M. Y., & Lentzsch, S. (2011). Targeting the Microtubular Network as a New Antimyeloma Strategy. *Molecular Cancer Therapeutics*, 10(10), 1886–1896.

[39] Fetiva, M. C., Liss, F., Gertzmann, D., Thomas, J., Gantert, B., Vogl, M., Sira, N., Weinstock, G., Kneitz, S., Ade, C., & Gaubatz, S. (2023). Oncogenic YAP mediates changes in chromatin accessibility and activity that drive cell cycle gene expression and cell migration. *Nucleic Acids Research*, 51(9), 4266–4283.

[40] Fischer, M., Grossmann, P., Padi, M., & DeCaprio, J. A. (2016). Integration of TP53, DREAM, MMB-FOXM1 and RB-E2F target gene analyses identifies cell cycle gene regulatory networks. *Nucleic Acids Research*, 44(13), 6070–6086.

[41] Fischer, M., Schade, A. E., Branigan, T. B., Müller, G. A., & DeCaprio, J. A. (2022). Coordinating gene expression during the cell cycle. *Trends in Biochemical Sciences*, 47(12), 1009–1022.

[42] Foos, G., Grimm, S., & Klempnauer, K. H. (1992). Functional antagonism between members of the myb family: B-myb inhibits v-myb-induced gene activation. *The EMBO Journal*, 11(12), 4619–4629.

[43] Fu, Z., Malureanu, L., Huang, J., Wang, W., Li, H., van Deursen, J. M., Tindall, D. J., & Chen, J. (2008). Plk1-dependent phosphorylation of FoxM1 regulates a transcriptional programme required for mitotic progression. *Nature Cell Biology*, 10(9), 1076–1082.

[44] García, P. & Frampton, J. (2006). The transcription factor B-Myb is essential for S-phase progression and genomic stability in diploid and polyploid megakaryocytes. *Journal of Cell Science*, 119(8), 1483–1493.

[45] Garibaldi, A., Carranza, F., & Hertel, K. J. (2017). Isolation of Newly Transcribed RNA Using the Metabolic Label 4-thiouridine. *Methods in molecular biology (Clifton, N.J.)*, 1648, 169–176.

[46] Gavet, O. & Pines, J. (2010). Progressive activation of CyclinB1-Cdk1 coordinates entry to mitosis. *Developmental cell*, 18(4), 533–543.

[47] Gentles, A. J., Newman, A. M., Liu, C. L., Bratman, S. V., Feng, W., Kim, D., Nair, V. S., Xu, Y., Khuong, A., Hoang, C. D., Diehn, M., West, R. B., Plevritis, S. K., & Alizadeh, A. A. (2015). The prognostic landscape of genes and infiltrating immune cells across human cancers. *Nature Medicine*, 21(8), 938–945.

[48] Giacinti, C. & Giordano, A. (2006). RB and cell cycle progression. *Oncogene*, 25(38), 5220–5227. Number: 38 Publisher: Nature Publishing Group.

[49] Gojo, I., Sadowska, M., Walker, A., Feldman, E. J., Iyer, S. P., Baer, M. R., Sausville, E. A., Lapidus, R. G., Zhang, D., Zhu, Y., Jou, Y.-M., Poon, J., Small, K., & Bannerji, R. (2013). Clinical and laboratory studies of the novel cyclin-dependent kinase inhibitor dinaciclib (SCH 727965) in acute leukemias. *Cancer Chemotherapy and Pharmacology*, 72(4), 897–908.

[50] Grant, G. D., Brooks, L., Zhang, X., Mahoney, J. M., Martyanov, V., Wood, T. A., Sherlock, G., Cheng, C., & Whitfield, M. L. (2013). Identification of cell cycle-regulated genes periodically expressed in U2OS cells and their regulation by FOXM1 and E2F transcription factors. *Molecular Biology of the Cell*, 24(23), 3634–3650.

[51] Gründl, M., Walz, S., Hauf, L., Schwab, M., Werner, K. M., Spahr, S., Schulte, C., Maric, H. M., Ade, C. P., & Gaubatz, S. (2020). Interaction of YAP with the Myb-MuvB (MMB) complex defines a transcriptional program to promote the proliferation of cardiomyocytes. *PLOS Genetics*, 16(5), e1008818. Publisher: Public Library of Science.

[52] Guiley, K. Z., Iness, A. N., Saini, S., Tripathi, S., Lipsick, J. S., Litovchick, L., & Rubin, S. M. (2018). Structural mechanism of MybMuvB assembly. *Proceedings of the National Academy of Sciences*, 115(40), 10016–10021. Publisher: Proceedings of the National Academy of Sciences.

[53] Guiley, K. Z., Liban, T. J., Felthousen, J. G., Ramanan, P., Litovchick, L., & Rubin, S. M. (2015). Structural mechanisms of DREAM complex assembly and regulation. *Genes & Development*, 29(9), 961–974.

[54] Hafner, M., Mills, C. E., Subramanian, K., Chen, C., Chung, M., Boswell, S. A., Everley, R. A., Liu, C., Walmsley, C. S., Juric, D., & Sorger, P. K. (2019). Multiomics Profiling Establishes the Polypharmacology of FDA-Approved CDK4/6 Inhibitors and the Potential for Differential Clinical Activity. *Cell Chemical Biology*, 26(8), 1067–1080.e8.

[55] Halasi, M. & Gartel, A. L. (2012). Suppression of FOXM1 Sensitizes Human Cancer Cells to Cell Death Induced by DNA-Damage. *PLOS ONE*, 7(2), e31761. Publisher: Public Library of Science.

[56] Hanada, N., Lo, H.-W., Day, C.-P., Pan, Y., Nakajima, Y., & Hung, M.-C. (2006). Co-regulation of B-Myb expression by E2F1 and EGF receptor. *Molecular Carcinogenesis*, 45(1), 10–17.

[57] Hanahan, D. & Weinberg, R. A. (2000). The Hallmarks of Cancer. *Cell*, 100(1), 57–70. Publisher: Elsevier.

[58] Huang, D. W., Sherman, B. T., & Lempicki, R. A. (2009). Systematic and integrative analysis of large gene lists using DAVID bioinformatics resources. *Nature Protocols*, 4(1), 44–57. Number: 1 Publisher: Nature Publishing Group.

[59] Iness, A. N., Felthousen, J., Ananthapadmanabhan, V., Sesay, F., Saini, S., Guiley, K. Z., Rubin, S. M., Dozmorov, M., & Litovchick, L. (2019). The cell cycle regulatory DREAM complex is disrupted by high expression of oncogenic B-Myb. *Oncogene*, 38(7), 1080–1092.

[60] Iness, A. N. & Litovchick, L. (2018). MuvB: A Key to Cell Cycle Control in Ovarian Cancer. *Frontiers in Oncology*, 8, 223.

[61] Iness, A. N., Rubinsak, L., Meas, S. J., Chaoul, J., Sayeed, S., Pillappa, R., Temkin, S. M., Dozmorov, M. G., & Litovchick, L. (2021). Oncogenic B-Myb Is Associated With Deregulation of the DREAM-Mediated Cell Cycle Gene Expression Program in High Grade Serous Ovarian Carcinoma Clinical Tumor Samples. *Frontiers in Oncology*, 11.

[62] Iwai, N., Kitajima, K., Sakai, K., Kimura, T., & Nakano, T. (2001). Alteration of cell adhesion and cell cycle properties of ES cells by an inducible dominant interfering Myb mutant. *Oncogene*, 20(12), 1425–1434. Number: 12 Publisher: Nature Publishing Group.

[63] Javaid, N. & Choi, S. (2021). CRISPR/Cas System and Factors Affecting Its Precision and Efficiency. *Frontiers in Cell and Developmental Biology*, 9, 761709.

[64] Johnson, T. K., Schweppe, R. E., Septer, J., & Lewis, R. E. (1999). Phosphorylation of B-Myb Regulates Its Transactivation Potential and DNA Binding*. *Journal of Biological Chemistry*, 274(51), 36741–36749.

[65] Kabadi, A. M., Ousterout, D. G., Hilton, I. B., & Gersbach, C. A. (2014). Multiplex CRISPR/Cas9-based genome engineering from a single lentiviral vector. *Nucleic Acids Research*, 42(19), e147.

[66] Kalinichenko, V. V., Major, M. L., Wang, X., Petrovic, V., Kuechle, J., Yoder, H. M., Dennewitz, M. B., Shin, B., Datta, A., Raychaudhuri, P., & Costa, R. H. (2004). Foxm1b transcription factor is essential for development of hepatocellular carcinomas and is negatively regulated by the p19ARF tumor suppressor. *Genes & Development*, 18(7), 830–850. Company: Cold Spring Harbor Laboratory Press Distributor: Cold Spring Harbor Laboratory Press Institution: Cold Spring Harbor Laboratory Press Label: Cold Spring Harbor Laboratory Press Publisher: Cold Spring Harbor Lab.

[67] Karnitz, L. M., Flatten, K. S., Wagner, J. M., Loegering, D., Hackbarth, J. S., Arlander, S. J. H., Vroman, B. T., Thomas, M. B., Baek, Y.-U., Hopkins, K. M., Lieberman, H. B., Chen, J., Cliby, W. A., & Kaufmann, S. H. (2005). Gemcitabine-Induced Activation of Checkpoint Signaling Pathways That Affect Tumor Cell Survival. *Molecular Pharmacology*, 68(6), 1636–1644. Publisher: American Society for Pharmacology and Experimental Therapeutics Section: Article.

[68] Karp, J. E., Smith, B. D., Levis, M. J., Gore, S. D., Greer, J., Hattenburg, C., Briel, J., Jones, R. J., Wright, J. J., & Colevas, A. D. (2007). Sequential flavopiridol, cytosine arabinoside, and mitoxantrone: a phase II trial in adults with poor-risk acute myelogenous leukemia. *Clinical Cancer Research: An Official Journal of the American Association for Cancer Research*, 13(15 Pt 1), 4467–4473.

[69] Kim, S.-T., Lim, D.-S., Canman, C. E., & Kastan, M. B. (1999). Substrate Specificities and Identification of Putative Substrates of ATM Kinase Family Members *. *Journal of Biological Chemistry*, 274(53), 37538–37543. Publisher: Elsevier.

[70] Klein, D. K., Hoffmann, S., Ahlskog, J. K., O'Hanlon, K., Quaas, M., Larsen, B. D., Rolland, B., Rösner, H. I., Walter, D., Kousholt, A. N., Menzel, T., Lees, M., Johansen, J. V., Rappsilber, J., Engeland, K., & Sørensen, C. S. (2015). Cyclin F suppresses B-Myb activity to promote cell cycle checkpoint control. *Nature Communications*, 6, 5800.

[71] Knight, A. S., Notaridou, M., & Watson, R. J. (2009). A Lin-9 complex is recruited by B-Myb to activate transcription of G2/M genes in undifferentiated embryonal carcinoma cells. *Oncogene*, 28(15), 1737–1747.

[72] Lam, E. W. F., Bennett, J. D., & Watson, R. J. (1995). Cell-cycle regulation of human B-myb transcription. *Gene*, 160(2), 277–281.

[73] Laoukili, J., Alvarez, M., Meijer, L. A. T., Stahl, M., Mohammed, S., Kleij, L., Heck, A. J. R., & Medema, R. H. (2008). Activation of FoxM1 during G2 Requires Cyclin A/Cdk-Dependent Relief of Autorepression by the FoxM1 N-Terminal Domain. *Molecular and Cellular Biology*, 28(9), 3076–3087.

[74] Li, X. & McDonnell, D. P. (2002). The Transcription Factor B-Myb Is Maintained in an Inhibited State in Target Cells through Its Interaction with the Nuclear Corepressors N-CoR and SMRT. *Molecular and Cellular Biology*, 22(11), 3663–3673. Publisher: Taylor & Francis.

[75] Lindqvist, A., van Zon, W., Karlsson Rosenthal, C., & Wolthuis, R. M. F. (2007). Cyclin B1-Cdk1 activation continues after centrosome separation to control mitotic progression. *PLoS biology*, 5(5), e123.

[76] Litovchick, L., Florens, L. A., Swanson, S. K., Washburn, M. P., & DeCaprio, J. A. (2011). DYRK1A protein kinase promotes quiescence and senescence through DREAM complex assembly. *Genes & Development*, 25(8), 801–813.

[77] Litovchick, L., Sadasivam, S., Florens, L., Zhu, X., Swanson, S. K., Velmurugan, S., Chen, R., Washburn, M. P., Liu, X. S., & DeCaprio, J. A. (2007). Evolutionarily Conserved Multisubunit RBL2/p130 and E2F4 Protein Complex Represses Human Cell Cycle-Dependent Genes in Quiescence. *Molecular Cell*, 26(4), 539–551.

[78] Littler, D. R., Alvarez-Fernández, M., Stein, A., Hibbert, R. G., Heidebrecht, T., Aloy, P., Medema, R. H., & Perrakis, A. (2010). Structure of the FoxM1 DNA-recognition domain bound to a promoter sequence. *Nucleic Acids Research*, 38(13), 4527–4538.

[79] Liu, N., Lucibello, F. C., Zwicker, J., Engeland, K., & Müller, R. (1996). Cell cycle-regulated repression of B-myb transcription: cooperation of an E2F site with a contiguous corepressor element. *Nucleic Acids Research*, 24(15), 2905–2910.

[80] Liu, Y., Chen, S., Wang, S., Soares, F., Fischer, M., Meng, F., Du, Z., Lin, C., Meyer, C., DeCaprio, J. A., Brown, M., Liu, X. S., & He, H. H. (2017). Transcriptional landscape of the human cell cycle. *Proceedings of the National Academy of Sciences*, 114(13), 3473–3478. Publisher: National Academy of Sciences Section: Biological Sciences.

[81] Lobingier, B. T., Hüttenhain, R., Eichel, K., Miller, K. B., Ting, A. Y., von Zastrow, M., & Krogan, N. J. (2017). An Approach to Spatiotemporally Resolve Protein Interaction Networks in Living Cells. *Cell*, 169(2), 350–360.e12.

[82] Lorvellec, M., Dumon, S., Maya-Mendoza, A., Jackson, D., Frampton, J., & García, P. (2010). B-Myb is Critical for Proper DNA Duplication During an Unperturbed S Phase in Mouse Embryonic Stem Cells. *Stem Cells*, 28(10), 1751–1759.

[83] Love, M. I., Huber, W., & Anders, S. (2014). Moderated estimation of fold change and dispersion for RNA-seq data with DESeq2. *Genome Biology*, 15(12), 550.

[84] Lüscher-Firzlaff, J. M., Lilischkis, R., & Lüscher, B. (2006). Regulation of the transcription factor FOXM1c by Cyclin E/CDK2. *FEBS letters*, 580(7), 1716–1722.

[85] Ma, J., Li, X., Su, Y., Zhao, J., Luedtke, D. A., Epshteyn, V., Edwards, H., Wang, G., Wang, Z., Chu, R., Taub, J. W., Lin, H., Wang, Y., & Ge, Y. (2017). Mechanisms responsible for the synergistic antileukemic interactions between ATR inhibition and cytarabine in acute myeloid leukemia cells. *Scientific Reports*, 7, 41950.

[86] Macosko, E. Z., Basu, A., Satija, R., Nemesh, J., Shekhar, K., Goldman, M., Tirosh, I., Bialas, A. R., Kamitaki, N., Martersteck, E. M., Trombetta, J. J., Weitz, D. A., Sanes, J. R., Shalek, A. K., Regev, A., & McCarroll, S. A. (2015). Highly Parallel Genome-wide Expression Profiling of Individual Cells Using Nanoliter Droplets. *Cell*, 161(5), 1202–1214.

[87] Mahat, D. B., Kwak, H., Booth, G. T., Jonkers, I. H., Danko, C. G., Patel, R. K., Waters, C. T., Munson, K., Core, L. J., & Lis, J. T. (2016). Base-pair-resolution genome-wide mapping of active RNA polymerases using precision nuclear run-on (PRO-seq). *Nature Protocols*, 11(8), 1455–1476. Bandiera_abtest: a Cg_type: Nature Research Journals Number: 8 Primary_atype: Protocols Publisher: Nature Publishing Group Subject_term: Gene expression analysis;RNA sequencing;Transcriptional regulatory elements;Transcriptomics Subject_term_id: gene-expression-analysis;rna-sequencing;transcriptional-regulatory-elements;transcriptomics.

[88] Major, M. L., Lepe, R., & Costa, R. H. (2004). Forkhead Box M1B Transcriptional Activity Requires Binding of Cdk-Cyclin Complexes for Phosphorylation-Dependent Recruitment of p300/CBP Coactivators. *Molecular and Cellular Biology*, 24(7), 2649–2661.

[89] Marceau, A. H., Brison, C. M., Nerli, S., Arsenault, H. E., McShan, A. C., Chen, E., Lee, H.-W., Benanti, J. A., Sgourakis, N. G., & Rubin, S. M. (2019). An order-to-disorder structural switch activates the FoxM1 transcription factor. *eLife*, 8, e46131.

[90] Matson, J. P., Dumitru, R., Coryell, P., Baxley, R. M., Chen, W., Twaroski, K., Webber, B. R., Tolar, J., Bielinsky, A.-K., Purvis, J. E., & Cook, J. G. (2017). Rapid DNA replication origin licensing protects stem cell pluripotency. *eLife*, 6, e30473.

[91] Meryet-Figuiere, M., Alaei-Mahabadi, B., Ali, M. M., Mitra, S., Subhash, S., Pandey, G. K., Larsson, E., & Kanduri, C. (2014). Temporal separation of replication and transcription during S-phase progression. *Cell Cycle*, 13(20), 3241–3248.

[92] Mukhopadhyay, N. K., Chand, V., Pandey, A., Kopanja, D., Carr, J. R., Chen, Y.-J., Liao, X., & Raychaudhuri, P. (2017). Plk1 Regulates the Repressor Function of FoxM1b by inhibiting its Interaction with the Retinoblastoma Protein. *Scientific Reports*, 7, 46017.

[93] Musa, J., Aynaud, M.-M., Mirabeau, O., Delattre, O., & Grünewald, T. G. (2017). MYBL2 (B-Myb): a central regulator of cell proliferation, cell survival and differentiation involved in tumorigenesis. *Cell Death & Disease*, 8(6), e2895–e2895. Number: 6 Publisher: Nature Publishing Group.

[94] Müller, G. A., Asthana, A., & Rubin, S. M. (2022). Structure and Function of MuvB Complexes. *Oncogene*, 41(21), 2909.

[95] Müller, G. A., Quaas, M., Schümann, M., Krause, E., Padi, M., Fischer, M., Litovchick, L., DeCaprio, J. A., & Engeland, K. (2012). The CHR promoter element controls cell cycle-dependent gene transcription and binds the DREAM and MMB complexes. *Nucleic Acids Research*, 40(4), 1561–1578.

[96] Müller, G. A., Wintsche, A., Stangner, K., Prohaska, S. J., Stadler, P. F., & Engeland, K. (2014). The CHR site: definition and genome-wide identification of a cell cycle transcriptional element. *Nucleic Acids Research*, 42(16), 10331–10350.

[97] Nakajima, T., Yasui, K., Zen, K., Inagaki, Y., Fujii, H., Minami, M., Tanaka, S., Taniwaki, M., Itoh, Y., Arii, S., Inazawa, J., & Okanoue, T. (2008). Activation of B-Myb by E2F1 in hepatocellular carcinoma. *Hepatology Research: The Official Journal of the Japan Society of Hepatology*, 38(9), 886–895.

[98] Narasimha, A. M., Kaulich, M., Shapiro, G. S., Choi, Y. J., Sicinski, P., & Dowdy, S. F. (2014). Cyclin D activates the Rb tumor suppressor by monophosphorylation. *eLife*, 3, e02872. Publisher: eLife Sciences Publications, Ltd.

[99] Ogata, K., Hojo, H., Aimoto, S., Nakai, T., Nakamura, H., Sarai, A., Ishii, S., & Nishimura, Y. (1992). Solution structure of a DNA-binding unit of Myb: a helix-turn-helix-related motif with conserved tryptophans forming a hydrophobic core. *Proceedings of the National Academy of Sciences of the United States of America*, 89(14), 6428–6432.

[100] Okumura, F., Uematsu, K., Byrne, S. D., Hirano, M., Joo-Okumura, A., Nishikimi, A., Shuin, T., Fukui, Y., Nakatsukasa, K., & Kamura, T. (2016). Parallel Regulation of von Hippel-Lindau Disease by pVHL-Mediated Degradation of B-Myb and Hypoxia-Inducible Factor . *Molecular and Cellular Biology*, 36(12), 1803–1817.

[101] Osterloh, L., von Eyss, B., Schmit, F., Rein, L., Hübner, D., Samans, B., Hauser, S., & Gaubatz, S. (2007). The human synMuv-like protein LIN-9 is required for transcription of G2/M genes and for entry into mitosis. *The EMBO journal*, 26(1), 144–157.

[102] Panagopoulos, A. & Altmeyer, M. (2021). The Hammer and the Dance of Cell Cycle Control. *Trends in Biochemical Sciences*, 46(4), 301–314. Publisher: Elsevier.

[103] Park, H. J., Costa, R. H., Lau, L. F., Tyner, A. L., & Raychaudhuri, P. (2008). Anaphase-Promoting Complex/Cyclosome-Cdh1-Mediated Proteolysis of the Forkhead Box M1 Transcription Factor Is Critical for Regulated Entry into S Phase. *Molecular and Cellular Biology*, 28(17), 5162–5171.

[104] Patro, R., Duggal, G., Love, M. I., Irizarry, R. A., & Kingsford, C. (2017). Salmon: fast and bias-aware quantification of transcript expression using dual-phase inference. *Nature methods*, 14(4), 417–419.

[105] Pattschull, G., Walz, S., Gründl, M., Schwab, M., Rühl, E., Baluapuri, A., Cindric-Vranesic, A., Kneitz, S., Wolf, E., Ade, C. P., Rosenwald, A., von Eyss, B., & Gaubatz, S. (2019). The Myb-MuvB Complex Is Required for YAP-Dependent Transcription of Mitotic Genes. *Cell Reports*, 27(12), 3533–3546.e7.

[106] Peña-Diaz, J., Hegre, S. A., Anderssen, E., Aas, P. A., Mjelle, R., Gilfillan, G. D., Lyle, R., Drabløs, F., Krokan, H. E., & Sætrom, P. (2013). Transcription profiling during the cell cycle shows that a subset of Polycomb-targeted genes is upregulated during DNA replication. *Nucleic Acids Research*, 41(5), 2846–2856.

[107] Pierce, A. M., Schneider-Broussard, R., Philhower, J. L., & Johnson, D. G. (1998). Differential activities of E2F family members: unique functions in regulating transcription. *Molecular Carcinogenesis*, 22(3), 190–198.

[108] Pilkinton, M., Sandoval, R., & Colamonici, O. R. (2007). Mammalian Mip/LIN-9 interacts with either the p107, p130/E2F4 repressor complex or B-Myb in a cell cycle-phase-dependent context distinct from the Drosophila dREAM complex. *Oncogene*, 26(54), 7535–7543.

[109] Ramírez, F., Ryan, D. P., Grüning, B., Bhardwaj, V., Kilpert, F., Richter, A. S., Heyne, S., Dündar, F., & Manke, T. (2016). deepTools2: a next generation web server for deep-sequencing data analysis. *Nucleic Acids Research*, 44(W1), W160–165.

[110] Reimer, K. A., Mimoso, C. A., Adelman, K., & Neugebauer, K. M. (2021). Co-transcriptional splicing regulates 3' end cleavage during mammalian erythropoiesis. *Molecular Cell*, 81(5), 998–1012.e7.

[111] Riba, A., Oravecz, A., Durik, M., Jiménez, S., Alunni, V., Cerciat, M., Jung, M., Keime, C., Keyes, W. M., & Molina, N. (2022). Cell cycle gene regulation dynamics revealed by RNA velocity and deep-learning. *Nature Communications*, 13(1), 2865. Number: 1 Publisher: Nature Publishing Group.

[112] Rivas, H. G. & DeCaprio, J. A. (2023). The Restriction Point. Publisher: Elsevier.

[113] Robinson, C., Light, Y., Groves, R., Mann, D., Marias, R., & Watson, R. (1996). Cell-cycle regulation of B-Myb protein expression: specific phosphorylation during the S phase of the cell cycle. *Oncogene*, 12(9), 1855–1864.

[114] Russo, J., Heck, A. M., Wilusz, J., & Wilusz, C. J. (2017). Metabolic Labeling and Recovery of Nascent RNA to Accurately Quantify mRNA Stability. *Methods (San Diego, Calif.)*, 120, 39–48.

[115] Sadasivam, S. & DeCaprio, J. A. (2013). The DREAM complex: Master coordinator of cell cycle dependent gene expression. *Nature reviews. Cancer*, 13(8), 585–595.

[116] Sadasivam, S., Duan, S., & DeCaprio, J. A. (2012). The MuvB complex sequentially recruits B-Myb and FoxM1 to promote mitotic gene expression. *Genes & Development*, 26(5), 474–489.

[117] Sala, A., Kundu, M., Casella, I., Engelhard, A., Calabretta, B., Grasso, L., Paggi, M., Giordano, A., Watson, R., Khalili, K., & Peschle, C. (1997). Activation of human B-MYB bycyclins. *Proceedings of the National Academy of Sciences*, 94(2), 532–536. Publisher: Proceedings of the National Academy of Sciences.

[118] Saldivar, J. C., Cortez, D., & Cimprich, K. A. (2017). The essential kinase ATR: ensuring faithful duplication of a challenging genome. *Nature Reviews. Molecular Cell Biology*, 18(10), 622–636.

[119] Saldivar, J. C., Hamperl, S., Bocek, M. J., Chung, M., Bass, T. E., Cisneros-Soberanis, F., Samejima, K., Xie, L., Paulson, J. R., Earnshaw, W. C., Cortez, D., Meyer, T., & Cimprich, K. A. (2018). An intrinsic S/G2 checkpoint enforced by ATR. *Science (New York, N.Y.)*, 361(6404), 806–810.

[120] Sanders, D. A., Gormally, M. V., Marsico, G., Beraldi, D., Tannahill, D., & Balasubramanian, S. (2015). FOXM1 binds directly to non-consensus sequences in the human genome. *Genome Biology*, 16(1), 130.

[121] Sanidas, I., Morris, R., Fella, K. A., Rumde, P. H., Boukhali, M., Tai, E. C., Ting, D. T., Lawrence, M. S., Haas, W., & Dyson, N. J. (2019). A Code of Mono-phosphorylation Modulates the Function of RB. *Molecular Cell*, 73(5), 985–1000.e6.

[122] Sanjana, N. E., Shalem, O., & Zhang, F. (2014). Improved vectors and genome-wide libraries for CRISPR screening. *Nature Methods*, 11(8), 783–784. Number: 8 Publisher: Nature Publishing Group.

[123] Saville, M. K. & Watson, R. J. (1998). The cell-cycle regulated transcription factor B-Myb is phosphorylated by cyclin A/Cdk2 at sites that enhance its transactivation properties. *Oncogene*, 17(21), 2679–2689.

[124] Schade, A. E., Fischer, M., & DeCaprio, J. A. (2019a). RB, p130ăand p107 differentially repress G1/S and G2/M genes after p53 activation. *Nucleic Acids Research*, 47(21), 11197–11208.

[125] Schade, A. E., Oser, M. G., Nicholson, H. E., & DeCaprio, J. A. (2019b). Cyclin D-CDK4 relieves cooperative repression of proliferation and cell cycle gene expression by DREAM and RB. *Oncogene*, 38(25), 4962–4976.

[126] Schmit, F., Korenjak, M., Mannefeld, M., Schmitt, K., Franke, C., von Eyss, B., Gagrica, S., Hanel, F., Brehm, A., & Gaubatz, S. (2007). LINC, a Human Complex That is Related to pRB-Containing Complexes in Invertebrates Regulates the Expression of G $_2$ /M Genes. *Cell Cycle*, 6(15), 1903–1913.

[127] Schöffski, P. (2009). Polo-like kinase (PLK) inhibitors in preclinical and early clinical development in oncology. *The Oncologist*, 14(6), 559–570.

[128] Skene, P. J. & Henikoff, S. (2017). An efficient targeted nuclease strategy for high-resolution mapping of DNA binding sites. *eLife*, 6, e21856. Publisher: eLife Sciences Publications, Ltd.

[129] Szmyd, R., Niska-Blakie, J., Diril, M. K., Renck Nunes, P., Tzelepis, K., Lacroix, A., van Hul, N., Deng, L.-W., Matos, J., Dreesen, O., Bisteau, X., & Kaldis, P. (2019). Premature activation of Cdk1 leads to mitotic events in S phase and embryonic lethality. *Oncogene*, 38(7), 998–1018. Number: 7 Publisher: Nature Publishing Group.

[130] Tan, Y., Raychaudhuri, P., & Costa, R. H. (2007). Chk2 mediates stabilization of the FoxM1 transcription factor to stimulate expression of DNA repair genes. *Molecular and Cellular Biology*, 27(3), 1007–1016.

[131] van Zon, W., Ogink, J., ter Riet, B., Medema, R. H., te Riele, H., & Wolthuis, R. M. F. (2010). The APC/C recruits cyclin B1-Cdk1-Cks in prometaphase before D box recognition to control mitotic exit. *The Journal of Cell Biology*, 190(4), 587–602.

[132] Walker, M., Black, E. J., Oehler, V., Gillespie, D. A., & Scott, M. T. (2009). Chk1 C-terminal regulatory phosphorylation mediates checkpoint activation by de-repression of Chk1 catalytic activity. *Oncogene*, 28(24), 2314–2323. Number: 24 Publisher: Nature Publishing Group.

[133] Wang, B., Varela-Eirin, M., Brandenburg, S. M., Hernandez-Segura, A., van Vliet, T., Jongbloed, E. M., Wilting, S. M., Ohtani, N., Jager, A., & Demaria, M. (2022). Pharmacological CDK4/6 inhibition reveals a p53-dependent senescent state with restricted toxicity. *The EMBO journal*, 41(6), e108946.

[134] Wang, I.-C., Chen, Y.-J., Hughes, D., Petrovic, V., Major, M. L., Park, H. J., Tan, Y., Ackerson, T., & Costa, R. H. (2005). Forkhead box M1 regulates the transcriptional network of genes essential for mitotic progression and genes encoding the SCF (Skp2-Cks1) ubiquitin ligase. *Molecular and Cellular Biology*, 25(24), 10875–10894.

[135] Wang, J., Rojas, P., Mao, J., Mustè Sadurnì, M., Garnier, O., Xiao, S., Higgs, M. R., Garcia, P., & Saponaro, M. (2021). Persistence of RNA transcription during DNA replication delays duplication of transcription start sites until G2/M. *Cell Reports*, 34(7), 108759.

[136] Wang, X., Kiyokawa, H., Dennewitz, M. B., & Costa, R. H. (2002). The Forkhead Box m1b transcription factor is essential for hepatocyte DNA replication and mitosis during mouse liver regeneration. *Proceedings of the National Academy of Sciences*, 99(26), 16881–16886. Publisher: Proceedings of the National Academy of Sciences.

[137] Watson, R. J., Robinson, C., & Lam, E. W. (1993). Transcription regulation by murine B-myb is distinct from that by c-myb. *Nucleic Acids Research*, 21(2), 267–272.

[138] Weinberg, R. A. (1995). The retinoblastoma protein and cell cycle control. *Cell*, 81(3), 323–330.

[139] Werwein, E., Schmedt, T., Hoffmann, H., Usadel, C., Obermann, N., Singer, J. D., & Klempnauer, K.-H. (2012). B-Myb promotes S-phase independently of its sequence-specific DNA binding activity and interacts with polymerase delta-interacting protein 1 (Pdip1). *Cell Cycle*, 11(21), 4047–4058.

[140] Whitfield, M. L., Sherlock, G., Saldanha, A. J., Murray, J. I., Ball, C. A., Alexander, K. E., Matese, J. C., Perou, C. M., Hurt, M. M., Brown, P. O., & Botstein, D. (2002). Identification of genes periodically expressed in the human cell cycle and their expression in tumors. *Molecular Biology of the Cell*, 13(6), 1977–2000.

[141] Wierstra, I. & Alves, J. (2006). Despite its strong transactivation domain, transcription factor FOXM1c is kept almost inactive by two different inhibitory domains. 387(7), 963–976. Publisher: De Gruyter Section: Biological Chemistry.

[142] Wissink, E. M., Vihervaara, A., Tippens, N. D., & Lis, J. T. (2019). Nascent RNA Analyses: Tracking Transcription and Its Regulation. *Nature reviews. Genetics*, 20(12), 705–723.

[143] Wu, L., Goodwin, E. C., Naeger, L. K., Vigo, E., Galaktionov, K., Helin, K., & DiMaio, D. (2000). E2F-Rb complexes assemble and inhibit cdc25A transcription in cervical carcinoma cells following repression of human papillomavirus oncogene expression. *Molecular and Cellular Biology*, 20(19), 7059–7067.

[144] Yesbolatova, A., Saito, Y., Kitamoto, N., Makino-Itou, H., Ajima, R., Nakano, R., Nakaoka, H., Fukui, K., Gamo, K., Tominari, Y., Takeuchi, H., Saga, Y., Hayashi, K.-i., & Kanemaki, M. T. (2020). The auxin-inducible degron 2 technology provides sharp degradation control in yeast, mammalian cells, and mice. *Nature Communications*, 11(1), 5701. Number: 1 Publisher: Nature Publishing Group.

[145] Yildirim, O., Izgu, E. C., Damle, M., Chalei, V., Ji, F., Sadreyev, R. I., Szostak, J. W., & Kingston, R. E. (2020). S-phase Enriched Non-coding RNAs Regulate Gene Expression and Cell Cycle Progression. *Cell Reports*, 31(6), 107629.

[146] Zhang, Y., Liu, T., Meyer, C. A., Eeckhoute, J., Johnson, D. S., Bernstein, B. E., Nusbaum, C., Myers, R. M., Brown, M., Li, W., & Liu, X. S. (2008). Model-based Analysis of ChIP-Seq (MACS). *Genome Biology*, 9(9), R137.

[147] Zhang, Z., Xue, S.-t., Gao, Y., Li, Y., Zhou, Z., Wang, J., Li, Z., & Liu, Z. (2022). Small molecule targeting FOXM1 DNA binding domain exhibits antitumor activity in ovarian cancer. *Cell Death Discovery*, 8(1), 1–8. Number: 1 Publisher: Nature Publishing Group.

[148] Zhao, B., Wei, X., Li, W., Udan, R. S., Yang, Q., Kim, J., Xie, J., Ikenoue, T., Yu, J., Li, L., Zheng, P., Ye, K., Chinnaiyan, A., Halder, G., Lai, Z.-C., & Guan, K.-L. (2007). Inactivation of YAP oncoprotein by the Hippo pathway is involved in cell contact inhibition and tissue growth control. *Genes & Development*, 21(21), 2747–2761.

[149] Zhao, H. & Piwnica-Worms, H. (2001). ATR-Mediated Checkpoint Pathways Regulate Phosphorylation and Activation of Human Chk1. *Molecular and Cellular Biology*, 21(13), 4129–4139. Publisher: Taylor & Francis _eprint: https://doi.org/10.1128/MCB.21.13.4129-4139.2001.

[150] Zhu, A., Ibrahim, J. G., & Love, M. I. (2019). Heavy-tailed prior distributions for sequence count data: removing the noise and preserving large differences. *Bioinformatics*, 35(12), 2084–2092.

[151] Ziebold, U., Bartsch, O., Marais, R., Ferrari, S., & Klempnauer, K.-H. (1997). Phosphorylation and activation of B-Myb by cyclin ACdk2. *Current Biology*, 7(4), 253–260. Publisher: Elsevier.

[152] Zona, S., Bella, L., Burton, M. J., Nestal de Moraes, G., & Lam, E. W.-F. (2014). FOXM1: An emerging master regulator of DNA damage response and genotoxic agent resistance. *Biochimica et Biophysica Acta*, 1839(11), 1316–1322.

[153] Zwicker, J., Liu, N., Engeland, K., Lucibello, F. C., & Müller, R. (1996). Cell cycle regulation of E2F site occupation in vivo. *Science (New York, N.Y.)*, 271(5255), 1595–1597.

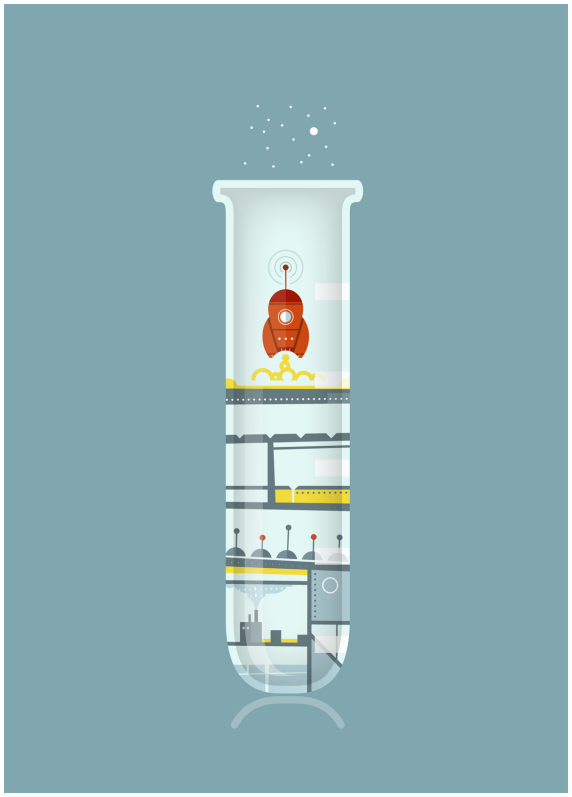

THIS THESIS WAS TYPESET using LaTeX, originally developed by Leslie Lamport and based on Donald Knuth's TeX. The body text is set in 11 point Egenolff-Berner Garamond, a revival of Claude Garamont's humanist typeface. The above illustration, "Science Experiment 02", was created by Ben Schlitter and released under CC BY-NC-ND 3.0. A template that can be used to format a PhD thesis with this look and feel has been released under the permissive MIT (X11) license, and can be found online at github.com/suchow/Dissertate or from its author, Jordan Suchow, at suchow@post.harvard.edu.